Biological Roles and Pharmacological Potentials of Marine 5-Thiohistidine Compounds

Thesis

Biological roles and pharmacological potentials of marine 5-thiohistidine compounds

Mariarita Brancaccio (M.Sc)

Doctor of Philosophy

The Open University, UK

School of Life, Health and Chemical Sciences

Stazione Zoologica Anton Dohrn, IT

Department of Biology and Evolution of Marine Organisms

September 2020

Director of studies:

Dr. Immacolata Castellano
Department of Biology and Evolution of Marine Organisms,
Stazione Zoologica Anton Dohrn, Naples, Italy

Internal Supervisor:

Dr. Anna Palumbo
Department of Biology and Evolution of Marine Organisms,
Stazione Zoologica Anton Dohrn, Naples, Italy

External Supervisor:

Prof. Dr. Florian Seebeck
Department of chemistry
University Basel, Switzerland

Abstract

5-thiohistidines are histidine-derived thiols first isolated from marine invertebrates in complex with other larger molecules or in free methylated forms. The biosynthesis of these compounds has developed in bacteria, microalgae, and invertebrates, but it has been lost in vertebrates and consequently in humans. Among them, ovothiols are methyl-5-thiohistidines first discovered in sea urchins, where they play a key role in the protection of the eggs from the oxidative burst associated with fertilization and early embryos from environmental cues. The key enzymes responsible for ovothiol biosynthesis, the sulfoxide synthase OvoA and the β-lyase OvoB, have been characterised and comparative genomics has revealed that its biosynthesis is much more widespread than previously thought.

Recently, it has been demonstrated that ovothiol A (N-p-methyl-5-thiohistidine), purified from sea urchin *Paracentrotus lividus* eggs, exhibits anti-proliferative and anti-inflammatory activity in an *in vitro* model of human hepatocarcinoma cells and in an *in vitro* model of human endothelial cells, respectively.

In this *scenario*, the aim of my thesis was to investigate the biological roles and pharmacological potential of 5-thiohistidines.

To study the biological role of this metabolite and to deepen the distribution and diversification of the ovothiol pathway in the marine world, we conducted an in-depth analysis on bacterial genomes. We highlighted that most bacteria, especially those living in acquatic environment, including several symbionts and parasites, evolved the biosynthetic pathways of ovothiol, in particular both OvoA and OvoB.

Moreover, to shed new light on the use of these molecules as new anti-inflammatory agents, we used an *in vivo* model of hepatic fibrosis and *in vitro* system of human keratinocytes to mimic skin inflammation. We identified the molecular mechanisms underlying the action of these molecules in human disorders by emphasizing their anti-inflammatory capacity.

Table of contents

Figures index

Tables index

List of abbreviations

ROS = Reactive Oxygen Species

RNS = Reactive Nitrogen Species

GSH = Glutathione

TSH = Trypanothione

MSH = Mycothiol

ovos = ovothiols

ovo A or ovo = ovothiol A

ovo B = ovothiol B

ovo C = ovothiol

SH = Thiol group

$R\text{-}S^-$ = Thiolate anion

H_2O_2 = Hydrogen Peroxide

OvoA = 5-histidylcysteine sulfoxide synthase

OvoB = β-lyase

EgtB = gamma-glutamyl hercynylcysteine sulfoxide synthase

MRE = Metal Responsive Elements

SRE = Stress Responsive Elements

AP-1 = Activator Protein 1 element

CRE = cAMP-Responsive element

TMH = N-α-trimethylhistidine

*Pl*OvoA = OvoA from *Paracentrotus lividus*

GPx = Glutathione peroxidase

Prx = Peroxiredoxin

MFP-4MI = 1-methyl-2- [3- trifluoromethylphenyl] -4-mercapto-imidazole

HepG2 = Human hepatocellular carcinoma cell line

HUVEC = Human endothelial cells

HSC = Hepatic stellate cells

ECM = Extracellular matrix

α-SMA = α-smooth muscle actin

MMP = Metalloproteinase

TIMP = Metalloproteinase inhibitor

TGF-β1 = Transforming growth factor beta1

GGT = γ-glutamyl transpeptidase

GST = Glutathione S-transferase

UV = ultraviolet radiation

IL-6 = Interleukin 6

IL-8 = Interleukin 8

TNF-α = Tumour necrosis factor

MAPK = Mitogen-activate protein kinase

Nrf2 = Erythroid-related factor 2

Keap-1 = Kelch-like ECH-associated protein 1

sMaf = Musculoaponeurotic fibrosarcoma protein

ARE = antioxidant response element

COX-2 = Cyclooxygenase 2

GGT = γ-Glutamyl transpeptidase

Thr = Threonine

DON = 6-diazo-5-oxo-L-norleucine

ES = Enzyme-Substrate

HG3= chronic B leukemic cell line

GpNA = γ-glutamyl-para-nitroanilide

GlyGly = glycyl-glycine

eqGGT = equine kidney GGT

erg = trimethyl-2-thiohistidine ergothioneine

DTT = Dithiothreitol

5-thio = 5-thiohistidine

HEK 293 = Human embryonic kidney cells

NADPH = Nitrate reductase

Col1a1= Collagen, type I, alpha 1

AST = Aspartate aminotransferase

ALT = Alanine aminotransferase

ALP = Alkaline phosphatase

CCl_4 = Carbon tetrachloride

H&E = haematoxylin/eosin

GAPDH = Glyceraldehyde 3-phosphate dehydrogenase

ERK = Extracellular signal-regulated kinase

JNK = C-Jun N-terminal kinases

HaCat = Human keratinocytes

IL-β1= Interleukin β1

p-ERK = Phospho- Extracellular signal-regulated kinase

p-JNK = Phospo-C-Jun N-terminal kinases

DMX = Dexamethasone

MT = Methyl transferase domains

Tyr417 = Tyrosine 417

G524 = Glycine 524

C525 = Cysteine 525

G528 = Glycine 528

R529 = Arginine 529

D545 = Aspartic acid 545

G599 = Glycine 599

D600 = Aspartic acid 600

A601 = Alanine 601

K240 = Lysine 240

Y125 = Tyrosine 125

N176 = Asparagine 176

D204 = Aspartic acid 204

H207 = Histidine 207

V100 = Valine 100

V101 = Valine 101

Y66 = Tyrosine 66

CHAPTER 1

General introduction

1.1 Marine 5-thiohistidines: biosynthesis and chemical structure

Living organisms are constantly exposed to oxidative stress conditions that can culminate in a pathological condition caused by the physiological unbalance between the production and elimination of oxidizing species by the antioxidant defence systems in the body. In this scenario, thiols play a crucial role in living organisms, as they contribute to maintain the cellular redox homeostasis by regulating the oxidation-reduction potentials and thiol-disulfide protein ratios. As thiols are also highly reactive towards electrophiles and oxidants, they protect the cell from reactive oxygen species (ROS) and reactive nitrogen species (RNS). and have a high affinity for metals (Winterbourn et al., 2008; Higdon et al., 2012; Nagy 2013).

The discovery, identification and characterization of intracellular thiols (figure 1) has been useful in expanding our chemical and biochemical knowledge on life processes, shedding light on different areas of research, including parasitology, chemical ecology, drug design (Hand and Honek, 2005).

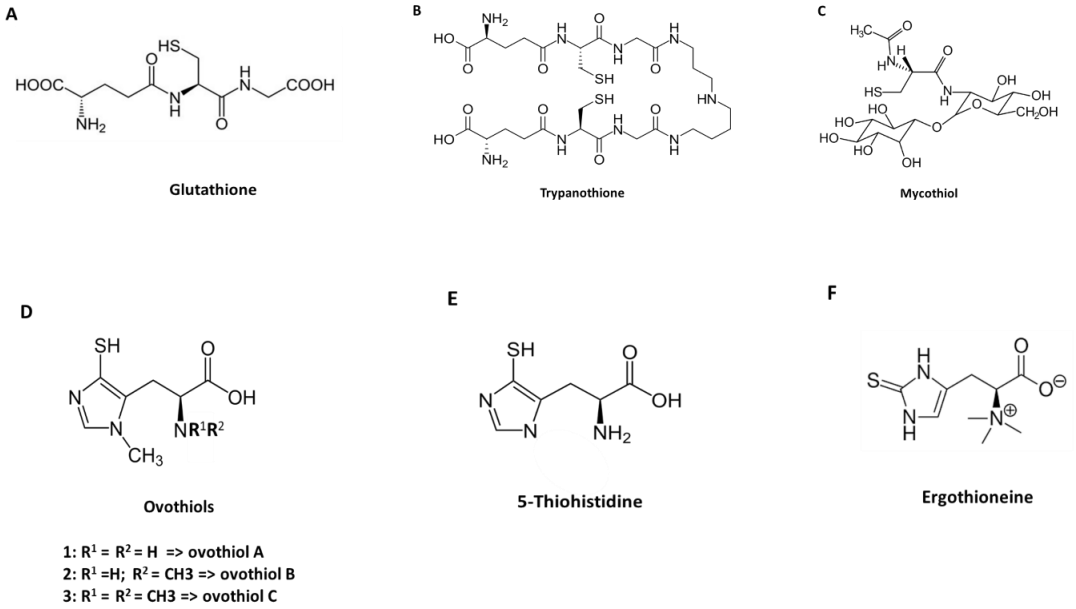

Figure 1. Chemical structure of naturally occurring thiols. A) Gluthathione; **B)** Trypanothione; **C)** Mycothiol; **D)** Ovothiols; **E)** 5-Thiohistidine; **F)** Ergothioneine.

In nature, glutathione (GSH) is the most abundant thiol in eukaryotic cells and in some bacteria such as *Escherichia coli*. GSH is a tripeptide made up of glutamic acid, cysteine and glycine (figure 1A).

In addition to GSH, there are other thiols characterized by the presence of cysteine: trypanothione (TSH) and mycothiol (MSH) (figure 1B and 1C).

TSH is an unusual form of glutathione containing two GSH molecules joined by a spermidine (polyamine) linker (figure 1B). It is found in parasitic protozoa such as *Leishmania* and *Trypanosoma*. These protozoan parasites are the cause of leishmaniosis, sleep sickness and Chagas disease. TSH was discovered by Alan Fairlamb (Fairlamb et al., 1985). Since this thiol is absent in humans and is essential for the survival of parasites, the enzymes that produce and use this molecule are targets for the development of new drugs for the treatment of these diseases. Instead, MSH is composed of a cysteine residue with an acetylated amino group linked to glucosamine (figure 1C), which is linked to inositol. It is present in the *Actinomycetes* bacteria (Newton et al., 1996).

In nature, there is also a second class of intracellular thiols which includes ergothioneine and 5-thiohistidines (figure 1D-F). This class of thiols derive from the amino acid histidine. Ergothioneine (erg) is a trimethyl-2-thioistidine (TMH) which has the sulfur group in the C2-H position on the imidazole ring (figure 1F). 5-thioistidines compounds include ovothiols (ovos), which differ for the presence of a methyl group (-CH3) on the imidazole ring of histidine (figure 1D). Depending on the nomenclature system adopted, the imidazole ring of ovothiols can be named: 3-N-methyl-5-thiohistidine, 1-N-methyl- 4-mercaptohistidine or π - N - methyl-5 –tiohistidine (Palumbo et al., 2018). In nature it is possible to recognize 3 forms: ovothiol A (ovo A), ovothiol B (ovo B) and ovothiol C (ovo C) which differ in the degree of methylation on the α-amino group of the side chain (figure 1D). On the other hand, 5-thiohistidine can occur also as an unmethylated form without any methyl group either on the imidazole ring and on the side chain of the α-amino group (figure 1E).

All these thiols may be indicated by the general formula R-SH in which the functional group –SH is referred to as a thiol group or as a sulphydryl group. The R-SH form can be deprotonated to originate the thiolate anion ($R\text{-}S^-$). The deprotonated form of thiolate anion is very reactive compared to the protonate one and acts as a nucleophile (LoPachin et al., 2007).

The capacity of a thiol group to be deprotonated depends on the acid dissociation constant (pKa), i.e. the pH at which that molecule is 50% in thiol form and 50% in thiolate form. This parameter is characteristic for each thiol group and at physiological pH (7.4) thiols with a relatively low pKa result

deprotonated and are consequently more reactive than those with a higher pKa (Wall et al., 2012) (figure 2).

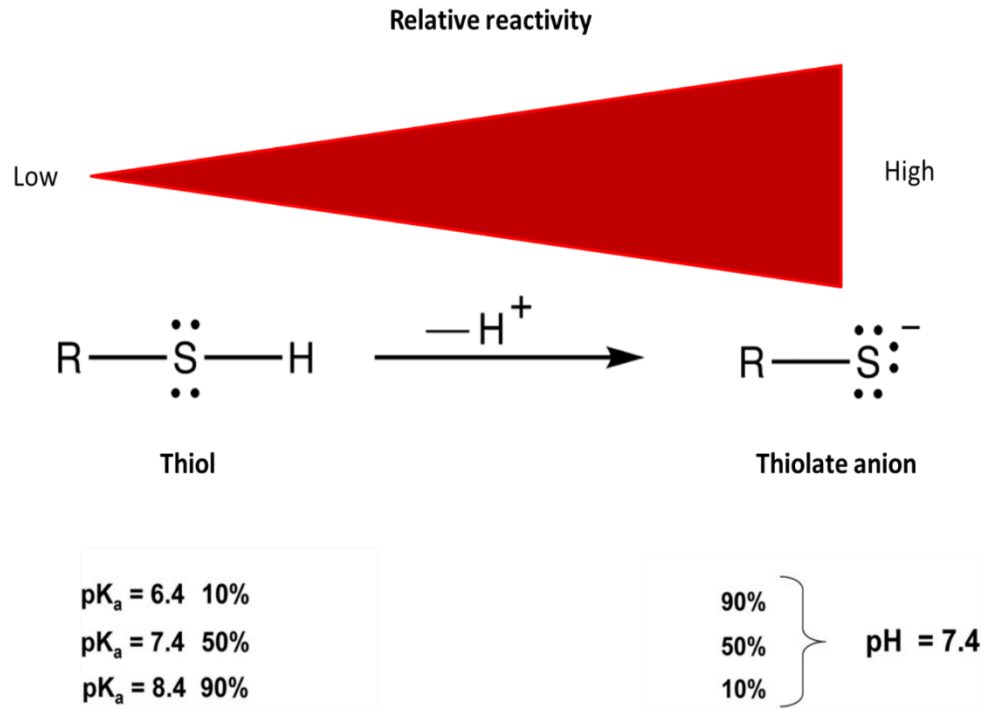

Figure 2. Relationship of thiol pKa and reactivity (modified from Wall et al; 2012)

The position of the thiol group on the imidazole ring of ovo gives it a very high reactivity compared to erg (Holler and Hopkins, 1988; Weaver and Rabenstein, 1995), in fact the pKa is equal to 1.4, an extremely low value, generating a redox potential of -0.09V. Consequently, the redox potential of these thiols is much more positive than other intracellular thiols such as GSH which has a pKa = 8.75 and a redox potential = -0.26 V (Marjanovic et al., 1995; Weaver and Rabenstein, 1995; Ariyanayagam and Fairlamb, 2001).

Therefore, these chemical characteristics make ovos particularly reactive and susceptible to oxidation. In fact, ovo reacts with hydrogen peroxide (H_2O_2) five times faster than GSH, forming water and the ovo disulphide, which, in turn, is reduced in a non-enzymatic way through the thiol-disulfide exchange with GSH (Turner et al, 1988) (figure 3) or by TSH (Fairlamb and Cerami 1992). The ability of ovos to be oxidized has made them efficient redox regulators (Turner et al., 1987; Holler and Hopkins, 1990; Bailly et al., 2000). In addition, this feature has stimulated scientific

interest in the synthesis of compounds derived from ovos to use them as anti-oxidative drugs (Zoete et al., 1997; Bailly et al., 2003).

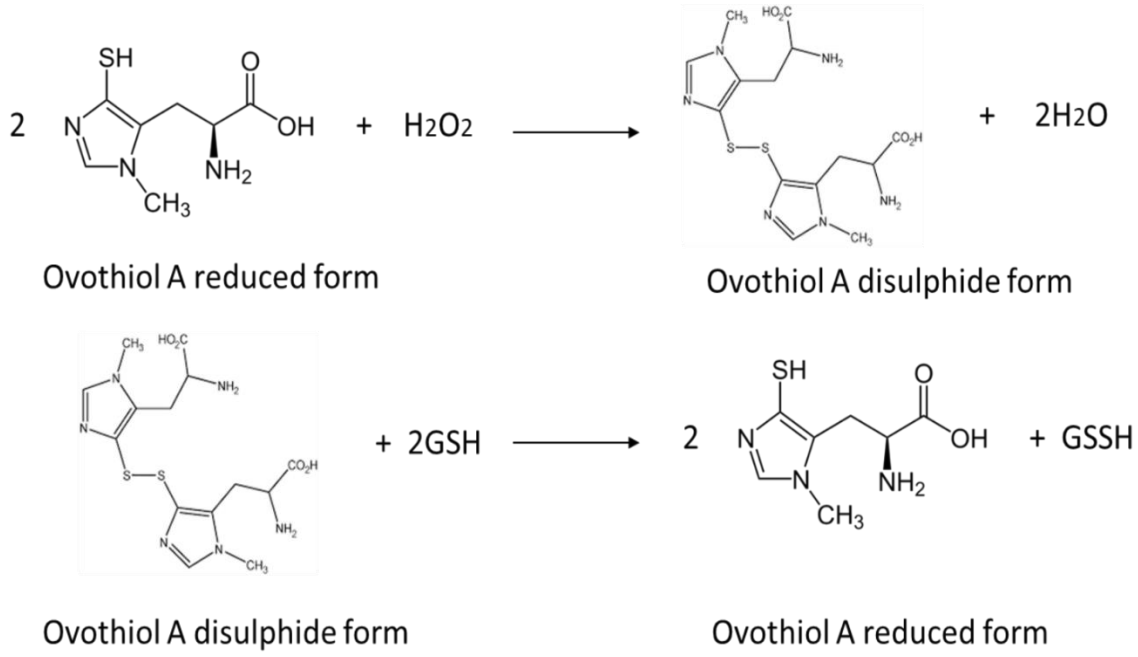

Figure 3. Thiol redox exchange reaction of ovothiol with glutathione.

In biological systems, ovo is produced thanks to three main enzymatic activities.

The biosynthetic activity of ovo was identified for the first time in raw extracts of the protist *Crithidia fasciculata*, following the incubation of cells with radiolabeled precursors (cysteine ^{35}S, methionine ^{35}S) (Steenkamp et al., 1996; Vogt et al., 2001).

More recently, the two enzymes responsible for ovo biosynthesis have been identified and characterized: 5-histidylcysteine sulfoxide synthase (OvoA) (Braunshausen and Seebeck, 2011, Seebeck, 2013) and β-lyase (OvoB) (Naowarojna et al., 2018).

OvoA is the first enzyme involved in ovo biosynthesis. This enzyme catalyzes the insertion of the cysteine sulfur atom in position C5 of the imidazole ring of histidine leading to the formation of the intermediate sulfoxide (figure 3). OvoA is an iron-dependent enzyme, identified and characterized in *Erwinia tasmaniensis* and *Trypanosoma cruzi*, which requires O_2 as an acceptor of four electrons for the formation of the C-S bond and sulfoxidation of the thioether bond (Braunshausen and Seebeck, 2011, Seebeck, 2013). The second enzyme involved in ovothiol biosynthesis is OvoB, a pyridoxal phosphate (PLP) dependent lyase that catalyzes the elimination of the cysteinyl moiety and the formation of 5-thiohistidine (figure 4) (Naowarojna et al., 2018). The last reaction consists in the

methylation of 5-thiohistidine by OvoA itself, thanks to the presence of a methyl transferase domain, to produce ovo A (Naowarojna et al., 2018).

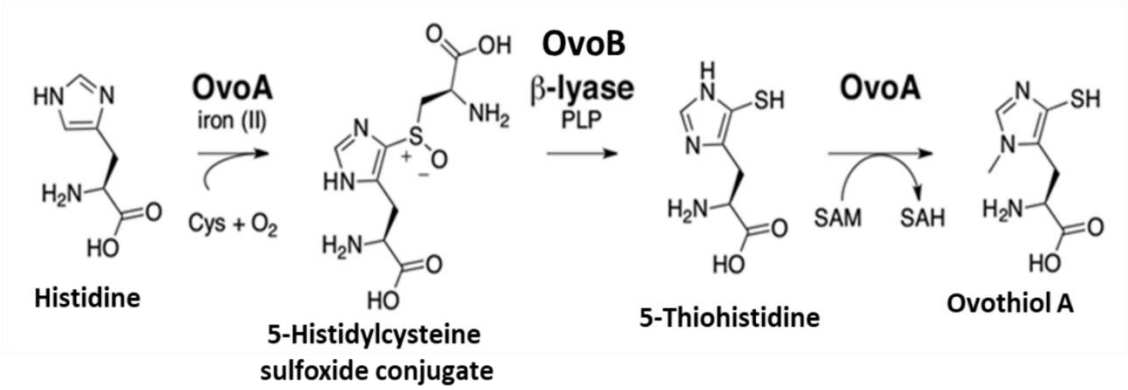

Figure 4. Ovothiol A biosynthesis.

The formation of the C-S bond by OvoA is similar to the reaction catalyzed by the gamma-glutamyl hercynylcysteine sulfoxide synthase, named EgtB, which takes part in the synthesis of erg. EgtB catalyzes the insertion of sulfur gamma-glutamyl-cysteine in the C2 position of TMH with the formation of the corresponding sulfoxide, which is then cleaved to give erg (figure 5) (Seebeck, 2010; Goncharenko et al., 2015).

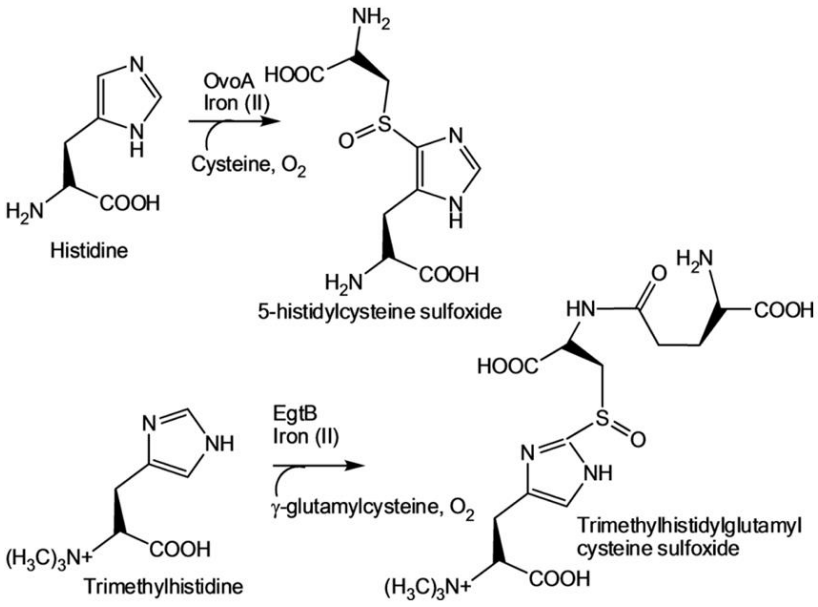

Figure 5. Comparison between OvoA and EgtB enzymatic reactions (Palumbo et al., 2018).

Recent studies have shown that enzymes homologous to OvoA are encoded in different genomes ranging from proteobacteria to animalia, prompting the concept that ovo biosynthesis is more widespread than previously thought (Castellano and Seebeck, 2018; Gerdol et al., 2019).

To investigate the specificity of the OvoA for different substrates, numerous kinetic studies have been performed using recombinant proteins from the bacteria *Erwinia tasmaniensis* and *Trypanosoma cruzi*. (Braunshausen and Seebeck, 2011; Mashabela and Seebeck, 2013). These studies have shown that OvoA presents greater flexibility in the choice of substrates compared to EgtB (Song et al., 2013; Song et al., 2014). In fact, OvoA can also accept TMH, the substrate of EgtB, leading to the formation of the intermediate precursor of erg. In this case, it is interesting to highlight how modulation of the methylation state of histidine (from histidine to TMH) leads to a change in the catalysis of OvoA, from an OvoA to a chemical EgtB type, i.e. insertion of the sulfur atom of the cysteine in the C5 or C2 position of the imidazole ring, respectively (Song et al., 2013).

The loci structure of the *ovoA* gene was recently characterized in sea urchin (Castellano et al., 2016) revealing a multi-intron-exon composition and the presence of Metal Responsive Elements (MRE) and Stress Responsive Elements (SRE) in the promoting regions of *ovoAs* from the purple sea urchin, *Strongylocentrotus purpuratus* and the Mediterranean one, *P. lividus*. The latter species showed two additional regulatory elements characterizing the *ovoA* gene, the Activator protein 1 (AP-1) element and the cAMP-Responsive (CRE) element (figure 5).

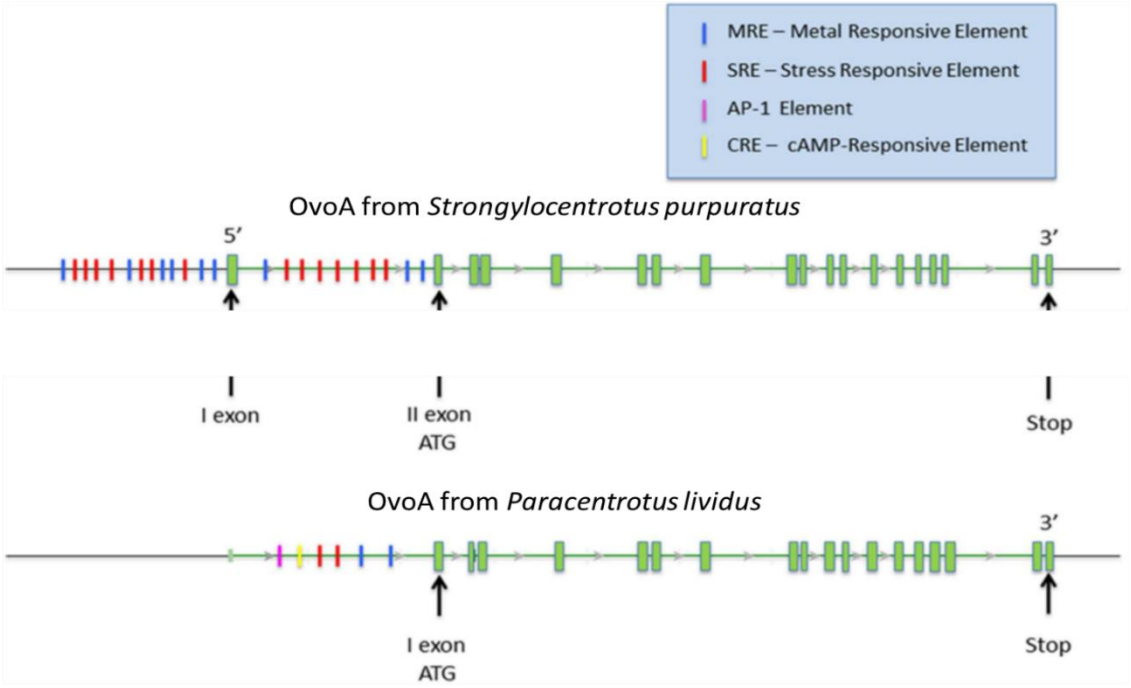

Figure 6. Gene structure of *ovoA* from sea urchin (modified from Castellano *et al.*, 2016).

The analysis of the protein primary structure revealed that the sea urchin OvoA is characterized by three characteristic domains, that are, starting from the N-terminal region: the domain of the DinB superfamily, which includes the iron binding motif HX3HXE (Braunshausen and Seebeck 2011); the formyl-glycyl (FG)E-sulphatase domain, which includes all the residues proposed to be involved in the recognition/binding of the substrates (cysteine and histidine) (Castellano et al., 2016); the C-terminal portion characterized by the presence of S-adenosyl methyl (SAM)-transferase domain (figure 7). The latter domain is absent in EgtB and represents a useful criterion for distinguishing between OvoA and EgtB.

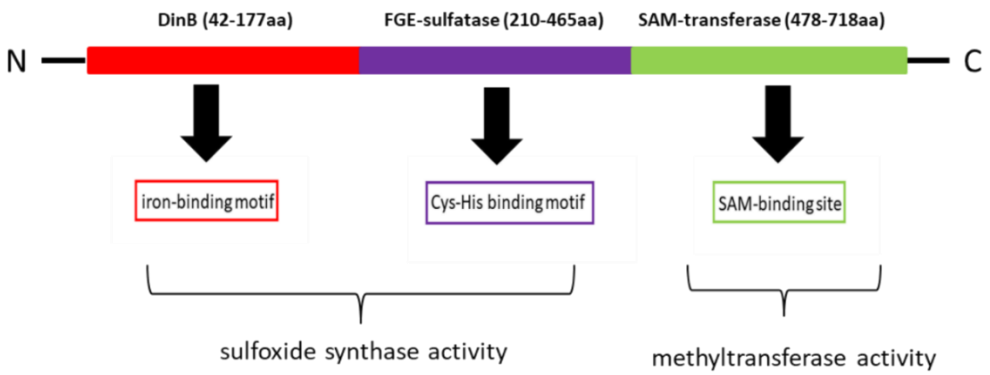

Figure 7. Protein characterization of OvoA from *P. lividus*

The evolutionary history of OvoA has also been studied in deep in metazoans (Gerdol et al., 2019). In detail, OvoA was found with a high degree of conservation in basal metazoans, like Porifera, Placozoa, Cnidaria (Anthozoa), in protostomes (Nemertea, Annelida, Mollusca, Brachiopoda) and deuterostomes. Among protostomes, *ovoA* gene was lost in Nematoda and Arthropoda. Among deuterostomes, OvoA was found in Echinodermata *(P. lividus* and *S. purpuratus*), Hemichordata (*Saccoglossus kowalevskii*), Urochordata (*Ciona intestinalis*), Cephalochordata, and Chondrichthyes. However, OvoA orthologous could not be identified in bony vertebrates. Furthermore, two events of secondary acquisition through horizontal gene transfer were identified in Rotifera and in Hydrozoa, respectively (figure 8).

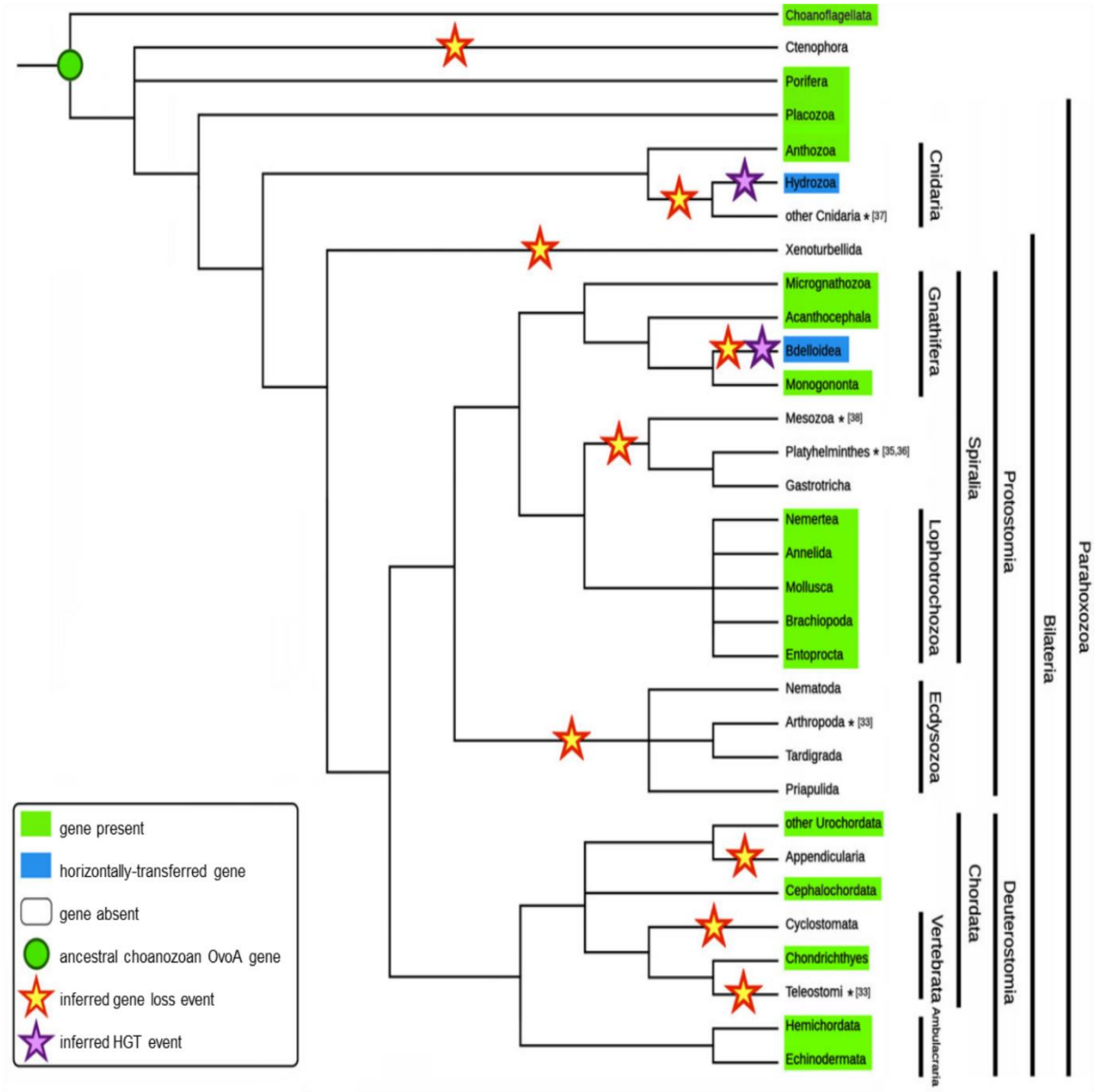

Figure 8. **Evolutionary history of OvoA in Metazoans.** The diagram is a representative of OvoA distribution in the currently accepted metazoan tree of life (Gerdol et al., 2019).

In addition, Milito and co-authors have shown that in diatoms OvoA homologous cluster into two main clades corresponding to centric and pennate diatoms (figure 9) (Milito et al., 2020), thus suggesting that OvoA protein diversified according to the phylogenesis of the two morphological groups (Medlin 2016). The authors highlighted the high degree of homology between OvoA from diatoms and OvoA from cyanobacteria, assuming that the OvoA gene present in diatoms was acquired through an endosymbiotic event by cyanobacteria. This hypothesis would support the conservation of OvoA in green and red algae. It is known that OvoA has never been found in plants, suggesting a gene loss event in this kingdom, while OvoA is preserved in diatoms, brown algae and

oomycetes; the absence of OvoA in plants is very interesting, suggesting that, as in the animal kingdom, OvoA was probably lost due to huge gene loss events during evolution (Milito et al., 2020). The conservation of this evolutionary pathway is probably due to its role in maintaining cellular homeostasis, which allows survival in different environmental niches.

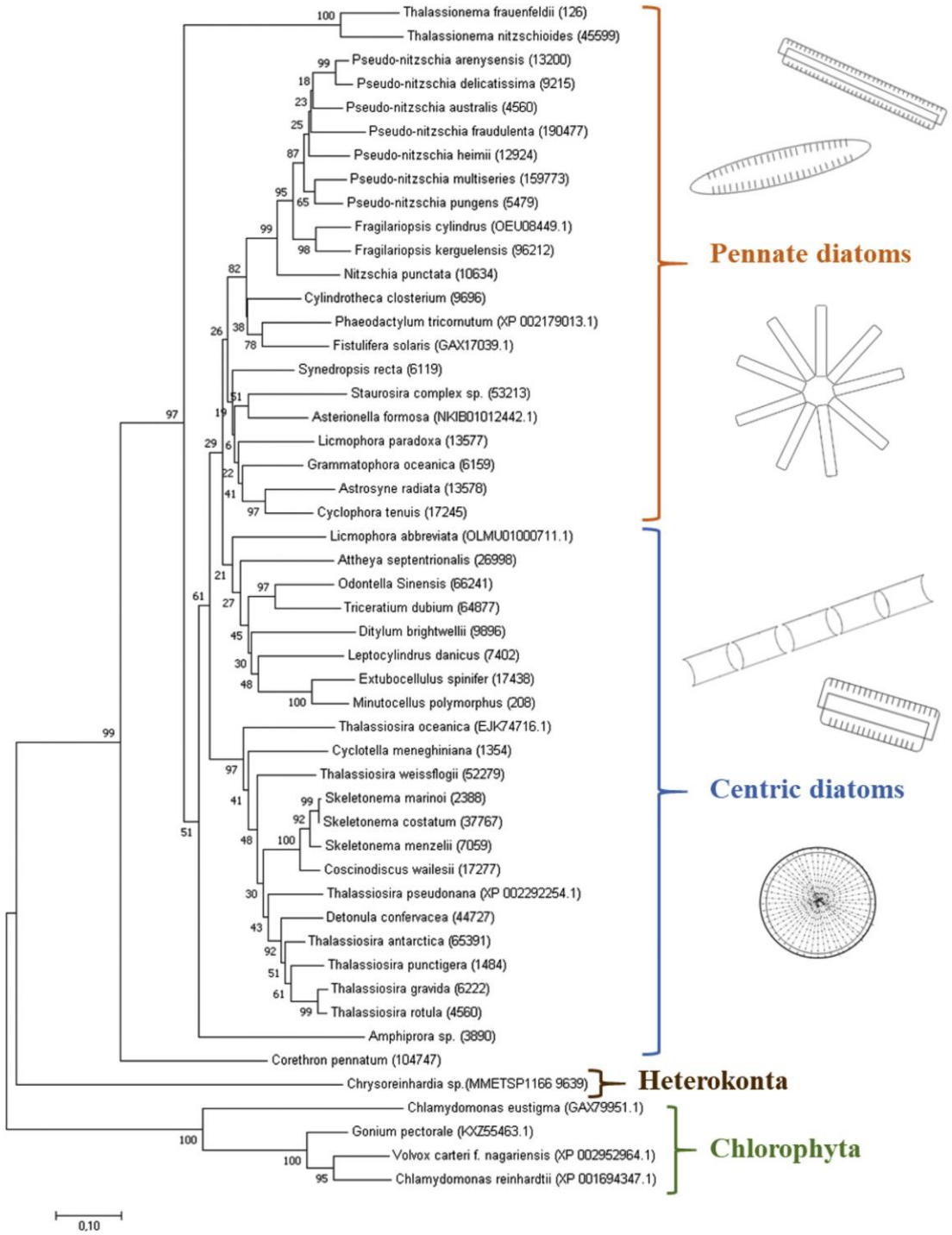

Figure 9. Evolutionary history of OvoA in Diatoms (Milito et al., 2020).

Catalytic activities of the OvoA and EgtB enzymes are considered evolutionarily distant, due to their different regioselectivity (insertion of the sulfur atom in the C5 or C2 position of the imidazole ring), the low sequence similarity and the presence in OvoA of the further methyltransferase domain.

Despite structural similarity (figure 1D and 1F), ovo and erg have very different physiochemical properties. Erg is less acidic and less reducing than ovo A. Ovo is much more reactive towards peroxides than erg. Ovo forms stable disulfides, whereas ergothioneine disulfides are hydrolyzed under physiological conditions. In addition, EgtB recognizes TMH as starting substrate while OvoA has histidine and cysteine as favourite substrates. These differences indicate that the two compounds may participate in different cellular processes, and therefore, may occur in different ecological niches.

However, a convergent evolutionary event has been suggested between the two enzymatic activities (Liao and Seebeck, 2017). In this work the authors demonstrated that OvoA-like from *Microcystis aeruginosa*, a species of freshwater cyanobacteria, was able to catalyse the synthesis of erg. In detail, due to some genetic mutations, the OvoA-like enzyme acquired EgtB-like activity ($EgtB_{ovo}$) capable of producing erg. In this enzyme tyrosine (Y) and alanine (A) in positions 451 and 452 respectively were replaced by asparagine (N) and tryptophan (W). To verify that these residues were necessary for the recognition of the substrate and the specificity of the enzyme, the authors performed a mutagenesis on OvoA from *Erwinia tasmaniensis* in position 451 and 452, by replacing YA with NW. The resulted mutated enzyme OvoA of *E. tasmaniensis* preferred TMH as a substrate rather than histidine. This discovery has shown that ancient ovo producing cyanobacteria have adapted to make erg. This adaption may have been induced by changes in the environment that rendered erg a more useful protectant than ovo. Probably, the ancestor of the sulfoxide synthase enzyme was an enzyme with a broader promiscuity of substrates, which underwent to gene duplication and diversification, into EgtB and OvoA.

1.1.1 Discovery and biological role of 5-thioistidines in nature

Ovothiol A was first isolated in millimolar concentrations from sea urchin eggs *P. lividus* (Palumbo et al., 1982; 1984) (figure 10). Following this discovery, ovo A was then identified in the eggs or ovaries of other Echinodermata, such as sea cucumber and several species of starfish (Palumbo et al., 1984; Turner et al., 1987), in the eggs and urine of the European squid *Loligo vulgaris* and in the urine of *Octopus Vulgaris* (Rossi et al., 1985). Later, at the end of the nineties, ovo A was found in the coelomatic fluid of sexually mature male marine worms and was suggested to act as a pheromone, triggering the release of eggs in females (Rohl et al., 1999; Breithaupt and Hardege, 2012). Moreover, recent studies have highlighted the presence of ovo A in mussels, *Mytilus galloprovincialis*, where it is involved in oogenesis and in the stress response to environmental contaminants (Diaz de Cerio et al., 2020) and in fish eye lenses where it is involved in the defence from environmental stressors (Yanshole et al., 2019). Finally, the non-methylated histidine derivative of ovo A, 5-thiohistidine, has been reported in the eggs of *O. vulgaris.* The other forms of ovo, B and C, have been found in other marine organisms. Ovo B was found in the ovaries of clams (Turner et al., 1987) and in the diatom *Skeletonema marinoi* (Milito et al., 2020) (figure 10), ovo C in the eggs of the sea urchins *Sphaerechinus granularis* (Palumbo et al., 1984) and *S. purpuratus* (Turner et al., 1986) (figure 10).

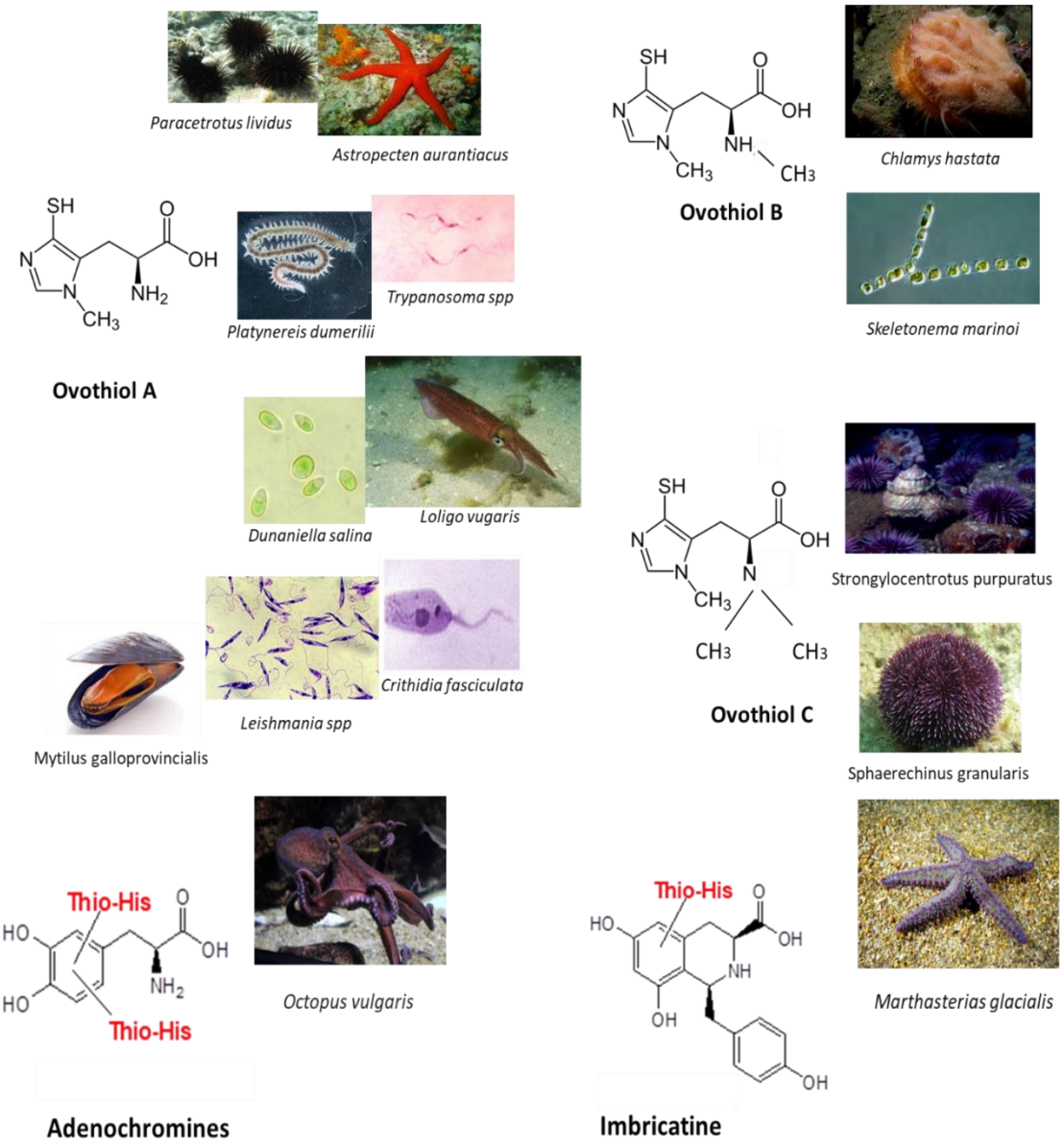

Figure 10. Occurrence of ovothiols in nature (modified from table 1, Palumbo et al., 2018).

The biological role of ovo A has been studied in sea urchins in particular in the fertilisation and developmental processes. Ovothiol has been proposed to protect sea urchin eggs from the deleterious effects of H_2O_2, which is produced during the high oxidative burst at fertilisation (Shapiro et al., 1990) (figure 11).

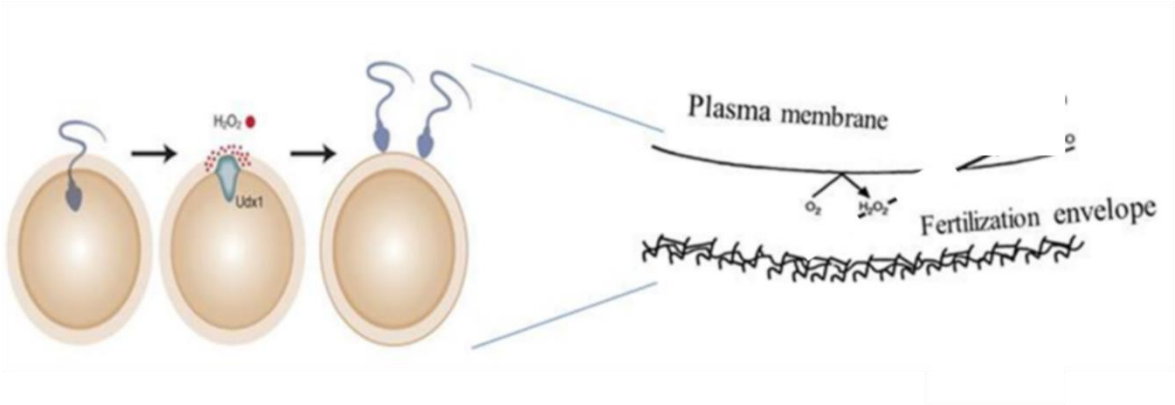

Figure 11. Proposed model for the biological role of ovo during sea urchin fertilisation (modified from Palumbo et al., 2018).

The expression of *ovoA* from *P. lividus* (*Pl*OvoA) was followed during sea urchin development by quantitative PCR (Castellano et al., 2016). Immediately after fertilisation, the expression of *Pl*OvoA reduced compared to the unfertilised eggs until early and swimming blastula stages. Subsequently, the expression increased significantly in the pluteus stage.

In addition, it has been suggested that during development, ovothiol protects sea urchin embryos from the oxidative stress produced by environmental pollutants (Castellano et al., 2016). In fact, the treatment of fertilized eggs of *P. lividus* with cadmium at concentrations that mimic those present in polluted seawater induced an increase in the gene expression of *Pl*OvoA and consequently the production of higher levels of ovo.

Moreover, other environmental factors such as toxic algal blooms have also been shown to regulate the expression of *Pl*OvoA. In fact, blastula stages of offspring of sea urchins cyclically exposed to the natural toxic bloom of the dinoflagellate *Ostreopsis cfr. ovata* showed a significant increase in *Pl*OvoA mRNA compared to control female embryos collected at the control site with negligible concentrations of *O. cf. ovata* (Castellano et al., 2016).

Based on these results, a mechanism for ovo biosynthesis was suggested. This mechanism implies that when sea urchins release gametes into sea water, after fertilisation, the embryos can be exposed to stressful agents present along the water column, such as natural toxins or heavy metals. These stressful agents can induce the production of ROS and the activation of redox sensitive transcription factors to bind MRE and /or SRE, promote the transcription of OvoA and finally the synthesis of ovo (figure 12). The presence of OvoA in most marine invertebrates with external fertilisation supports

the hypothesis that ovo could protect the eggs and embryos of these organisms from environmental damage when released into seawater (Castellano et al., 2016).

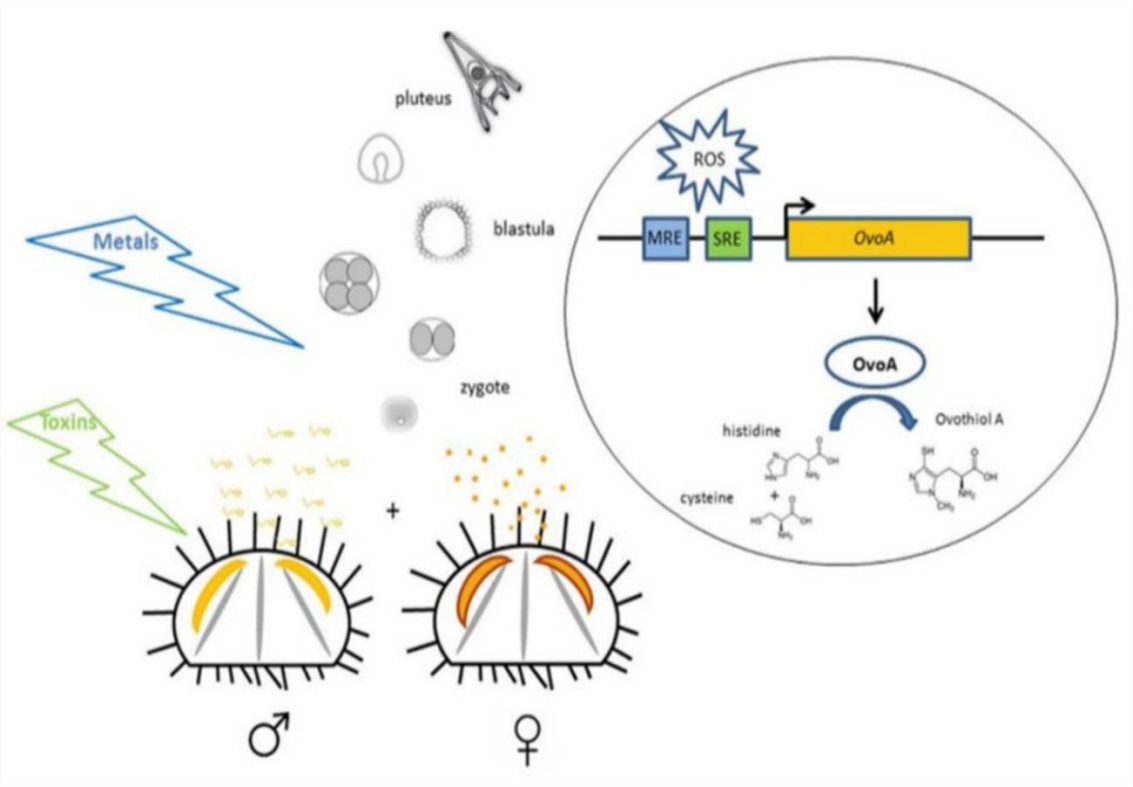

Figure 12. Proposed model for the biological role of ovothiol in sea urchins (Castellano et al., 2016).

At the same time, the presence of OvoA also in marine organisms with internal fertilisation, such as cartilaginous fish, indicated a wider role of OvoA, probably related to the processes of embryonic development (Castellano et al., 2016). In addition to marine invertebrates, ovo A is also widespread in the microbial world. In particular, it is present in several species of protozoa of the Trypanosomatidae family, such as the pathogenic parasites Leishmania spp., *T. cruzi* and *T. brucei*, where it should have played a key role in protecting them from oxidative stress during infection (Spies and Steenkamp, 1994 ; Ariyanayagam and Fairlamb, 2001), providing parasites with an efficient self-defence mechanism for decomposing the S-nitroso groups of nitrosoglutathione and dinitrotrypanothione, formed by the high levels of nitric oxide released by macrophages (Murray and Nathan, 1999; Vogt and Steenkamp, 2003; Krauth-Siegel and Leroux, 2012). Furthermore, several photosynthetic microorganisms are capable of producing ovo A, such as the green microalga *Dunaliella salina*, in which it has been reported to be a redox regulator in chloroplasts (Selmar-

Reimer et al., 1991) and the microalga *Euglena gracilis*, where the presence of different OvoA transcripts in light and dark conditions has allowed to hypothesise a light-dependent regulation (O'Neill et al., 2015).

The thiohistidine unit is also present as a component in larger structures of some marine species, such as adenochrome and imbricatine (figures 10). Adenochrome, the red iron-binding pigment present in the branchial hearts of *O. vulgaris*, is a mixture of peptides made up of glycine and three isomeric adenochromines, derived from the conjugation of 5-thiohistidine with 3,4-dihydroxyphenylalanine (dopa) quinone enzymatically generated by L-DOPA (Ito et al., 1979a, b). The physiological function of adenochrome is already obscure. However, the presence of adenochrome in branchial hearts as an iron chelating agent, together with the peptide's ability to bind other metal ions (copper, lead, cadmium), suggested its possible involvement in the detoxification mechanism of metal ions.

Ovo is also present in the structure of the imbricatine (figures 10), a cytotoxic alkaloid of the starfish *Dermasterias imbricate*, formed by the thiohistidine linked, through a thioether bond, to a nucleus of isochinoline (Pathirana and Andersen, 1986; Burgoyne et al., 1991). Imbricatine has the ability to elicit escape responses in the prey of the starfish, causing the detachment and response of swimming in the sea anemone *Stomphia coccinea* at very low concentrations. When analysed separately, the two subunits of imbricatine, i.e. benzyltetrahydroisoquinoline and thioistidine, have been shown to be almost inactive (Elliott et al., 1989).

Until now, the best source of ovo is represented by sea urchin eggs. Initially, ovo A was isolated as disulfide from *P. lividus* eggs by fractionation of the aqueous extract of the sea urchin eggs by sequential ion exchange and gel filtration chromatography (Palumbo et al., 1982). Recently, the procedure has been modified (Russo et al., 2014). In fact, the sea urchin egg homogenate was freed from proteins by treatment with acid ethanol overnight and from the lipid component by extraction of ethyl ether. The aqueous phase was then purified by sequential ion exchange chromatography to provide a pure ovo A disulfide. From 10 g of sea urchin eggs 2.5 mg of ovo A can be obtained (figures 13).

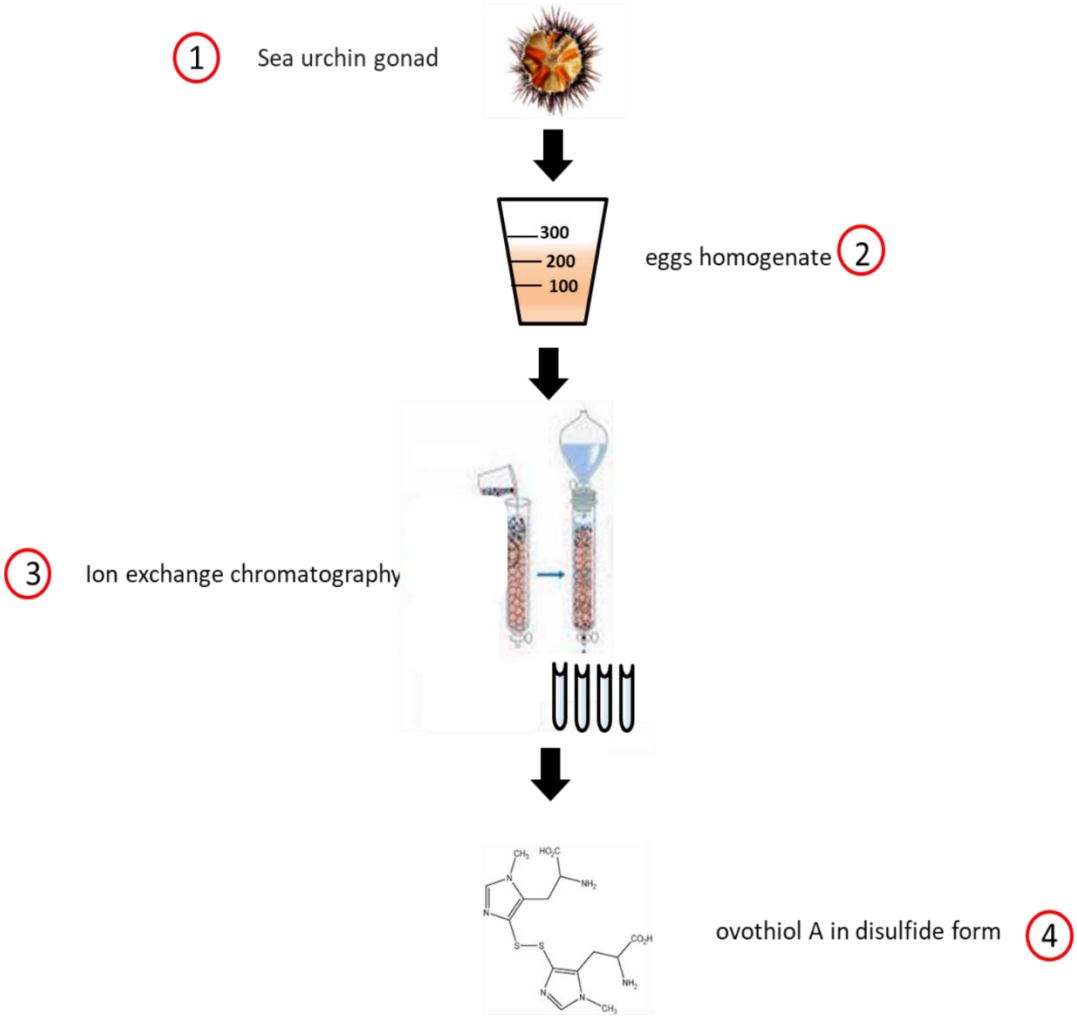

Figure 13. Ovothiol A extraction.

The initial studies on the synthesis of ovothiol were motivated by the need to confirm the structural assignment of the ovo compounds A and C isolated from different sources (Holler et al., 1989). Currently, the chemical methods for the synthesis of ovo are really cumbersome, the experimental protocols used so far have proved to be non-reproducible and expensive (reviewed in Palumbo et al., 2018). Therefore, ovothiol synthesis still remains a topic of strong scientific debate and a field still to be explored to find more efficient and less expensive ways to produce such molecules.

Instead, the synthesis of 5-thioistidine, the precursor of ovo, not methylated on the imidazole ring has been recently developed in a feasible way (Daunay et al., 2016).

1.1.2 Pharmacological potential of 5-thiohistidines in human diseases

Sulfur plays a key role in biology as component of numerous natural compounds from plants, bacteria, fungi or animals. Thanks to their biochemical properties, the sulfur-containing compounds have promising anti-oxidative, anti-inflammatory and anti-tumor activities (Jacob et al., 2006).

Among thiols, ovos have interesting redox activities which make these compounds attractive from a pharmacological point of view.

They can catalyze the H_2O_2 reduction similar to peroxidase, unlike erg, which reduces various oxidants but apparently not H_2O_2. In humans, the catalytic removal of peroxides to give water and alcohols is afforded by the enzymes glutathione peroxidase (GPx) and peroxiredoxin (Prx) (Rhee et al., 2005). GPx mimetics represent highly interesting tools in artificial enzyme research for potential pharmacological applications (Wang et al., 2017). However, most GPx mimics are not suitable for therapeutic use as they contain selenium or tellurium. In this context, ovos and its derivatives of chemical synthesis have been proposed as a less toxic alternative (Bailly et al., 2000; Zoete et al., 2000). In particular, the synthetic derivative of ovo 1-methyl-2- [3- trifluoromethylphenyl] -4-mercapto-imidazole (MFP-4MI) (figure 14) has proven to be a promising neuroprotective agent in the mouse brain (Vamecq et al., 2003).

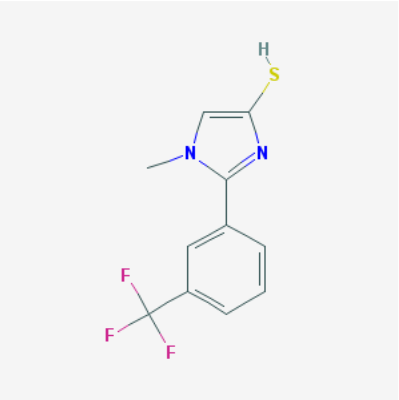

Figure 14. 1-methyl-2-[3-trifluoromethylphenyl]-4-mercapto-imidazole (MFP-4MI) 2D structure (pubchem.ncbi.nlm.nih.gov; PubChem CID: 10308114).

More recent studies have shown that ovo, purified from *P. lividus* sea urchin eggs, affects the proliferative activity of a human hepatocellular carcinoma cell line (HepG2) (Russo et al., 2014). In particular, treatment with ovo A decreases the proliferation of cancer cells in a dose dependent

manner. This process is concomitant with the activation of an autophagic process, revealed by phase contrast and fluorescence microscopy (figure 15), together with the expression of specific autophagic molecular markers, LC3 II and Beclin-1. The ability of ovo A to induce autophagy in cancer cell lines reveals a correlation between the biological/pharmacological activity of ovos and the metabolism of cancer (Lozy and Karantza, 2012).

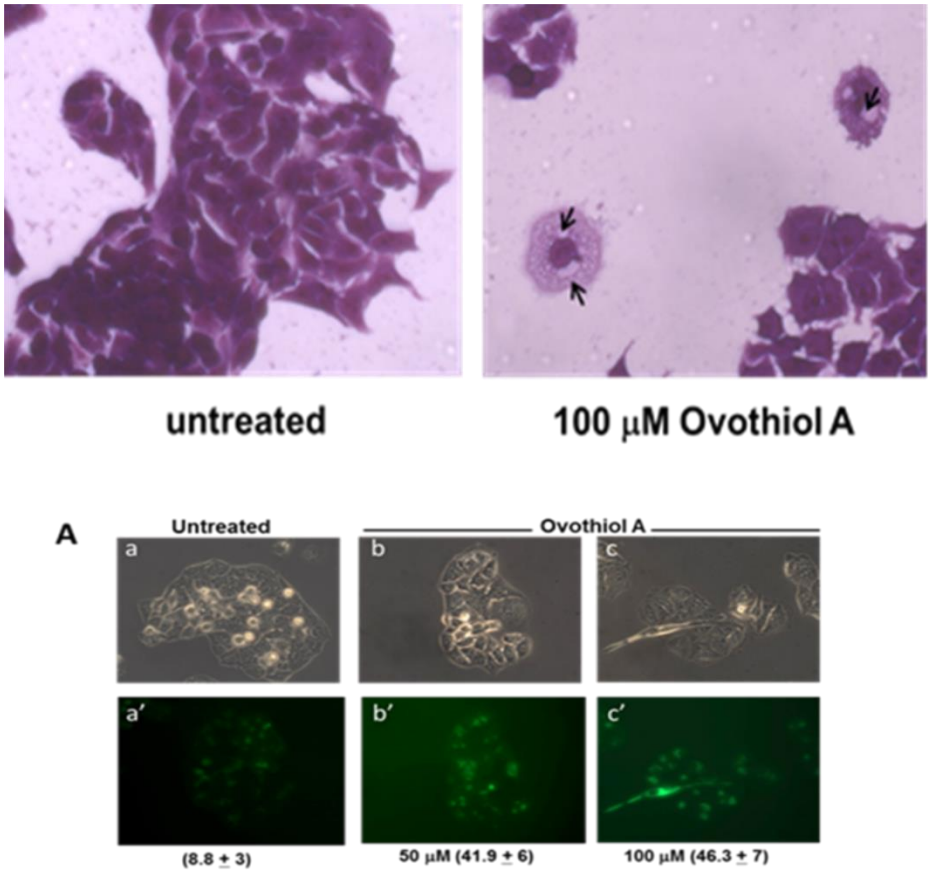

Figure 15. Ovothiol A induces autophagy-dependent cell death in Hep-G2 cells (Russo et al; 2014).

In addition, ovo A has also been shown to have anti-inflammatory activity in human endothelial cells (HUVEC) derived from the umbilical cord of women suffering from gestational diabetes (figure 16) (Castellano et al., 2018). In particular, the authors showed that in cells stimulated by the tumor necrosis factor α (TNF-α), ovo A induced the downregulation of the expression of specific adhesion molecules (V-CAM and I-CAM) and the decrease in the monocyte-HUVEC interaction (figure 16), which is the biological process responsible for the formation of the atherosclerotic plaques. This event has been associated with the reduction of ROS and RNS and the increase in the bioavailability of nitric oxide. These results indicate the potential anti-atherogenic properties of the natural

antioxidant ovo A and support its therapeutic potential in pathologies related to cardiovascular diseases associated with oxidative/ inflammatory stress and endothelial dysfunction.

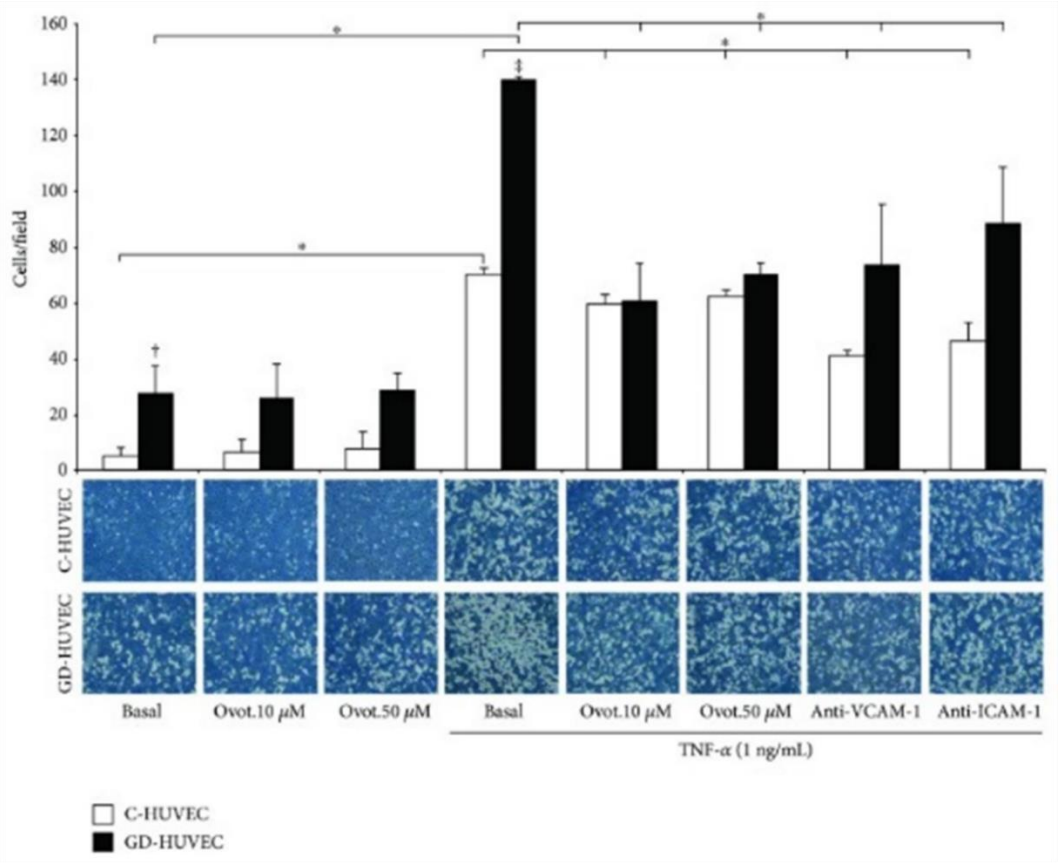

Figure 16. Effect of ovothiol A on TNF-α-induced monocyte interaction in endothelial cells (Castellano et al.; 2018)

Therefore, ovo A may be considered a promising anti-inflammatory agent to be used as a food supplement and /or as a preventive drug for the treatment of chronic diseases related to inflammation, like atherosclerotic processes and cardiovascular diseases. Despite the peculiar chemical properties of ovos and the great pharmacological potential of these molecules, further studies will be needed to evaluate their activities on other biological systems.

1.2. Model systems

1.2.1. Liver fibrosis

Liver fibrosis is an inflammatory process, involving the excessive accumulation of connective tissue in the liver, thus generating scars that represent the response to chronic and repeated damage of liver cells. Generally, fibrosis progression implies the disruption of the liver architecture and finally its functionality, while regeneration of hepatocytes attempts to replace and repair damaged tissues (Bedossa and Paradis 2003). When these changes are widespread, cirrhosis is diagnosed (figure 17) (Pearson et al 2007; Punche et al 2013).

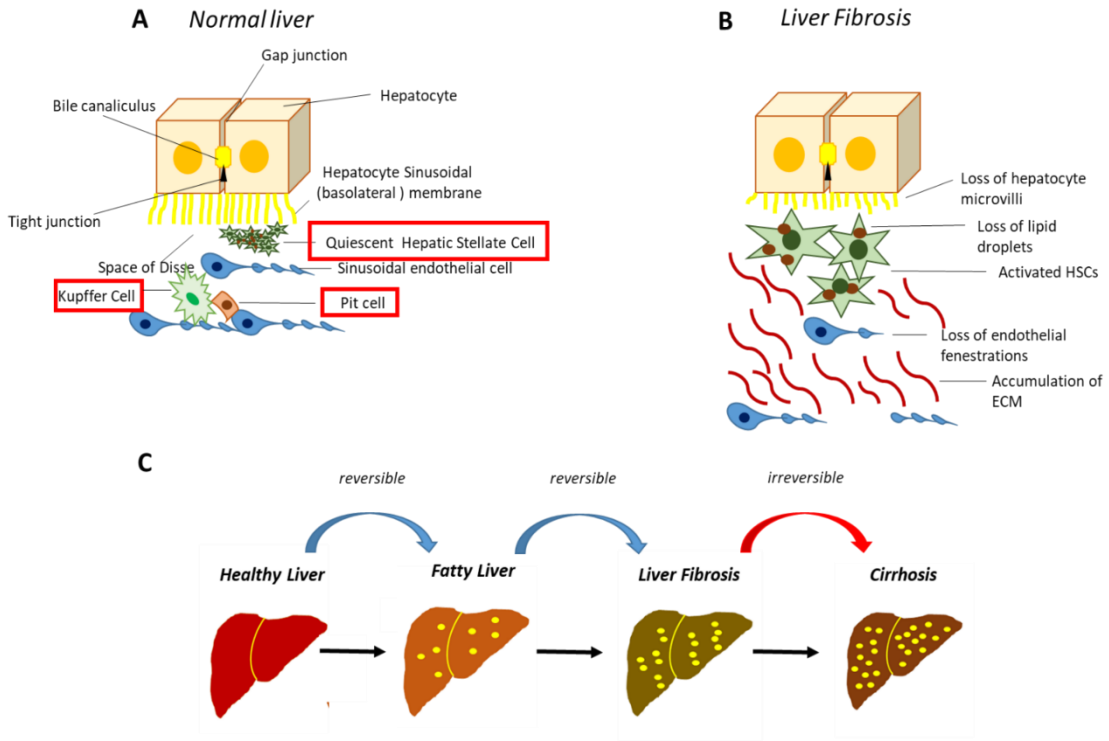

Figure 17. Normal and fibrotic liver architecture. **(A)** In the healthy liver the hepatocytes are closely joined by gap junctions. The liver sinusoid, a large fenestrated capillary, is mainly constituted by sinusoidal endothelial cells (SECs), Kupffer cells, specialized hepatic macrophages, and the Pit cells, the natural killer lymphocytes of the liver. The space between the hepatocytes and the sinusoid, called "the space of Disse", hosts the hepatic stellate cells (HSCs); **(B)** following HSCs activation, there is a massive accumulation of extracellular matrix (ECM) as well as the loss of microvilli in the hepatocytes and the loss of fenestrae in SECs; **(C)** stages of hepatic fibrosis. (Milito et al.; 2019)

Various types of chronic liver damage can cause fibrosis: chronic inflammatory lesions, chronic viral hepatitis (hepatitis B or C), bacterial (brucellosis), fungal and parasitic infections (echinococcosis), congenital errors of metabolism, lipid accumulation, iron overload, intense and prolonged use of

some drugs (methotrexate, methyldopa and chlorpromazine) and exposure to toxic agents (alcohol) (figure 18).

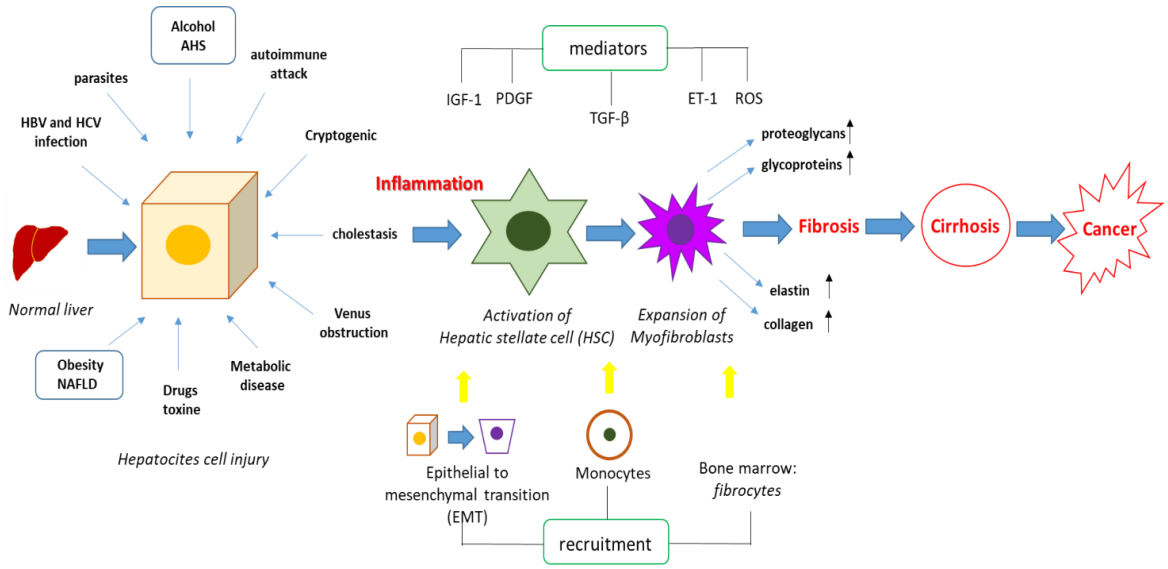

Figure 18. Pathogenesis of liver fibrosis. Liver fibrosis can be induced by different insults, which can trigger cell death processes in the hepatocytes, leading to the release of profibrogenic mediators such as the TGF-β, the platelet-derived growth factor (PDGF), insulin-like growth factor-1 (IGF-1), endothelin 1 (ET-1), and ROS. These can activate HSCs, promoting their differentiation into myofibroblasts, as well as they can stimulate the epithelial to mesenchymal transition and the recruitment of circulating monocytes and fibrocytes from bone marrow. The combination of these events leads to an increased expression and secretion of elastin, collagen, proteoglycans and glycoproteins, causing the accumulation of the ECM and therefore the fibrotic process. This represents a prerequisite for cirrhosis and cancer. (Milito et al.; 2019)

There is also a congenital form of liver fibrosis, an autosomal recessive disorder that primarily affects the hepatobiliary and renal system (Jiang et al 2019).

In the initial stage, liver fibrosis can regress if the cause of lesions is removed, conversely when the lesions become chronic or repeated, the fibrosis becomes permanent and it can also lead to death (Povero et al., 2010; Bataller and Brenner 2015).

The pathophysiology underlying liver fibrosis consists in the activation of perivascular hepatic stellate cells (HSC) (Ito cells, which accumulate lipids) leading to the start of the fibrotic process (Pearson et al 2007; Punche et al 2013). At the same time, the increase in HSC proliferation causes the activation of myofibroblasts, connective tissue cells with contractile capacity. These cells produce excessive amounts of abnormal extracellular matrix (ECM) (made up of collagen, glycoproteins and glycans) and extracellular matrix proteins. As a result, ROS and inflammatory mediators are released. Indeed, high intracellular concentrations of ROS are known to induce redox

imbalance in the liver and are involved in the apoptotic and necrotic process of hepatocytes (Arazu et al, 2016).

Oxidative stress in the liver plays a key role in activating the transformation of pleiotropic cytokines. At the molecular level, the increased expression of α-smooth muscle actin (α-SMA) and procollagen-I are both associated with the ability of the activated HSCs to depose collagens and other matrix proteins in the extracellular space (Novo et al., 2015). Furthermore, activated HSCs present an altered regulation of matrix remodelling enzymes, such as metalloproteinases (MMPs) and their tissue inhibitors (TIMPs), modulating matrix degradation and production, respectively (Hemmann et al., 2015). Another key player in fibrosis development is the pleiotropic cytokine transforming growth factor β1 (TGF-β1), which is secreted in the latent form and, when active, induces the activation of HSCs and modulates the expression and secretion of a number of proteases and their regulators, including MMPs and TIMPs (Li et al., 2015). TGF-β1 can also auto-induce its own production thus subsequently amplifying its actions (Weng et al 2009; D'Argenio et al 2013).

In addition, oxidative stress is a key player in triggering liver damage; the finely regulated levels of glutathione (GSH) contribute to maintain a healthy liver, preserving its functionality. GSH is synthesized within the cell and partially released into the extracellular space along a concentration gradient. In the extracellular space, GSH is hydrolysed by γ-glutamyl transpeptidase (GGT), a dimeric enzyme located on the surface membrane. GGT is highly expressed in the liver, where it is responsible for GSH metabolism and detoxification mechanisms, together with glutathione S-transferase (GST), a family of phase II metabolic isozymes, known for their ability to catalyse the conjugation of the reduced form of GSH - through the sulfhydryl group - to the electrophilic centre of the xenobiotic substrates, making them more soluble in water and more sensitive to detoxification (Aitken et al.,2006; Castellano and Merlino 2012; 2013).

Several studies demonstrated the efficacy of different natural products and phytochemicals present in foods and used as food extracts (such as sulforaphane, S-allylcysteine, curcumin, proanthocyanidins, garlic extract, coffee, and grape skin or seeds) to prevent or reduce liver fibrosis progression by different mechanisms in several animal models (D'argenio et al., 2010 and 2013; Milito et al, 2019). In this context, ovothiols from marine invertebrate species, represent promising

bioactive compounds to reverse the fibrotic phenotype thanks to their pharmacological potential (Russo et al., 2014; Castellano et al., 2018).

1.2.2. Human skin disorders

Skin disorders vary greatly in symptoms and severity. They can be temporary or permanent, and may be painless or painful. Some can be caused by external injuries, while others may be dependent on genetic factors. Some skin lesions are minor, and others can be life-threatening.

The skin is the most external barrier of the body and is therefore exposed to a high number of pathogens such as *Staphylococcus* and *Streptococcus* (Scudiero et al., 2020). It also represents our defence against exposure to sunlight (D'Orazio et al., 2013); as a result, it provides several defence mechanisms. The skin is made up of three layers - namely the epidermis, dermis and hypodermis - starting from the outermost layer (Figure 19). The barrier that prevents the entry of microbial agents and the defence against ultraviolet (UV) rays is provided by the corneum layer (Figure 19), which represents the outermost layer of the skin, belonging to the epidermis (Figure 19).

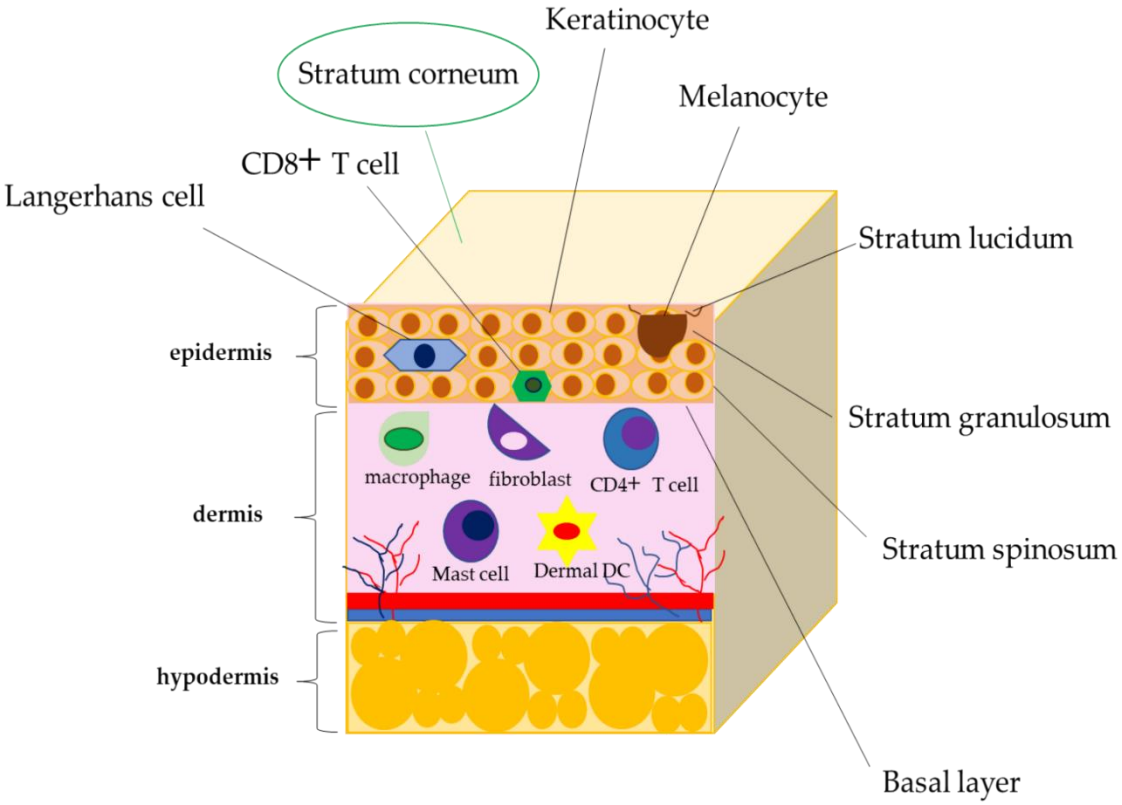

Figure 19. Skin organization. (Scudiero et al.; 2020)

Furthermore, within the epidermis, various immune sentinels, like macrophages, are activated only in case of skin damage. The activation of these sentinels causes downstream the activation of numerous pro-inflammatory cytokines: *interleukin 6* (IL-6), *interleukin 8* (IL-8) and *tumor necrosis factor* (TNF-α), which are known to play a key role in mediating cell damage and the pathogenesis of chronic inflammatory diseases (Damjanov and Vojinovic 2009; Ding et al, 2009; Kovarikova et al, 2004).

Furthermore, TNF-α mediates the activation of the transcription factor NF-κB, which in turn induces the activation of numerous pro-inflammatory genes. In addition, exposure to pro-inflammatory agents or UV rays causes the activation of the mitogen-activate protein kinase (MAPK) (Carlsen et al., 2004; Muthusamy et al., 2009; Leng et al., 2009). MAPKs play a key role in the regulation of skin homeostasis (Leng et al., 2009; Neves et al., 2009; Ivanova et al., 2009). In addition, excessive exposure to UV radiation generates skin damage that may be due to hyper production of ROS (Haywood et al., 2003). ROS accumulation can modulate the expression of redox sensitive genes and regulate erythroid-related factor 2 (Nrf2), an oxidative stress marker (Hseu et al.,2012). Under non-stimulating conditions, Nrf2 is negatively regulated by Kelch-like ECH-associated protein 1 (Keap-1) (Kaspar et al., 2009); conversely, on stimulation, Nrf2 moves to the nucleus, where it forms a heterodimer complex with the small musculoaponeurotic fibrosarcoma protein (sMaf). This binds to the antioxidant response element (ARE), triggering the transcription of genes coding for phase II detoxification enzymes (Kaspar et al., 2009; Kim et al., 2010) and inhibiting the transcription of pro-inflammatory genes including cyclooxygenase 2 (COX-2) (Ahmed et al., 2016).

Previous studies have shown that erg, produced mainly in fungi and cyanobacteria (Krauth-Siegel et al., 2012; Braunshausen and Seebeck 2011), protects human keratinocytes from damage induced by UVA rays (figure 20) (Hseu et al., 2015). In fact, the pretreatment of human keratinocytes with erg blocks the activation of ROS and the fragmentation of DNA and, at the same time, it re-establishes the expression levels of the key actors involved in autophagy and apoptosis (Caspase 3/9 and Bcl-2 /Bax, respectively) (figures 20).

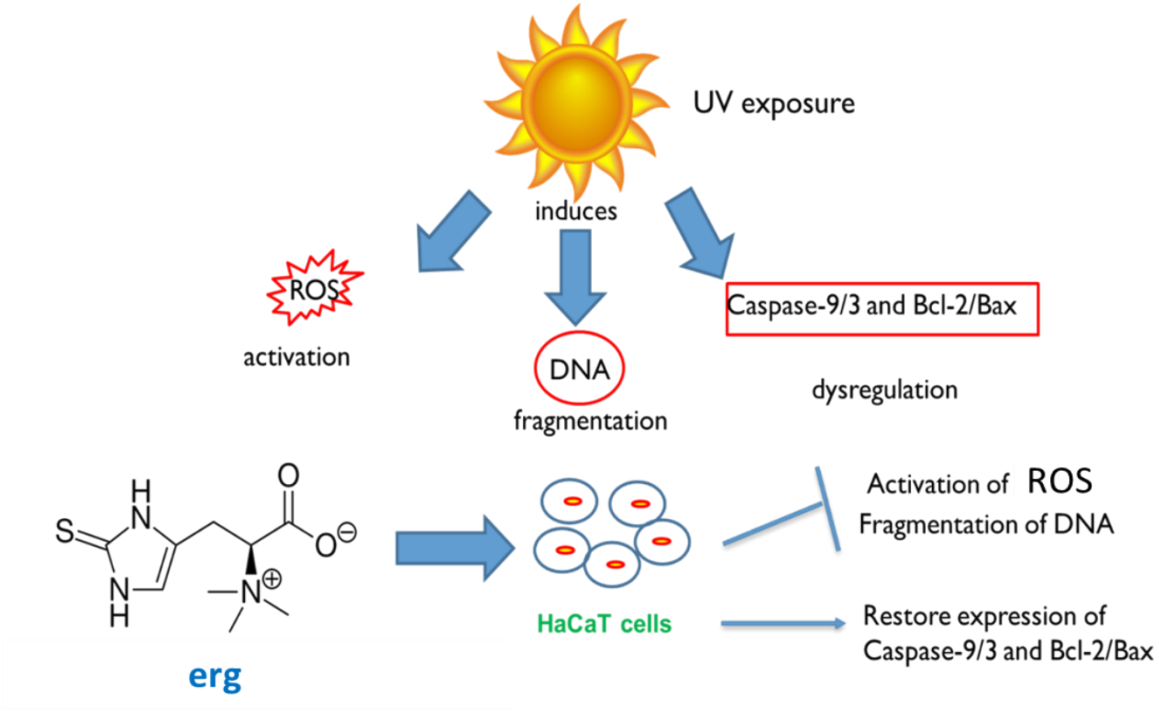

Figure 20. Photoprotective role of ergothioneine.

In addition, recently, ovos have been found in the sea anemone under stress induced by UV radiation (Tarrant et al., 2018)

The onset of skin inflammatory condition can represent a stage where you can test the anti-oxidative and anti-inflammatory activity of 5-thiohistidines, as natural protective molecules against skin disorders.

CHAPTER 2

Interplay between Gamma-glutamyl transpeptidase and 5-thiohistidines

2.1. Aims of the study

Recently, Russo and co-authors showed that the treatment of human hepatocarcinoma cells (HepG2) with ovo A caused a decrease in cell proliferation through an autophagy mechanism (Russo et al., 2014). In this case, most of ovo administered to the cells remained in the medium, suggesting that this compound could interact with a surface membrane protein complex. Among the membrane-bound enzymes expressed in liver cells, the most representative is γ-Glutamyl transpeptidase (GGT), that became the main candidate of our investigations to study a direct interaction with 5-thiohistidines.

GGT is an enzyme belonging to the transferase class. A transferase, in biochemistry, is an enzyme that catalyses the transfer of a functional group from one molecule (named donor) to another (named acceptor). GGT has been isolated from various sources, ranging from bacteria to mammals. GGT is found expressed in high concentrations as a cell membrane protein in the liver, bile ducts and kidney. Mammalian GGTs are heterologously glycosylated and embedded in the plasma membrane by a N-terminal trans-membrane peptide, whereas bacterial homologous are generally soluble and localised in the periplasmic space by an N-terminal signal peptide or secreted in the extracellular environment (reviewed in Castellano et al., 2012 and 2013). All GGTs are encoded by a single gene and are translated as a unique polypeptide, which then undergoes an auto-proteolytic cleavage into a large and a small subunit. The molecular weights of the two chains are generally found to be within 38–72 kDa for the large subunit and from 20 to 66 kDa for the small subunit (Marchesini et al., 2005; Nakayama et al., 1984; Suzuki et al., 1986; Ogawa et al., 1991), respectively. Such a high variation in the molecular masses can be explained by the high glycosylation of the animal and plant enzymes (Martin and Slovin 2000; Lancaster and Shaw 1994).

In detail, GGT hydrolyses extracellular glutathione (GSH), catalysing the cleavage of the γ-glutamyl group from a donor compound and the transfer of this group to an acceptor compound by ping-pong mechanism (figure 21) (Castellano et al., 2012 and 2013). The enzymatic reactions catalysed by GGT are reported in figure 22. These enzymes catalyse the cleavage of the γ-glutamyl linkage of γ-glutamyl compounds, such as GSH, and the transfer of the γ-glutamyl moiety to other amino acids or short peptides. In vivo, the primary reaction catalysed by human GGT is the hydrolysis, in which water, rather than amino acids, acts as the acceptor molecule during the cleavage of the γ-glutamyl

bond (West et al.; 2011). In the first step of a ping-pong mechanism, the oxygen atom of the N-terminal Thr residue attacks the carbonyl of the γ-glutamyl-compound to form a γ-glutamyl-enzyme intermediate. This intermediate can then react with water to release glutamate in a hydrolysis reaction or with an amino acid or di-peptide to give a transpeptidation reaction forming new γ-glutamyl compounds.

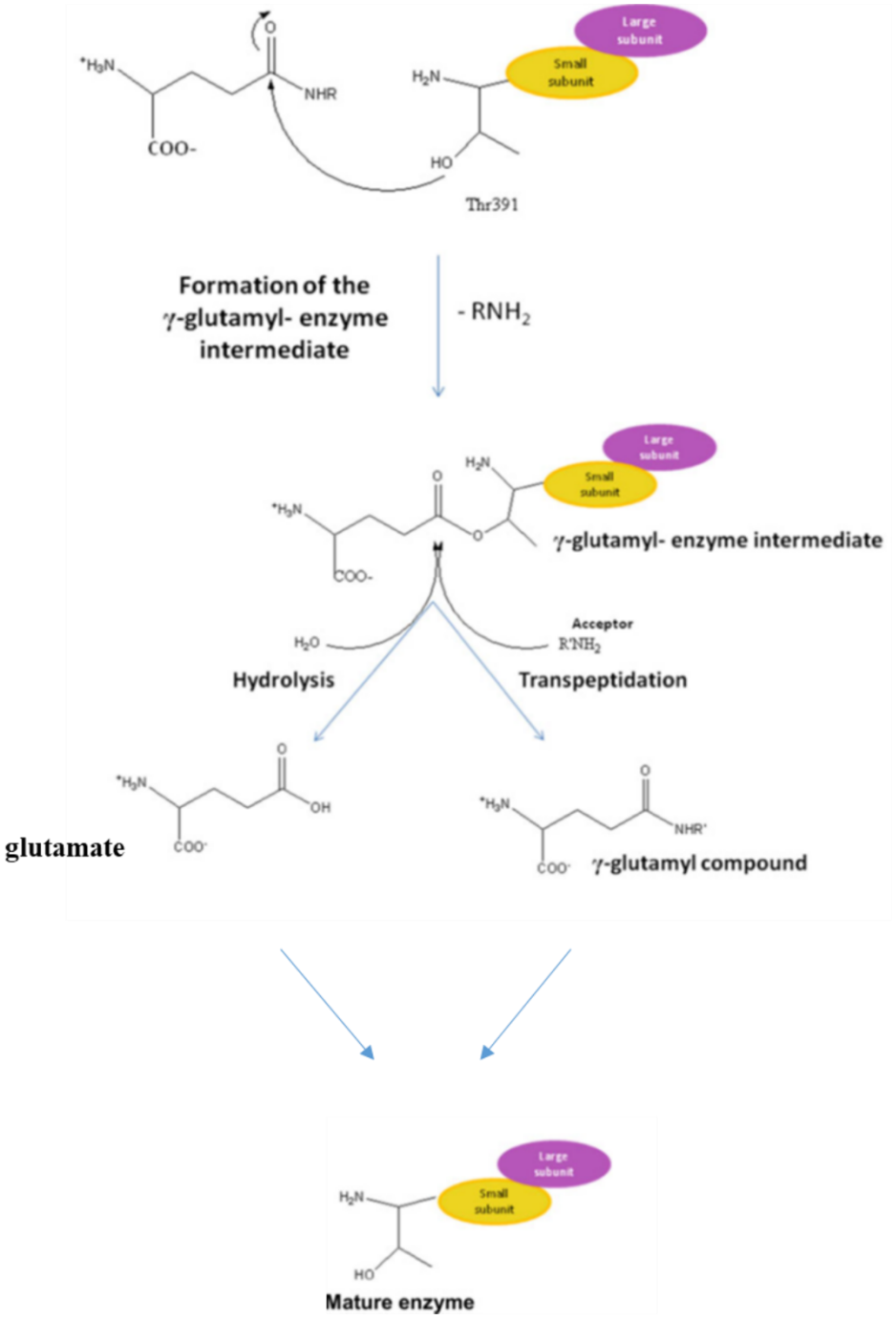

Figure 21. Proposed reaction mechanism of GGT (modified form Castellano and Merlino 2012)

GSH represents the physiological substrate of GGT, it acts as a γ-glutamyl donor in the initial hydrolysis reaction, then cysteinyl-glycine is released and split into cysteine and glycine by the dipeptidases of the cell surface. In the second reaction catalysed by GGT (transpeptidation), the γ-glutamyl group is transferred from the γ -glutamyl-GGT complex to water to release glutamate or to a second substrate (the acceptor), usually consisting of amino acids or dipeptides. Therefore, GGT is implicated in the recovery of amino acids through the cell membrane and in the metabolism of GSH (Hanigan 2014).

Several human cancers, including hepatocellular carcinoma and renal cell carcinoma, exhibit high levels of GGT activity. Increasing GGT levels in these tumours improves their resistance to chemotherapy due to the ability of GGT to recycle GSH (Hanigan et al., 1999a and b; Hanigan 2014, Pompella et al., 2006; Corti et al., 2010). In fact, elevated GSH levels in tumours have been shown to cause an increase in the resistance of chemotherapy and radiotherapy and also prevent the onset of apoptotic cascade in cancer cells (Benlloch et al., 2005 and 2006).

In recent years, researchers have focused their attention on identifying new GGT inhibitors to use as new compounds in therapies for the treatment of GGT-dependent diseases, such as certain types of cancer, renal ischemia /reperfusion-induced lesion and asthma (Corti et al., 2010; Yamamoto et al., 2011; Tuzova et al., 2014).

To date, the main GGT inhibitors tested in clinical or pre-clinical trials include glutamine analogues and other amino acid derivatives such as acivicin, 6-diazo-5-oxo-L-norleucine (DON) (figure 22), azaserin (Terzyan et al., 2017; Tate and Meister 1978) (figure 22), sulfur derivatives of L-glutamic acid (Lherbet and Keillor 2004) and γ-(monophenyl) analogues of phosphonoglutamate (Han et al., 2006 and 2007).

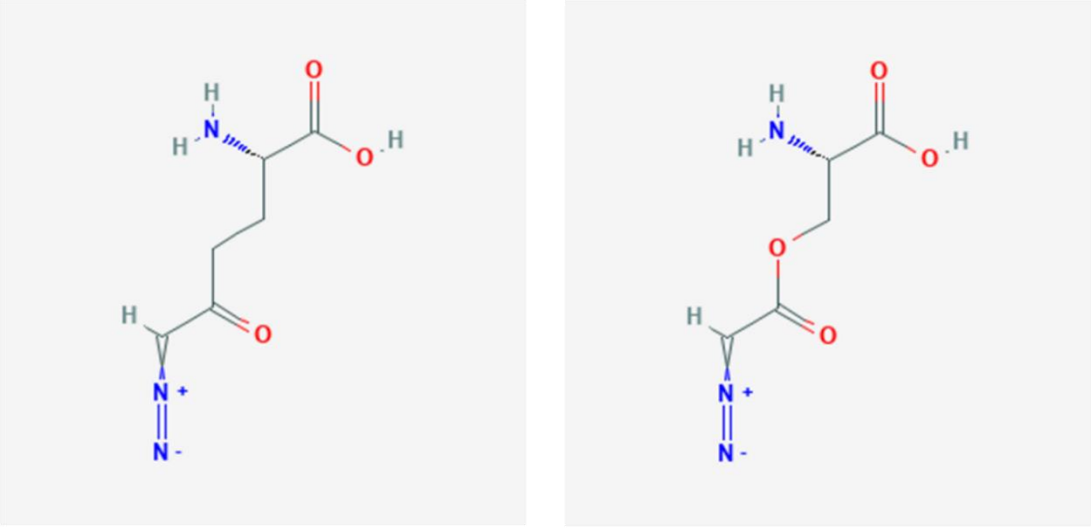

Figure 22. 6-diazo-5-oxo-L-norleucine (DON; CID: 9087) and Azaserin (CID: 460129) 2D structure (pubchem.ncbi.nlm.nih.gov; PubChem).

However, most of these compounds have cytotoxic activity (Ahluwalia et al., 1990; Lyons et al., 1990; Taylor et al., 1991) due to their interference with essential pathways such as the recycling of glutamate involved in neurotransmission. Among the monophenyl analogues of phosphonoglutamate, only the butanoic acid derivative GGsTop was found to be inactive on glutamine amidotransferase (Kamiyama et al., 2016) and effective for the treatment of oral mucositis (Shimamura et al., 2019). In contrast, serine borate was found to be too weak as inhibitor (Tate and Meister 1978; Terzyan et al., 2015). In addition, a class of non-competitive inhibitors, structurally different and less toxic than the glutamine analogues, has been developed. These compounds do not interact with the γ-glutamyl-binding site, but bind the acceptor site (King et al., 2009). However, further studies are needed to confirm their therapeutic potential.

Non-competitive inhibitors are able to bind both the active site of the enzyme and other sites different from the active site. They are therefore able to bind the free enzyme or the enzyme bond to its substrate (Enzyme-Substrate, ES). They are a particular type of mixed inhibitor. Their binding to the enzyme generates a conformational change of the enzyme itself, which can result in the inhibition of the bond between the enzyme and the substrate. In this case, as there is no competition between the inhibitor and the substrate, the strenght of inhibition depends exclusively on the concentration of the inhibitor itself. Conversely, when a competitive inhibitor binds to the active site it prevents substrate binding. The effect is to decrease the concentration of the free enzyme available to react. Finally, an

uncompetitive inhibitor is an inhibitor that follows an uncompetitive (reversible) inhibition mechanism, i.e. the inhibitor binds to a site other than that of the substrate, present only in the ES complex: it interacts only with ES and not with E. In practice, non-competitive inhibition (as well as mixed) occurs only in enzymes with two or more substrates (Westley, A. M., and Westley, J, 1996).

The first objective of my PhD project was to characterise the interactions of 5-thioistidines: 5-methyl-thioistidine (ovo) and des-methylated 5-thiohistidine with the membrane-bound human GGT (hGGT) in order to discover new therapeutic agents in the treatment of GGT-positive- diseases. For example, in liver pathologies such as fibrosis, cirrhosis, hepatitis and liver cancer, the dosage of GGT is used as a biomarker for the appearance and progression of the disease (Hanigan et al., 1999a and B; Hanigan 2014, Pompella et al., 2006; Corti et al., 2010). Similarly, in leukemia, a proliferative malignancy that can infiltrate multiple different organs throughout the human body, including the liver, a correlation between the increase in GGT and the severity of the disease has been examined, assuming that subjects with high GGT have a worse life expectancy and a poor prognosis, and hypothesising GGT as a prognostic marker (Hampel et al., 2016; Hampel et al., 2017; Kreiniz et al., 2017). In this project, we decided to use HepG2 and chronic B leukemic cell line (HG3) as cell lines to test the use of ovo as a GGT inhibitor because both are GGT over-expressing cells (Corti et al; 2010). In particular, chronic B-cell leukemia has been reported to cause secondary liver malignancy, resulting in an over-expression of GGT that causes drug resistance to traditional chemotherapy (Esfahani et al; 2011).

The choice of comparing ovo and 5-thio is due to two main reasons: 1. at structural level, ovo differs from 5-thio for a methyl group on the imidazole ring, which could affect the interaction with GGT; 2. ovo was purified from sea urchin eggs, while 5-thio was produced by chemical synthesis, consequently the comparison of their biological activities is essential to determine if the compound of chemical synthesis can be used for further studies.

2.2. Materials and methods

2.2.1 Enzyme isolation and GGT activity assay

GGT was isolated from human liver cancer cell line (HepG2) and chronic B leukemic cell line (HG3) as described by King et al. (King et al., 2009). Cells were homogenized in 4 volumes of 25 mM TrisCl, pH 7.5, containing 0.33 M sucrose, 0.2 mM EDTA, 1 µM leupeptin, and 1.4 µg/ml aprotinin and centrifuged at 9,000 x g. Supernatant was spun at 100,000 x g for 1 h. The microsomal pellet, resuspended in 25 mM TrisCl, pH 7.35, 0.5% Triton X-100, 1 µM leupeptin, 1.4 µg/ml aprotinin, was centrifuged again at 100,000 x g for 1 h. The supernatant was aliquoted, stored at -80 °C, and then assayed for GGT protein expression and activity. GGT activity was determined by a colorimetric test. The assay buffer contained 100 mM TrisCl, pH 7.8, or 1X PBS, pH 7.4. Each reaction contained 1 mM γ-glutamyl-para-nitroanilide (GpNA) as a donor substrate and 40 mM glycyl-glycine (GlyGly) as an acceptor substrate. The formation of product, p-nitroaniline, was continuously monitored at room temperature at 405 nm using a Bio-Rad 680 microplate reader with Microplate Manager 5.2 (Bio-Rad) software. One unit of GGT activity was defined as the amount of GGT that released 1 µmol of p-nitroaniline/min at room temperature using 10000 M^{-1} cm^{-1} as the molar absorption coefficient, derived as reported previously (Lottenberg and Jackson 1983). All the substrates for GGT assay [GpNA, GlyGly, and equine kidney GGT (eqGGT)] and the compounds tested as inhibitors [trimethyl-2-thiohistidine ergothioneine (erg), 6-diazo-5-oxo-L-norleucine (DON), and dithiothreitol (DTT)] were purchased from Sigma-Aldrich. The compound 5-thiohistidine (5-thio) was produced according to Daunay (Daunay et al., 2016) and kindly provided by Prof. Florian Peter Seebeck, University of Basel. Ovothiol was purified by sea urchin eggs, as previously described (Russo et al., 2014).

2.2.2 Inhibition assay of GGT by thiohistidine compounds

Equine GGT (EqGGT) was used to carry out kinetics studies. The assay buffer contained 100 mM Na_2HPO_4, pH 7.4, with 3.2 mM KCl, 1.8 mM KH_2PO_4, and 27.5 mM NaCl. The concentrations of the substrate GpNA and the acceptor GlyGly were varied as indicated in the figure legends. The inhibitor compounds were added before the enzyme at different concentrations: ovothiol (ovo) and 5-thiohistidine (5-thio) were used at 5, 10 and 20 µM; instead DON and erg were used at 100, 200 and 300 µM.

Aliquots of 0.5–1 µl of GGT (1 mg/ml) were added to start the reaction, which was time-monitored as described above using a Cary100 spectrophotometer (Agilent). The initial velocity of the reaction was derived from the linear part of the kinetics. Data were nonlinear fitted to the Michaelis–Menten equation using Kaleidagraph™ 4.1 software (Synergy). The apparent inhibition constant (*Ki*) were calculated using the following equation.

$$V_{max}{}' = V_{max}/ [1 +[I]/K_i]$$

in which V_{max} and $V_{max}{}'$ represent the V_{max} in the absence or presence of [I], the concentration of the inhibitor. The apparent K_i values obtained at each inhibitor concentration were averaged to obtain a unique value of apparent K_i for each compound. Kinetic parameters and their corresponding standard errors were evaluated using a simple weighting method (Student's *t* test).

The reversibility of the inhibition was assessed using a dilution method described previously (Costanzo et al., 2016). Briefly, the enzyme eqGGT 7 µM was pre-incubated at 37 °C for different time points with the inhibitors or with DTT, as a control, in a total volume of 60 µL of water. After a 50-fold dilution of the incubation mixture, the residual enzyme activity was measured. The concentrations of the inhibitors in the pre-incubation mix were 400 µM of DON, 20 µM of ovo and 20 µM of 5-thio, respectively. To study the effect of the reduced forms of ovo and 5-thio, DTT was added at 5 mM for the time indicated. The mix assay containing 1X PBS, 1 mM of GpNA and 20 mM of GlyGly, and the amount of product released was monitored as described above. The percentage of recovered enzyme activity was referred to that measured for the enzyme pre-treated under identical experimental conditions in the absence of inhibitors.

2.2.3 Cytotoxicity assays

For cytotoxicity assays, human embryonic kidney cells (HEK 293) were plated in 384-multiwell plates (2 $x10^3$ cell/well) by a pipetting robot (Freedom Evo-2 200 Liquids Handler, Tecan, Männedorf, Switzerland) and treated with ovo and 5-thio, at the indicated concentrations for 24–48 h. Cytotoxicity was assessed by resazurin-based assays (CellTiter-Blue® Cell Viability Assay, Promega, Madison, WI, USA) according to the manufacturer's recommendations using a Spark® multimode microplate reader (TECAN). Experiments were performed in triplicate. Data were expressed as units of fluorescence $560_{Ex}/590_{Em}$ nm.

2.2.4 GSH assay

Total GSH levels were determined using a GSH Assay kit (Sigma). Briefly, cell culture media were added with 3 volumes of 5% 5-sulfosalicylic acid and mixed. Subsequently, 7 volumes of 5% 5-sulfosalicylic acid were added, mixed, incubated for 5 min at 4 °C, and finally centrifuged at 10,000 x g for 10 min. Diluted samples of the supernatants were used for the assay procedure where, following incubation with GSH reductase and NADPH, GSH was totally recovered in the reduced form, and its concentration was determined by monitoring the reduction of 5,5-dithiobis(2-nitrobenzoic acid) to 5-thio-2-nitrobenzoic at 412 nm using a Thermo Scientific™ Multiskan™ FC microplate photometer.

2.2.5 Western blot Analysis

For GGT detection, microsomal extracts (5 µg) were run on a 12% SDS-polyacrylamide gel according to Laemmli (Laemmli 1970). Following electrophoresis, proteins were transferred onto a polyvinylidene difluoride membrane (Millipore) using a Bio-Rad Trans-Blot apparatus and detected mouse anti-GGT monoclonal antibody (sc-166908 from Santa Cruz Biotechnology) incubated at 4 °C overnight. The appropriate secondary antibody anti-Mouse (NA931VS, Amersham ECL Mouse IgG, HRP-linked whole Ab from Citeab) was added at 37 °C for 1h, and immunoreactive proteins were detected using enhanced chemiluminescence (Western-BrightTM ECL detection kit, Advansta) according to the manufacturer's instructions. Protein expression levels were analysed by means of

densitometric analysis using ImageJ software and normalized with respect to total protein content determined by Bradford (Bradford 1976) assay and checked by Coomassie Blue gel staining, as housekeeping proteins were too variable in these cancer cell cultures.

2.2.6 Statistical analysis

All statistical analyses were performed using the GraphPad Prism 4 software (GraphPad Software Inc., La Jolla, USA). Data were expressed as the mean ± standard deviation. Comparisons among groups were made by Student's t test. Values of $p < 0.05$ were considered as significant. For each experiment 3 biological samples were tested in triplicate.

2.3. Results

2.3.1. Marine 5-thiohistidines inhibit GGT activity

To understand if thiohistidine compounds could affect the enzymatic activity of GGT, we performed enzymatic tests using both human GGT (hGGT) isolated from membranes of HepG2 or HG3 cells and commercial eqGGT showing high percentage of identity with hGGT, keeping fixed and saturated the concentrations of GpNa and of the acceptor GlyGly, respectively, and by varying the concentrations of the compounds under examination (Figure 23). Residual GGT activity in the presence of ovo, isolated from *P. lividus* eggs in its disulfide form, was compared with that in the presence of the desmethylated form, 5-thiohistidine (5-thio), the trimethyl-2-thiohistidine erg stabilized in thione form, the previously characterized GGT inhibitor DON (Terzyan et al., 2017), and dithiothreitol (DTT), used as a negative control (Figure 24). Under these conditions, 50% GGT inhibition was obtained at 16 µM for ovo, 15 µM for 5-thio, compared with 282 µM for DON, which was abandoned in clinical trials for toxicity (Lyons et al., 1990), and with 297 µM for erg. Similar results were obtained with eqGGT in the presence of the different compounds. The addition of DTT did not induce any GGT-inhibitory action, thus excluding the possibility that the observed inhibitory effect was due to the intrinsic ability of an unspecific thiol to reduce cysteine or disulfides.

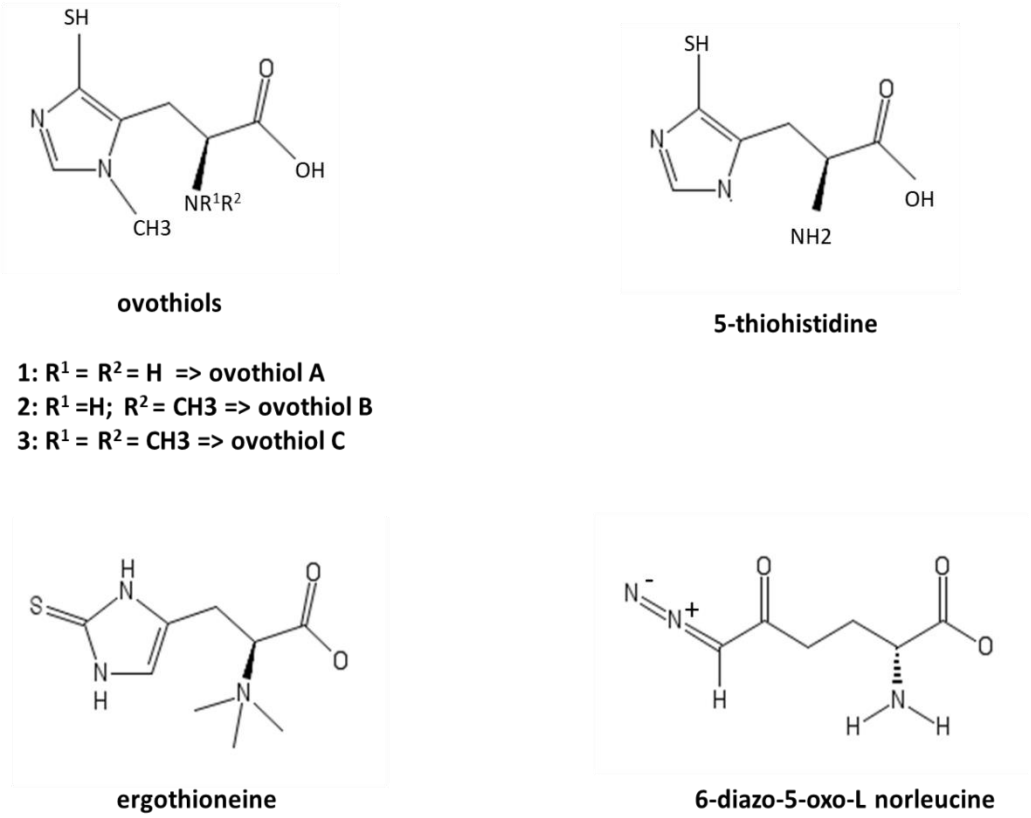

Figure 23. Comparison of sulfur-containing histidines and DON. Chemical structures of ovo, 5-thio, erg, and DON.

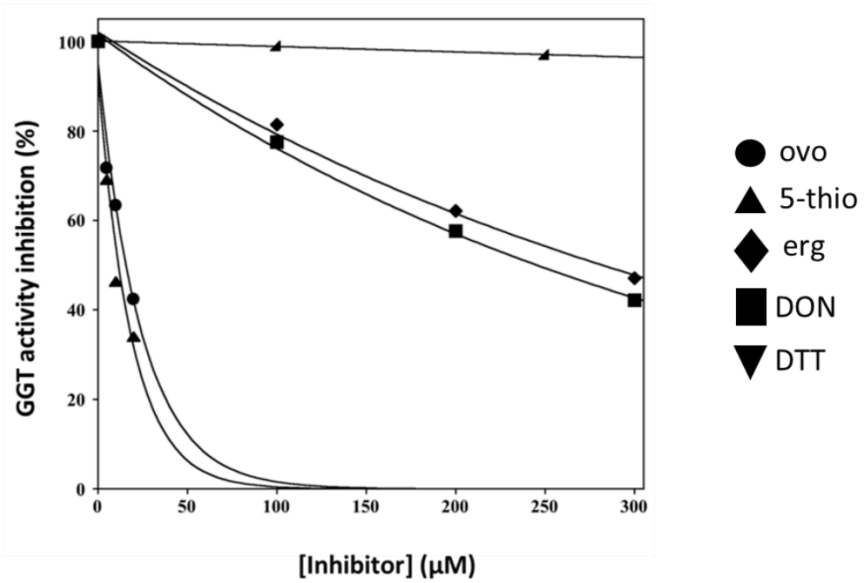

Figure 24. Inhibition of GGT activity. GGT activity was measured in the presence of 40 mM GlyGly and 3 mM GpNA using the following concentrations of ovo and 5-thio (5, 10 and 20 µM); of erg and DON (100, 200 and 300 µM) and of DTT (100 and 250 µM) and reported as a percentage of the activity measured in the absence of the inhibitor (21 units).

2.3.2. Kinetic analysis of GGT inhibition by 5-thiohistidines

To determine the mechanism of 5-thiohistidines-driven inhibition of GGT, kinetics of eqGGT activity were analysed, in the absence or presence of the inhibitor, varying each of the substrates with the second maintained at a fixed concentration. In detail, when GlyGly (the acceptor substrate) concentration varied, GpNA was maintained at 3 mM (Figure 25); *viceversa*, GlyGly was maintained at 40 mM when GpNA concentration varied (Figure 26). The effect of different concentrations of ovo, 5-thio, DON, and erg on the kinetics of eqGGT is shown in representative Michaelis– Menten graphs reported in figure 25 and 26. The behavior of ovo and 5-thio inhibition (Figure 25A, 25B and 26A, 26B) accounted for a non-competitive-like inhibition. In fact, the extrapolation of the fitting on the x axis approached very similar K_m values, whereas a decrease of V_{max} was observed in all cases. These data indicate that ovo and 5-thio have the same affinity for the free enzyme and the covalent E–γ-glutamyl complex, both when GpNA binds as donor substrate and GlyGly binds as acceptor. Similar kinetic behaviours with decreased V_{max} and roughly constant K_m values were also obtained in the presence of DON (Figure 25C and 26C) and erg (Figure 25D and 26D). The apparent K_i values obtained from nonlinear fitting in the Michaelis– Menten equation are reported in Table 1. The apparent K_i values obtained for each compound indicated that, among those tested, ovo and 5-thio are more potent inhibitors compared with erg and DON, thus confirming the data reported in Figure 25 and 26.

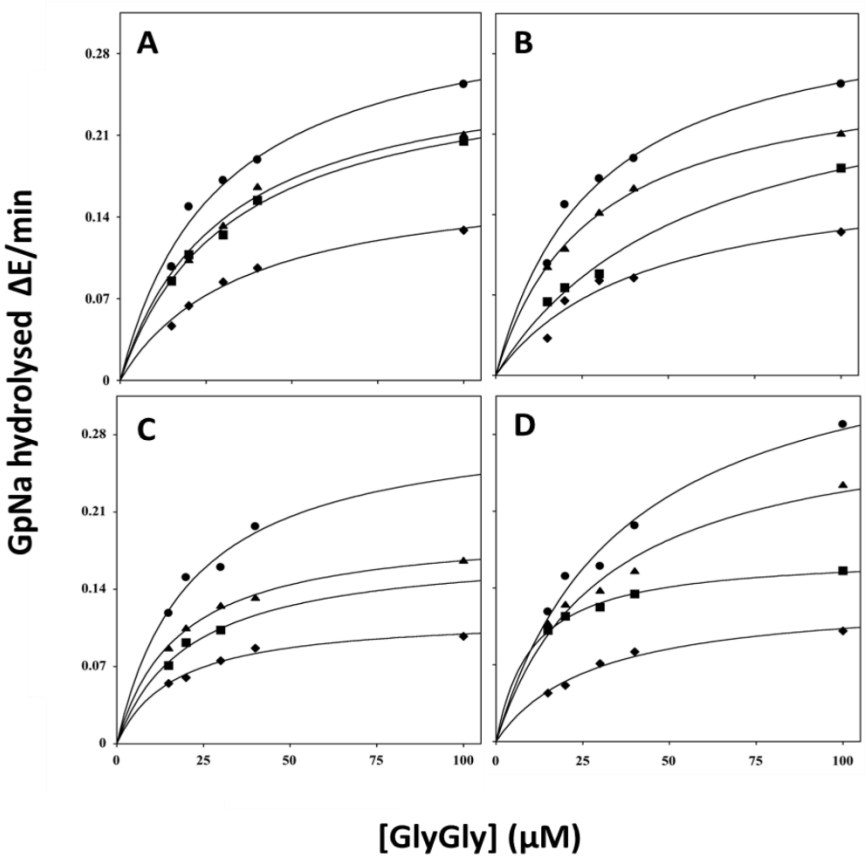

Figure 25. Kinetic analysis of GGT inhibition (a). EqGGT activity was assayed as reported under "Experimental procedures" in the presence of 3mM GpNA and the indicated concentrations of GlyGly (**A, B, C**, and **D**). Michaelis– Menten plots were obtained in the absence (closed circle) or presence of 5 (closed triangles), 10 (closed squares), or 20 (closed diamonds) µM ovo and 5-thio (A and B) and 100 (closed triangles), 200 (closed squares), or 300 (closed diamond) µM erg and DON (C and D).

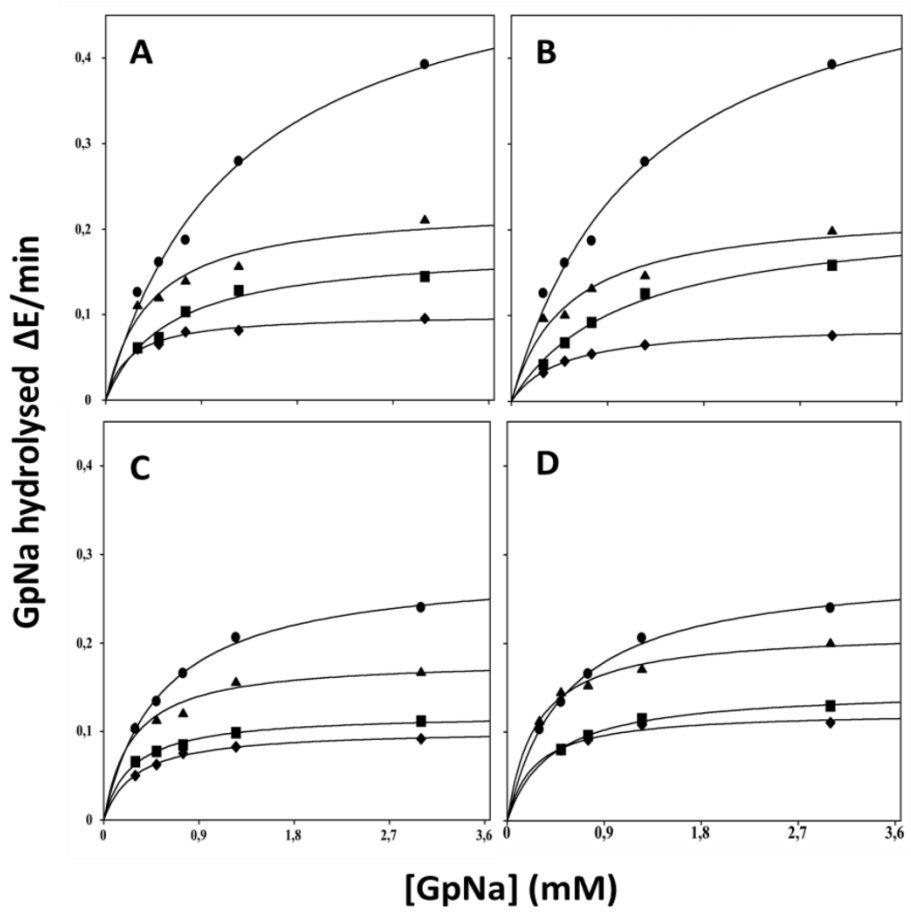

Figure 26. Kinetic analysis of GGT inhibition (b). EqGGT activity was assayed as reported under "Experimental procedures" in the presence of 40Mm GlyGly and the indicated concentrations of GpNA (**A**, **B**, **C**, and **D**). Michaelis– Menten plots were obtained in the absence (closed circle) or presence of 5 (closed triangles), 10 (closed squares), or 20 (closed diamonds) µM ovo and 5-thio (A and B) and 100 (closed triangles), 200 (closed squares), or 300 (closed diamond) µM erg and DON (C and D).

Table 1. Inhibition constants of GGT activity by sulfur-containing compounds. Data of apparent K_i were obtained as reported under "Experimental procedures" and are expressed as mean ± S.D. (n= 3).

Compounds	Fixed substrate	Variable substrate	Apparent K_i (µM)
Ovo	GpNA	GlyGly	21 ± 7
5-thio	GpNA	GlyGly	17 ± 1.5
DON	GpNA	GlyGly	141 ± 27
Erg	GpNA	GlyGly	171 ± 3
Ovo	GlyGly	GpNA	7 ± 1
5-thio	GlyGly	GpNA	7 ± 1.7
DON	GlyGly	GpNA	83 ± 11
Erg	GlyGly	GpNA	111 ± 10

2.3.3. 5-thiohistidines inhibit membrane-bound GGT of human cancer cells

In order to understand whether 5-thiohistidines inhibit GGT linked to the membrane of human tumour cells, we used two tumour cell lines: HepG2 and HG3 cells and two non-tumour cell lines: lymphocytes and human embryo kidney (HEK 293).

To evaluate the protein expression of GGT in these cell lines, we performed an immunoblotting using a specific antibody against hGGT. Both tumour cell lines showed a significant higher expression of the GGT membrane-bound form (64 kDa) compared to normal lymphocytes and HEK 293 (Figure 27A and 27B). Curiously, the molecular weight of GGT in HEK 293 was apparently lower than in GGT from HepG2 and HG3, probably due to differences in the state of protein glycosylation. These results confirmed that the tumour cell lines used in this study expressed higher GGT levels compared to non-malignant cells, HEK293 and lymphocytes.

In addition, to investigate whether ovothiol inhibited membrane-bound GGT in dividing cells, we treated HG3 cells with 20 µM ovo and we evaluated the expression of GGT after 2 and 24 h.

This concentration was chosen on the basis of the Ki of ovo (see Table 1).

Treatment with ovo did not induce significant changes in GGT expression respect to untreated cells at 2 hours, except for a slight decrease in GGT expression at 24 h (Figure 27C and 27D).

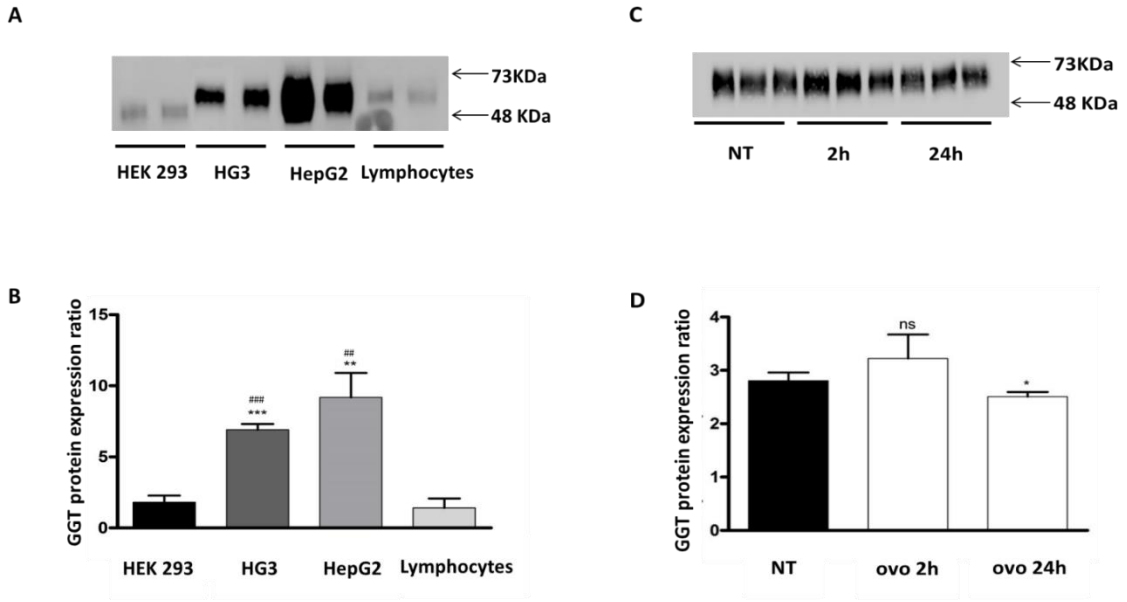

Figure 27. Protein expression analysis of hGGT. (A) Representative Western blot using hGGT-specific antibody against microsomal extracts of HG3 and HepG2 human cancer cells compared with normal lymphocytes and HEK 293 cells. **(B)** Protein expression levels were quantified by densitometric analysis using ImageJ software and normalized *versus* total protein content: ** ($p < 0.01$) and *** ($p < 0.001$) represent significance compared to HEK 293 cells; $^{\#\#}$ ($p < 0.01$) and $^{\#\#\#}$ ($p < 0.001$) represent significance compared to lymphocytes. *Error bars* represent S.D. The significance was determined by Student's *t* test and post hoc analysis. **(C)** Representative Western blot performed with hGGT-specific antibody using microsomal extract of HG3 cells. **(D)** Protein expression levels analyzed by densitometric analysis and normalized to total protein content (n=3). * ($p < 0.05$), represent significance compared to non treated cells (NT). *Error bars* represent S.D. The significance was determined by Student's *t* test and post hoc analysis. (modified from Brancaccio et al., 2019)

2.3.4 GGT activity and GSH content in human cancer cells

To investigate the activity of GGT after treatment with ovo, we treated the HG3 cells with 20 µM of ovo for 2 and 24 h, then we carried out a partial purification of the enzyme and measured the activity of GGT.

The activity of GGT was normalised towards the total protein content. In this case we observed a significant decrease of GGT activity both at 2 hours and at 24 hours of treatment, when compared with the non treated cells (NT) (Figure 28A). In addition, we evaluated the GSH content in the medium of the cell cultures after treatment with ovo, in order to understand whether ovo treatment could inhibit GGT and consequently block the hydrolysis of extracellular GSH. In our experiment we observed that the reduction of GGT activity was concomitant to a significant increase in GSH at 24 h outside the cells (Figure 28B), thus confirming the blocking of GSH hydrolysis.

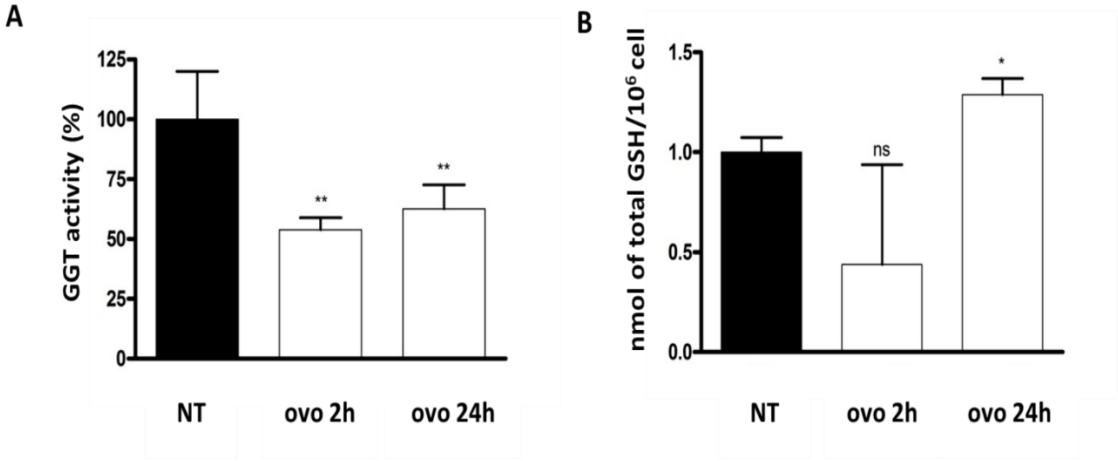

Figure 28. GGT activity and GSH content in HG3 upon treatment with ovothiol. (A) Enzymatic activity of GGT evaluated on cell microsomal extracts containing membrane-bound GGT. The activity of GGT was normalized to the densitometric value of GGT protein band detected by immunoblotting (*n*=6). ** (p <0.01) represent significance compared to non treated cells (NT). *Error bars* represent S.D. The significance was determined by the Student's *t* test and post hoc analysis. **(B)** The levels of GSH were determined in the medium of cells. GSH content was normalized *versus* the number of cells (*n*=6). * (p <0.05), represent significance compared to non treated cells (NT). *Error bars* represent S.D. The significance was determined by the Student's *t* test and post hoc analysis. (modified from Brancaccio et al.,2019)

2.3.5. Mechanism of inactivation of GGT by 5-thiohistidine compounds

To reveal whether the inhibition mechanism of our compounds was reversible or not, we carried out the following experiment. We pre-incubated eqGGT with ovo, 5-thio and DON for 2 hours and the residual enzyme activity was measured at different time points after diluting the pre-incubation mixture in the buffer reaction. The pre-treatment kinetics indicated that DON acted as an irreversible inhibitor and therefore as an inactivator of GGT, since, after dilution, the activity was not restored and decreased with the incubation time (Figure 29). Instead, an opposite trend was observed for 5-thio and ovo, for which the activity was restored in a time-dependent manner after dilution (Figure 29). This finding indicates a reversible inhibition mechanism for 5-thio and ovo. In addition, in order to evaluate whether the inhibitory activity of ovo and 5-thio was ascribed only to the disulphide forms of these compounds or also due to the reduced forms, we added DTT to the reaction mixture. The addition of DTT did not affect the activity of GGT in any way (Table 2), indicating that the inhibitory species are indeed the disulfide forms of ovo and 5-thio. We therefore demonstrated that ovo and 5-thio act as non-competitive inhibitors when in disulphide form and their interaction is reversible. Instead, DON is an inactivator, which irreversibly modify the enzyme. This could explain the reason

for its cellular toxicity. Therefore, following this result, we decided to perform cytotoxicity tests on our compounds.

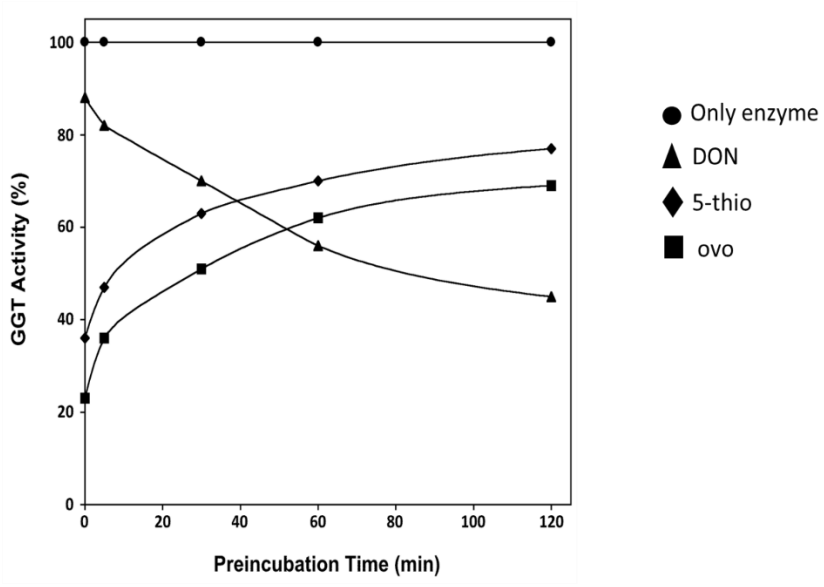

Figure 29. Inhibition of eqGGT by 5-thiohistidines. EqGGT was preincubated at 37 ˚C with 400 µM of DON, 20 µM of 5-thio, 20 µM of ovo, or in the absence of compounds for the indicated times. Immediately following the pre-incubation, the mix was assayed for GGT activity as reported in the Materials and Methods section. Experiments were performed in quadruplicate and data were reported as percentage of enzyme activity in the presence of the inhibitors with respect to the enzyme without the inhibitor. (modified from Milito et al., 2019)

Table 2. Time-dependent inhibition of eqGGT activity by 5-thiohistidines ± DTT. The % of residual GGT activity after the incubation with 5 mM of DTT, 20 µM of ovo, 20 µM of 5-thio, ovo± DTT or 5-thio ± DTT at the same concentrations, or in the absence of the compounds at 0, 30 and 60 min, is reported**.**

Time (min)	eqGGT	DTT	Ovo	5-thio	DTT+ovo	DTT+5-thio
0	100%	93%	39%	33%	94%	86%
30	100%	89%	60%	47%	83%	71%
60	100%	72%	72%	59%	73%	60%

2.3.6 Cytotoxycity

To verify whether ovo and 5-thio are cytotoxic towards normal cells, we treated non-malignant HEK 293 cells for 24 and 48 h at different concentrations (5, 20, 50 100 µM) of ovo and 5-thio, and measured cell vitality. As reported above, HEK 293 cells express low levels of GGT in comparison to malignant cells such as HepG2 and HG3 (figure 27). Our results indicated that the compounds showed no cytotoxic activity when compared cell viability against the untreated samples. Moreover, after 24 h treatment, we observed a slight increase in cell proliferation at the lowest concentration of 5 µM (Figure 30A and 30B). This phenomenon may account for an adaptive response of the cell known as hormesis, which deserves further investigations.

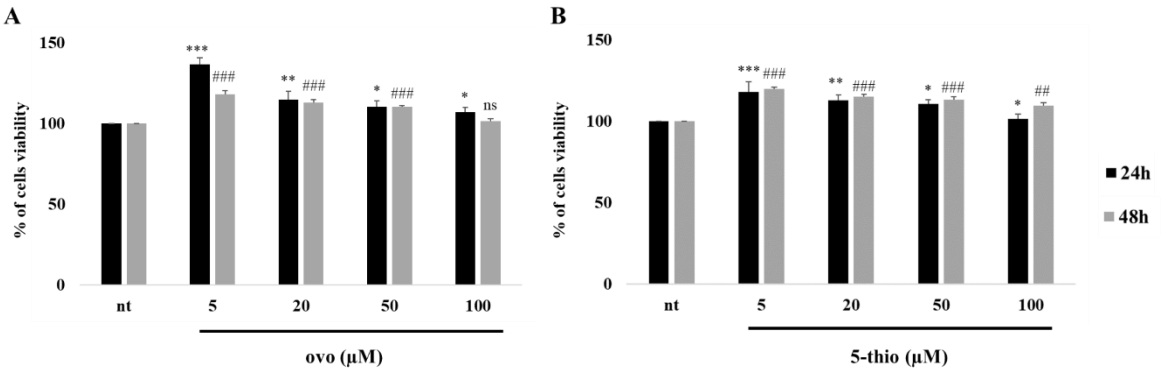

Figure 30. Effect of ovo and 5-thio on HEK 293 cells. (A) and **(B)** HEK 293 cells were treated for 24 and 48 h with ovo and 5-thio at four different concentrations (5, 20, 50 and 100µM). Cell viability was measured by a resazurin-based assay (n = 3). Results were reported as percentage of cell viability. Data were reported as mean±SD. The significance was determined by the t-test student: * ($p < 0.05$), ** ($p < 0.01$) and *** ($p < 0.001$) represent significance compared to NT at 24h; $^{\#}$($p < 0.05$), $^{\#\#}$ ($p < 0.01$) and $^{\#\#\#}$ ($p < 0.001$) represent significance compared to NT at 48h

2.4. Discussion

GGT is known to play a key role in maintaining cellular homeostasis, particularly in detoxification processes. In addition, the increased expression of GGT is involved in tumor progression, in the birth of drug resistance, in neurodegenerative diseases and in pathologies such as asthma and renal ischemia (Corti et al.,2010; Yamamoto et al.,2011; Tuzova et al., 2014). Therefore, for example, the use of GGT inhibitors can help to improve chemotherapy treatment by limiting the supply of cysteine to cancer cells and blocking the accumulation of intracellular GSH (Ruoso and Hedley 2004; Lieberman et al., 1996).

Previous studies conducted on metastatic liver melanoma in animal models have used acivicin in combination with traditional chemotherapy to deplete cancer cells in GSH. In 90% of cases it was possible to visualise the reversal of the tumour phenotype, thus leading to complete recovery (Mena et al., 2007).

However, most of GGT inhibitors known to date are toxic and /or have reduced efficacy; therefore, it is necessary to discover new inhibitors that exhibit greater efficacy and lower toxicity (Castellano et al., 2012).

In this study we discovered that GGT is a direct target of ovo and its demethylated form 5-thio, shedding light on a new class of GGT inhibitors, i.e. 5- thioistidines. Kinetic studies on hGGT and eqGGT in the presence of these compounds pointed to a non-competitive- like inhibition relative to the donor and the acceptor substrate.

Although in a strictly non-competitive inhibition we should find identical K_i values, regardless of whether the donor or acceptor substrate varies, the differences found (see table 1) could lie in the complex ping-pong mechanism of GGT (see figure 21). In particular, the mechanisms by which one or more products are released before all substrates are bound to the enzyme are known as ping-pong mechanisms. In the case of GGT the γ-glutamyl-group of the first substrate (the donor GpNA) is removed from the substrate by the enzyme E, thus forming a stable enzyme form in which the γ-glutamyl-group is firmly bound (often covalently) to the enzyme (ping phase). In the second part of the reaction, the γ-glutamyl-group is again moved from the enzyme to the second substrate (the acceptor GlyGly) to form the the γ-glutamylated product, consequently regenerating the original

form of the enzyme E (pong phase). These reactions are also called, double shift reactions (note that in these reactions, the two substrates never meet on the surface of the enzyme).

Competitive inhibition has been reported to often be an inappropriate basis for the design of potential therapeutic agents. Consequently, the use of non-competitive inhibitors is probably much more effective (Westley et al., 1996). Moreover, a reversible mode of action for GGT inhibitors could provide the additional advantage of a rapid inhibition rate (Ramsay and Tipton 2017) as well as being easier to modulate *in vivo*, and thus preserving the physiological GGT activity and resulting in lower toxicity. Therefore, ovo and 5-thio can be very advantageous inhibitors of the GGT enzymatic activity compared to competitive inhibitors.

In particular, when inhibitors compete with the physiological substrate, they can cause its significant accumulation, which can have unfavourable consequences. In addition, it can be extremely unfavourable when an irreversible inhibitor can covalently modify the enzyme, thus leading to the total loss of enzymatic activity.

Furthermore, the results obtained show that both ovo and 5-thio have an inhibitory capacity of about 10 times stronger than known inhibitors (DON), without showing any cytotoxicity. Indeed, cell death is not observed *in vitro* on HEK 293 cells, up to 100 µM of ovo or 5-thio.

In contrast, erg appears as a very weak inhibitor of GGT activity.

These results may suggest that the 5-thiohistidines disulfide form has a strong inhibitory capacity against GGT, caused either by the steric hindrance of the structure or by the greater reactivity of the –SH group compared to the erg which is generally stabilised in the thione form.

Moreover, these studies confirmed molecular docking analysis showing that disulfide forms of ovo and 5-thio enter the hGGT binding pocket, and interact with key residues in the donor and the acceptor binding sites, which are the same as those involved in the formation of the tetrahedral intermediate of the physiological substrate GSH, whereas erg is far from establishing the same interactions (Milito et al, 2019). This may explain the stronger inhibitory power of 5-thiohistidine disulfides in inhibiting hGGT compared to erg (Brancaccio et al, 2019). In addition, the simulations suggested that both ovo and 5-thio in disulfide form can also interact with one or two residues in the acceptor site. This finding can explain the stronger inhibitory activity of both molecules compared

to DON and the reduced forms of ovo and 5-thio, whose interactions involve only residues at the donor binding site (Milito et al, 2019).

In addition, the treatment of HG3 cells with ovo does not induce significant changes in GGT expression respect to untreated cells at 2 hours, except for a slight decrease in GGT expression at 24 h (Figure 27C and 27D). However, we observed a significant decrease in GGT activity (Figure 28A) with a consequent increase in GSH levels 24 h after treatment (Figure 28B). Therefore, a strong inhibition of GGT can block the metabolism of extracellular GSH, and consequently the recycling of cysteine and glycine. These effects can cause the reduction of the intracellular GSH synthesis and in general of protein synthesis and consequently cell proliferation.

These data suggest that 5-thiohistidine derivatives can be finely modulated in *in vitro* and *in vivo* studies, thanks to their reversible mode of action. In particular, 5-thio has the advantage of being efficiently obtained by chemical synthesis (Daunay et al,2016); hence, it can be considered a valid alternative to ovo, whose synthesis is tricky.

2.5. Conclusions and perspectives

In conclusion, for the first time, a class of sulfur-containing compounds from the marine world (ovo and 5-thio) has been shown to inhibit GGT through a non-competitive and reversible mechanism, causing no cytotoxicity of normal GGT expressing cells, while arresting proliferation of GGT-over-expressing cells.

Future studies will be needed to test these compounds in positive GGT pathologies in order to validate their use as alternative therapies.

CHAPTER 3

Therapeutic potential of 5-thiohistidines for the treatment of liver fibrosis

3.1. Aims of the study

Liver fibrosis represents a worldwide health problem for its growing incidence and prevalence, and its evolution towards cirrhosis, which is associated with high morbidity and mortality. It is a complex process caused by chronic hepatic injury, which leads to an excessive increase in extracellular matrix (ECM) accumulation and fibrogenesis. In the normal liver, three types of cells coexist: the hepatocytes with the microvilli necessary for liver detoxification, the inactivated HSC and the Kuppfer cells (Figure 31A). Kupffer cells are specialized macrophages located in the liver, which are part of the "macrophage system". They are found to be altered in most liver diseases. Activation of Kupffer cells is responsible for the early stages of liver damage. Liver damage occurs with a double-hit system, involving first the activation of the Kupffer cells or of the hepatic magrophages and then that of the immune system. This activation promotes the transcription of pro-inflammatory cytokines (tumor necrosis factor or TNFα) and the production of superoxides. TNFα is then absorbed by HSCs in the liver, leading to collagen synthesis and fibrosis. Fibrosis can eventually lead to liver cirrhosis or loss of liver function (Haubrich, 2004).

After liver damage, we can observe the loss of hepatocytes, the activation of HSC and the accumulation of ECM (Figure 31B). This process is regulated by several factors including: TGF-β, the most important pro-fibrogenic marker, released by macrophage cells after liver damage; α-SMA (alpha smooth muscle actin) released by myofibroblast cells, activated after cell injury; Col1a1 (Collagen, type I, alpha 1) (Figure 31). The fibrotic process consists in the accumulation of collagen fibers, generating fibrotic scars. The main player of this process is TIMP-1 (inhibitor of metallopeptidase -1), which inhibits the activity of the metalloproteases during fibrosis and favours the accumulation of ECM (Figure 31).

In addition, the appearance of hepatic fibrosis leads to both morphological alterations of the liver and to the increase of the serological levels of the enzymes involved in liver metabolism: aspartate aminotransferase (AST), alanine aminotransferase (ALT), alkaline phosphatase (ALP) (Iluz-Freundlich et al., 2020) and γ-glutamyl transferase (GGT) (Koenig and Seneff 2015) (Figure 32).

Furthermore, serum GGT is clinically recognised as the most useful marker for the diagnosis of alcoholic liver disease, (Irie et al., 2007), which can turn into fibrosis and then in liver cirrhosis.

Moreover, Bodewes and coauthors have reported that an increase in the serum GGT of pediatric patients with cystic fibrosis can be used as an alarm bell to know the risk of liver cirrhosis (Bodewes et al., 2015). The increase of the GGT values greater than 35 U/L was associated with the probability of the appearance of cirrhosis within two years. Consequently, GGT can be used as a biomarker in liver damage, and its inhibition, therefore, can represent a pharmacological approach for the treatment of liver fibrosis.

In addition, several natural products, including sulphur containing compounds, have been investigated for their antifibrotic effects (Milito et al., 2019), although the molecular mechanisms underpinning their action are partially still obscure. Thus, there is an urgent need to develop antifibrotic treatments that can prevent, halt, or even reverse liver fibrosis or cirrhosis (Schuppan and Kim 2013). As we have previously discovered that GGT is inhibited by marine 5-thioistidines through a reversible and non-competitive mechanism, and that the administration of 5-thioistidines in HEK 293 cells does not generate cellular cytotoxicity, in this study, in collaboration with University of Naples "Federico II" we decided to investigate for the first time the effect of ovothiol A, isolated from sea urchin eggs on an *in vivo* mouse model of liver fibrosis.

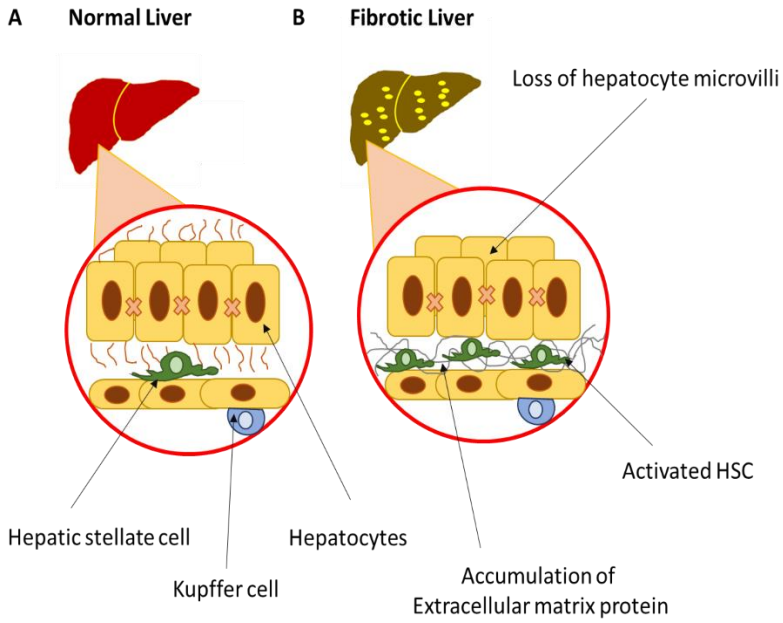

Figure 31. Normal and fibrotic liver architecture. (A) In the healthy liver the hepatocytes present the microvilli necessary for liver detoxification, HSC and the Kupffer cells are inactivated. **(B)** In the fibrotic liver there is the loss of the microvilli of the hepatocytes, the activation of the HSC and the accumulation of ECM.

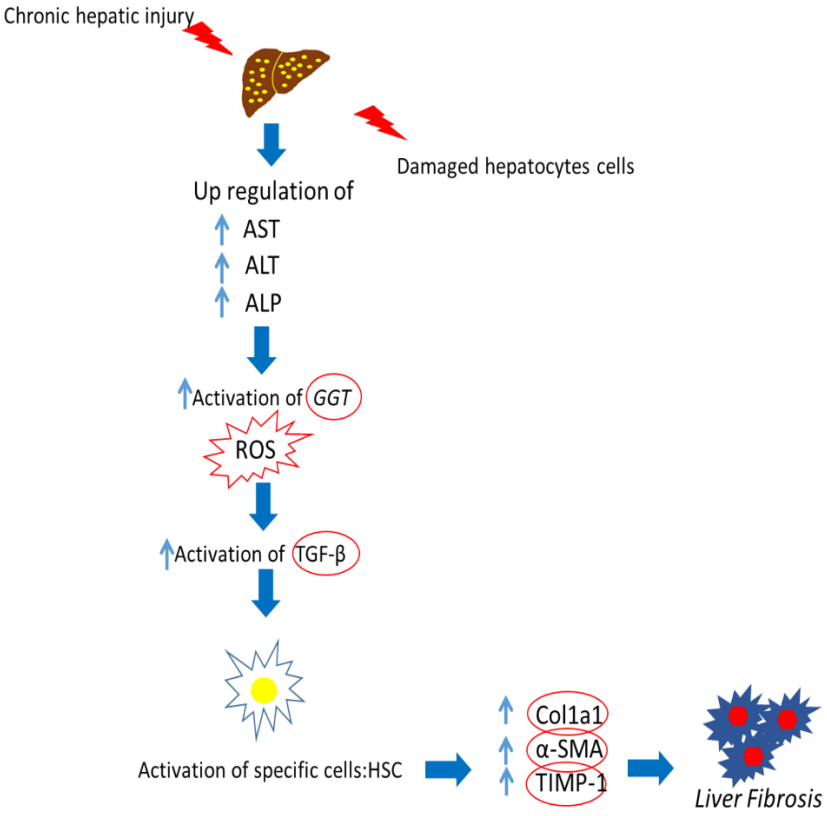

Figure 32. Molecular mechanisms of the fibrotic process. During chronic liver damage, the levels of liver enzymes (AST, ALT, ALP, GGT) increase, causing an accumulation of ROS, TGFβ activation, which stimulates the activation of HSC which in turn promote the activation and up regulation of α-SMA, Col1a1, and TIMP-1; culminating in the liver fibrotic process.

3.2. Materials and methods

3.2.1. Experimental model and animal treatment

Male balb-c albino mice (20–25 g) were housed in a room at a mean constant temperature of 22°C with a 12 h light–dark cycle and free access to standard pellet chow and water. The study was approved by Federico II University School of Veterinary Medicine Animal Care N° 104/2015-PR. Liver fibrosis was induced in mice by intraperitoneal (ip) injection of carbon tetrachloride (CCl_4) 0.2 mL/100 g body weight (b.w.) in refined olive oil (1: 1) twice a week for 7 weeks according to a well-established protocol (Issa et al., 2003). Two experimental groups were designed as follows: (1) mice receiving CCl_4 and ip injection of the disulfide form of ovothiol A 50 μg/g b.w. 3 times a week for 7 weeks (n = 7); (2) control group receiving CCl_4 and ip injection of vehicle (aqueous solution) alone (n = 7) with the same timing. Ovothiol A was prepared as described by Russo et al., 2014. The dose of administration was chosen on the basis of a previous work demonstrating that at this posology an ovothiol analogue induced no toxicity in not injured mice and neuroprotection in mice affected by brain injury (Vamecq et al., 2003). A group of 5 normal mice was also included in the study. The animals were then killed under anaesthesia, and their livers were harvested at peak of fibrosis (3 days after the final injection of CCl4). After harvesting, livers were divided with a minimum of two lobes fixed in formalin for histologic analysis and histochemistry, and the remaining tissue was snap-frozen for RNA and protein extraction. Serum was also collected from each mouse to analyze biochemical parameters.

3.2.2. Histology and biochemical parameters

Formalin-fixed paraffin-embedded tissue was cut into 4 μm sections by using routine techniques and mounted onto slides with coverslips. Representative sections of each fixed liver were stained with haematoxylin/eosin (H&E) for routinely observations. For the detection of collagen content, sections were stained with Sirius red/Fast green, according to standard protocols. All histological analyses were performed by an experienced histopathologist in a blinded manner. For each mouse, 64 fields of a constant raster of 31mm2 were analyzed at 100-foldfinal magnification. For semiautomated

morphometry, a Sony 3CCD (model DXC-950P) video microscope equipped with a motor stage and the Quantimed 500MC (Leica, Germany) software were used. Serum AST, ALT, and ALP levels were determined to assess liver function by using standard laboratory techniques and equipment (Roche Diagnostics, Germany).

3.2.3. RNA extraction and cDNA synthesis

Total RNA was extracted from frozen tissue by homogenization in Trizol Reagent according to the manufacturer's protocol (Life Technologies). The amount of total RNA extracted was estimated measuring the absorbance at 260nm and the purity by 260/280 and 260/230nm ratios by Nanodrop (ND-1000 UV-Vis Spectrophotometer; NanoDrop Technologies). The integrity of RNA was evaluated by agarose gel electrophoresis. For each sample, 1200 ng of total RNA extracted was retrotranscribed with iScriptTM cDNA synthesis kit (Bio-Rad), following the manufacturer's instructions.

3.2.4. Gene expression by Real-Time qPCR.

For real-time qPCR experiments, the data from each cDNA sample were normalized using the mouse housekeeping gene GAPDH (glyceraldehyde 3-phosphate dehydrogenase). In the case of GAPDH, TGF-β, α-SMA, Col1a1, and GGT-1, the specific primers were designed based on the nucleotide sequences downloaded by NCBI database (accession numbers) using Primer3WEB v.4.0.0. GAPDH primer forward 5′-GGTGAAGGTCGGTGTGAACG-3′, primer reverse 5′-CTCGCTCCTGGAAGATGGTG-3′; TGF-β primer forward 5′- TGCGCTTGCAGAGATTAAAA-3′, primer reverse 5′-CTGCCGTACAACTCCAGTGA-3′; α-SMA primer forward 5′-CTGACAGAGGCACCACTGAA-3′, primer reverse 5′-CATCTCCAGAGTCCAGCACA-3′; Col1a1 primer forward 5′-ACAGTCGCTTCACCTACAGC-3′, primer reverse 5′-TGGGGTGGAGGGAGTTTACA-3′ GGT-1 primer forward 5′-TGCTCGGTGACCCAAAGTTT-3′, primer reverse 5′-TTCAGAGGATGGCAGTGCTG-3′. A final concentration of 1.4 pmol/μL for each primer and 1 FastStart SYBR Green Master Mix (total volume of 10 μL) were used for the reaction mix. PCR amplifications were performed in a ViiATM 7 real-time PCR system (Applied

Biosystems) thermal cycler using the following thermal profile: 95°C for 10 min, one cycle for cDNA denaturation; 95°C for 15 sec and 60°C for 1 min, 40 cycles for amplification; 72°C for 5 min, one cycle for final elongation; and one cycle for melting curve analysis (from 60°C to 95°C) to verify the presence of a single product. Each assay included a no-template control for each primer pair. Specificity of amplification reactions was verified by melting curve analysis. The efficiency of each primer pair was calculated according to standard method curves using the equation E = 10–1/slope. Five serial dilutions were set up to determine Ct values and reaction efficiencies for all primer pairs. Standard curves were generated for each oligonucleotide pair using the Ct values versus the logarithm of each dilution factor, and PCR amplifications were performed in a ViiATM 7 real-time PCR system (Applied Biosystems) thermal cycler using the standard protocol previously reported. To capture intra-assay variability, all real-time qPCR reactions were carried out in triplicate. Fluorescence was measured using ViiATM 7 Software (Applied Biosystems). The expression of the genes was analyzed and internally normalized against GAPDH using relative expression software tool (REST) software based on the Pfaffl method (2002). Relative expression ratios above two cycles were considered significant. Experiments were performed in triplicate for 7 different biological samples.

3.2.5. Protein analysis

Liver samples, about 20/30 mg, were homogenized in 1mL of RIPA lysis buffer (1X) containing a 50mM Tris-HCl (pH 7.6), 150mM NaCl, 5mM EDTA, 0.5% NP-40, 0.5% Sodium deoxycholate, 10% SDS, phosphatase, and protease inhibitor cocktail (Roche). Liver homogenates were run on 12% SDS/polyacrylamide gel according to Laemmli. Following electrophoresis, proteins were transferred onto a PVDF (Millipore) membrane (Bio-Rad Trans-Blot Apparatus) and detected using a mouse anti-TGF-β polyclonal antibody (Sigma-Aldrich, USA), mouse anti-GGT monoclonal antibody (Santa Cruz Biotechnology, USA), rabbit anti-α-SMA monoclonal antibody (Santa CruzBiotechnology, USA), rabbit TIMP-1 polyclonal antibody (Elabscience), and as an internal control mouse anti-GAPDH monoclonal antibody (Santa Cruz Biotechnology, USA). All primary antibodies were incubated at 4°C overnight. The appropriate secondary antibody was added, and

immunoreactive proteins were detected using the ECL (WesternBrightTM detection kit ECL, Advansta, USA) according to the manufacturer's instructions. Protein expression levels were analyzed by means of densitometric analysis using the Image J software.

3.2.6. Enzyme isolation and GGT activity

Tissues were homogenized with Potter-Elvehjem tissue homogenizer at 4°C in 5 volumes of 25mM Tris-HCl, pH7.5, 0.2mM EDTA, containing 0.33M sucrose, 1 μM leupeptin, and 1.4 μg/mL aprotinin [33]. The homogenate was centrifuged at 9000 × g for 20 min; the supernatant was spun at 100,000 × g for 1 h to spin down nuclei, mitochondria, and cellular debris. The pellet was homogenized in 25mM Tris-HCl, pH7.35, 0.5% Triton X-100, 1 μM leupeptin, 1.4 μg/mL aprotinin, and then centrifuged again at 100,000 × g for 1 h. The supernatant was aliquoted and stored at −80°C and then assayed for GGT protein expression and activity. GGT activity was determined by a colorimetric test. The assay buffer contained 100mM Tris-HCl pH7.8 or PBS 1X pH7.4. Each reaction contained 1mM of γ-glutamyl-para-nitroanilide (GpNa) as a donor substrate and 40mM glycylglycine (GlyGly) as an acceptor substrate. The product formation, p-nitroaniline, was continuously monitored at room temperature at A405nm using a Bio-Rad 680 microplate reader with Microplate Manager 5.2 (Bio-Rad) software. One unit of GGT activity was defined as the amount of GGT that released 1 μmol of p-nitroaniline/ min at room temperature.

3.2.7. Glutathione assay

Total glutathione levels were determined by Glutathione Assay Kit (Sigma). Briefly, frozen liver tissues were ground with a pestle and a mortar in the presence of liquid nitrogen to prepare a fine powder. Then, 100mg of powder was added to 3 volumes of 5% 5-sulfosalicylic acid and mixed. Then, other 7 volumes of 5% 5-sulfosalicylic acid were added, mixed, left for 5 min at 4°C, and finally centrifuged at 10,000 × g for 10 min. Diluted samples of the supernatants were used for the assay procedure, in which following the incubation with glutathione reductase and NADPH, glutathione was totally recovered in the reduced form and thus determined by monitoring the

reduction of 5,5-dithiobis (2-nitrobenzoic acid) to 5-thio-2- nitrobenzoic at 412nm by a Thermo Scientific™ Multiskan™ FC Microplate Photometer.

3.2.8. Statistical analysis

As appropriate, comparisons among groups were made by Student's t-test or analysis of variance ANOVA followed by Bonferroni or Tukey's multiple comparison tests. Values of $p < 0\ 05$ were considered significant.

3.3. Results

3.3.1. Effect of ovothiol on liver histology and serum biochemical markers.

In order to evaluate the effect of ovo in liver fibrosis, the compound was injected intraperitoneally into a group of mice affected by liver fibrosis induced by treatment with carbon tetrachloride (CCl_4). Another group, formed by mice with liver fibrosis, received only vehicle injection (figure 33). Then, the histology and functionality of the liver were examined in both mice groups as well as in non-treated healthy mice (figure 33).

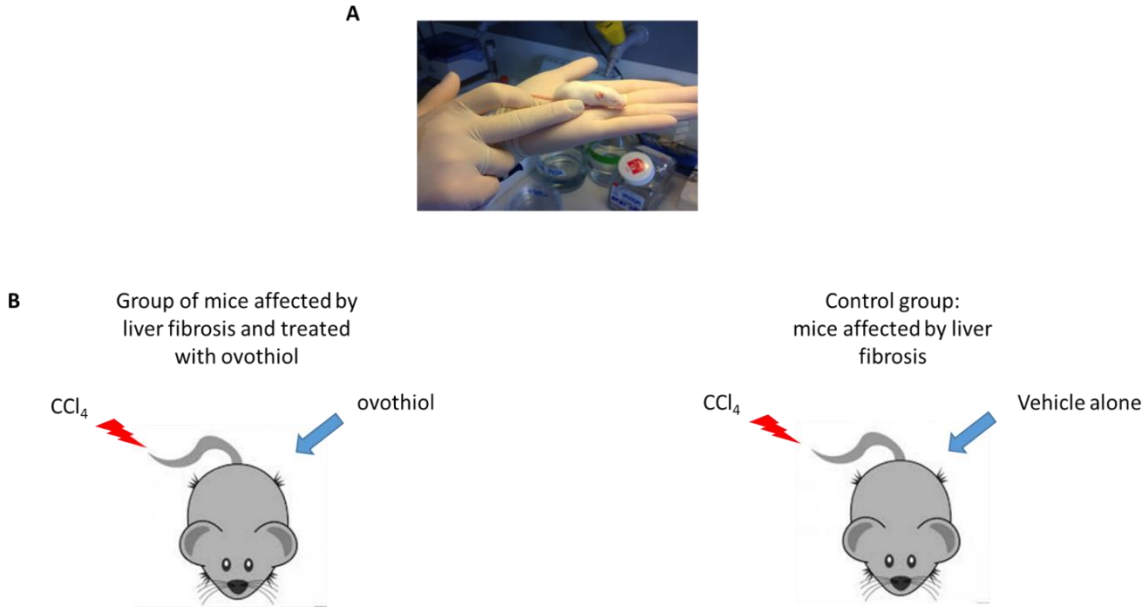

Figure 33. *In vivo* mouse model of liver fibrosis. (A) Representative image of Male balb-c albino mouse. **(B)** Schematic representation of the experimental plan.

Histological analysis of hepatic tissue of mice treated with CCl_4 for 7 weeks compared with healthy mice tissue confirmed that the injection of CCl_4 caused the progression of hepatic fibrosis, as demonstrated by the increase of red coloured collagen fibres showing established septa linking hepatic veins (see Figure 34A, c–d compared to a and b). Ovo treatment significantly reduced hepatic fibrosis as shown by the reduction of red coloured collagen fibres (Figure 34(A), e–f compared to c and d). The amount of collagen was reduced in fibrotic mice treated with ovo compared to those treated with vehicle alone (2.7 ± 0.9% vs 5.8 ± 1.2%, $p < 0\ 05$). Serum levels of liver enzymes, AST, ALT, and ALP were assayed to evaluate liver functionality. Levels of AST and ALT increased in

mice affected by hepatic fibrosis, whereas the treatment with ovo led to a significant reduction in AST and ALT levels (Figure 34 B). Conversely, serum ALP levels in mice with hepatic fibrosis did not significantly differ among the treatment groups.

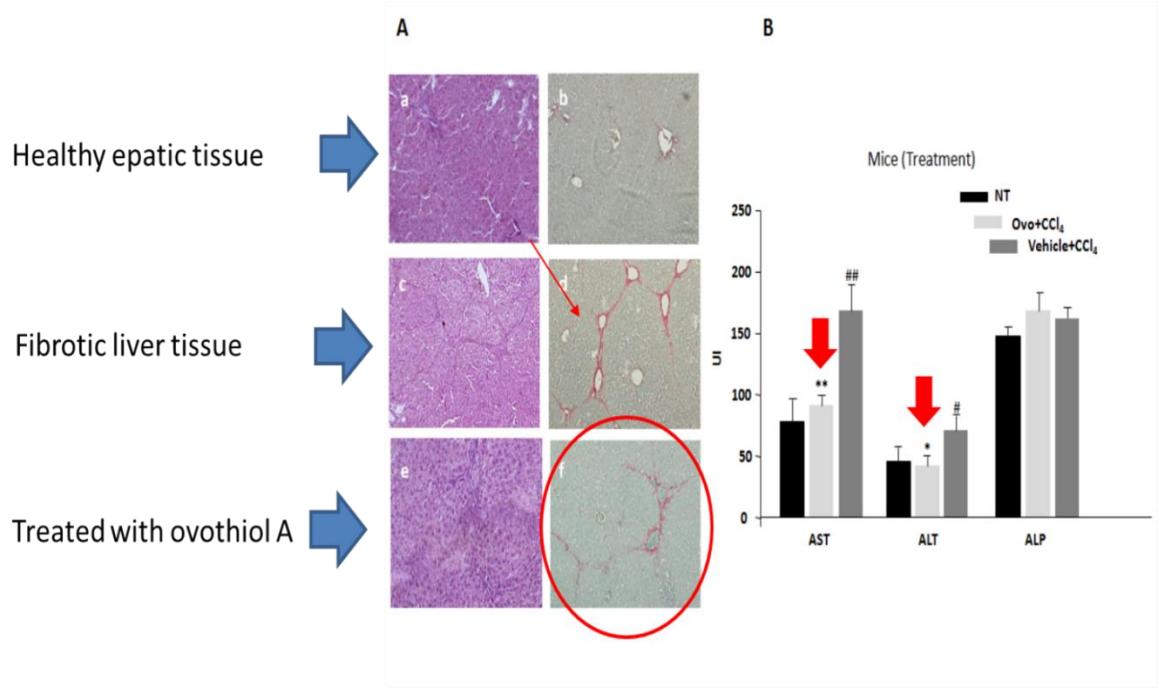

Figure 34. **Liver histology and serum biochemical parameters. (A)** Histological analysis. H&E staining and sirius red dye to highlight the collagen fibers of liver section: (a, b) healthy hepatic tissue; (c, d) fibrotic liver tissue induced by CCl_4; (E, F) liver tissue with hepatic fibrosis treated with ovo. (B) Evaluation of serum levels of liver enzymes. The levels of AST, ALT, and ALP were determined in the serum from mice affected by liver fibrosis and treated with ovo or control solution. Data are expressed as mean ± SD, n = 7. The significance was determined by the ANOVA and post hoc analysis: ($^{*}p < 0\ 05$) and ($^{**}p < 0\ 01$) represent significance compared to vehicle + CCl_4; ($^{\#}p < 0\ 05$) and ($^{\#\#}p < 0\ 01$) compared to non-treated (NT) healthy mice. (modified from Brancaccio et. al., 2018)

3.3.2. Ovothiol treatment influences the gene expression of biomarkers of liver fibrosis

To evaluate the transcript regulation of specific liver fibrotic markers, gene expression analysis was carried out by real-time qPCR on TGF-*β*, *α*-SMA, GGT, and fibrillary type collagen 1 (Col1a1) and compared to gene expression in healthy mice. A significant increase in gene expression for TGF-*β*, *α*- SMA, and Col1a1 was observed in mice affected by liver fibrosis and treated with vehicle compared to healthy mice (Figure 35), whereas no significant variation was shown for GGT expression levels. On the other hand, samples from mice treated with ovothiol A showed a slight but significant downregulation of mRNA of TGF-*β* and *α*-SMA, whereas the gene expression of Col1a1 and GGT were not affected.

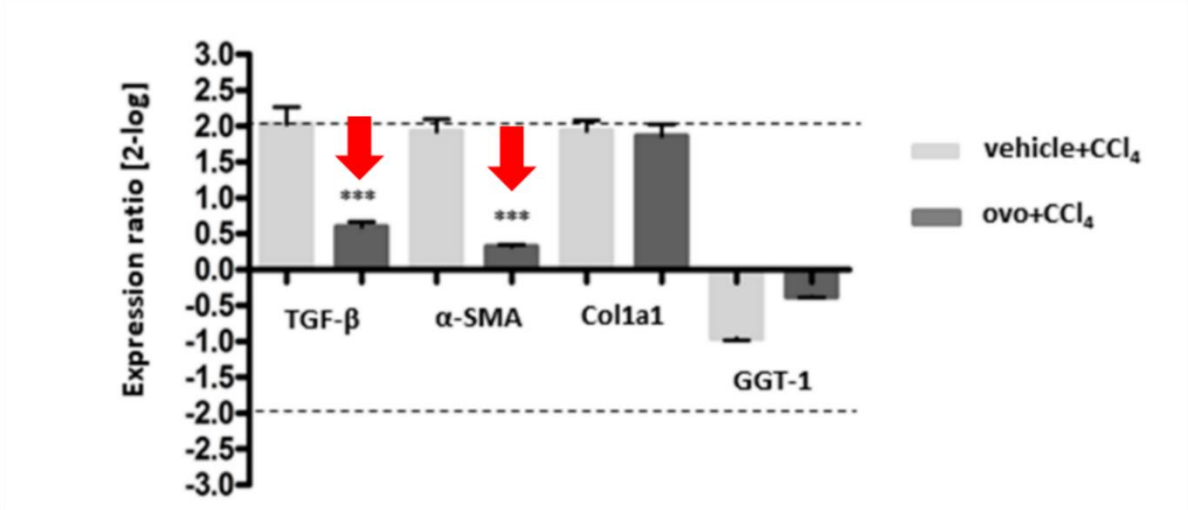

Figure 35. Gene expression analysis of markers of liver fibrosis by real-time qPCR. The levels of gene expression of the fibrotic markers in tissues after treatment with ovo or control solution were compared to tissues from healthy mice (reference baseline). Data were analyzed through the REST software, which considers fold differences ≥ +/−2 to be significant. (∗∗∗p < 0 001) represents the significance compared to the treated mice with vehicle + CCl4. (modified from Brancaccio et. al., 2018)

3.3.3. Ovothiol treatment affects protein expression of key players in liver fibrosis

The protein expression of the hepatic fibrogenic markers, TGF-*β*, *α*-SMA, and TIMP1 was evaluated by Western blot analysis (Figure 36A). In mice affected by liver fibrosis, the levels of TGF-*β*, *α*-SMA, and TIMP1 significantly increased compared to healthy mice. After treatment with ovo, the protein expression of TGF-*β*, *α*-SMA, and TIMP1 significantly decreased compared to mice with

hepatic fibrosis (Figures 36A–36D). In addition, the presence of GGT in the liver tissue was also evaluated by immunoblot of microsomal extracts containing membrane-bound GGT.

We decided to carry out this experiment to understand if ovo affected the protein expression of GGT. GGT is synthesised as a single 64 kDa precursor polypeptide, which undergoes self-proteolysis to form the mature protein composed of two subunits, the largest of which is around 50 kDa (Figure 37A). The antibody used in this study is directed against a peptide in the major subunit, therefore, it is able to recognise both the large subunit and the precursor. In the liver microsomal extracts of healthy mice, 62% of the total GGT was present in the mature form, while in the fibrotic tissues, the mature form significantly decreased to 36%. Conversely, the treatment with ovo induced an increase in mature protein up to 44% of the total content of GGT (Figures 37A and 37B). Finally, the presence of GGT was also evaluated in mice serum. In all three groups of mice, the serum contained only one band recognised by GGT antibody corresponding to the size of the large subunit of the mature form (Figure 37C).

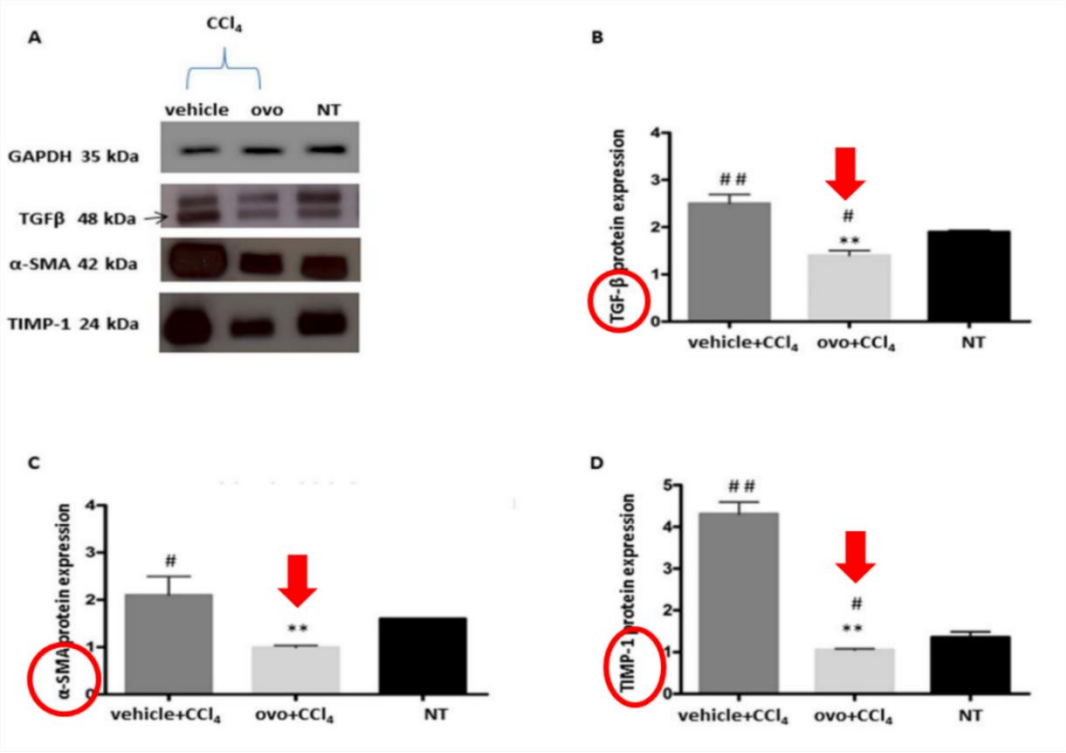

Figure 36. Protein expression of liver fibrosis markers. (A) A representative experiment of Western blot analysis of cytosolic extracts obtained from hepatic tissues of mice treated with ovothiol A or vehicle, after induction of liver fibrosis, compared to samples of healthy mice (NT), using antibodies specific for TGF-*β*, *α*-SMA, and TIMP1. Histograms of the densitometry analysis of protein bands obtained by Western blot for liver markers: **(B)** TGF-*β*; **(C)** *α*-SMA; and **(D)** TIMP1. Data were normalized for GAPDH. Data are expressed as mean ± SD, *n* = 7. The significance was determined by ANOVA test. (#*p* < 0 05) and (##*p* < 0 01) represent significance compared to NT; (∗∗*p* < 0 01) represents significance compared to the treated with vehicle + CCl_4. (modified from Brancaccio et. al., 2018)

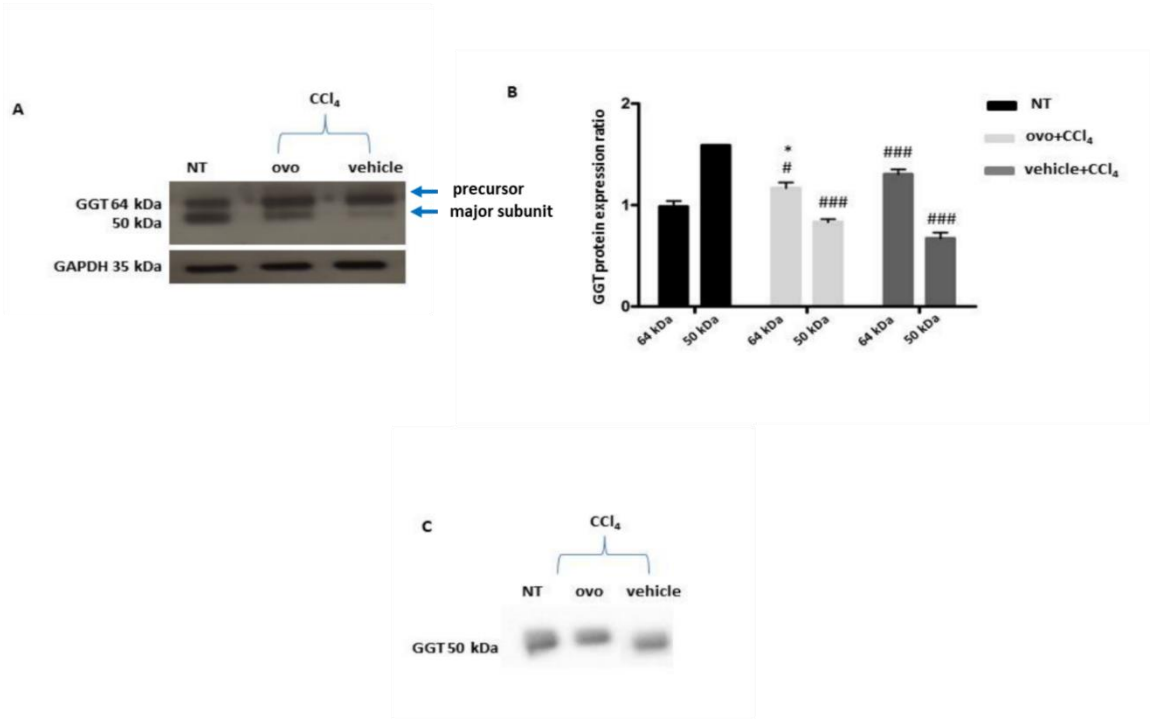

Figure 37. Protein expression of GGT. (A) Representative Western blot performed with GGT-specific antibody using microsomal extracts of hepatic tissues of mice with liver fibrosis treated with ovo or control solution compared to non-treated healthy mice (NT). **(B)** Histogram of the densitometric analysis of the GGT bands at 64 and 50 kDa. Data were normalized for GAPDH. **(C)** Representative Western blot performed on mice serum using GGT-specific antibody. Data are expressed as mean ± SD, $n = 6$. Statistical significance was determined by the one-way ANOVA test; (#$p < 0\ 05$) and (###$p < 0\ 001$) represent the significance compared to the corresponding NT band;($*p < 0\ 05$) represents the significance compared to fibrotic mice treated with control solution. (modified from Brancaccio et. al., 2018)

3.3.4. Ovothiol affects membrane-bound GGT activity

GGT activity was determined in liver microsomal extracts and normalised against the amount of the mature protein, which represents the active form of the enzyme, compared to the inactive precursor polypeptide (Castellano and Merlino 2012, 2013). GGT activity significantly increased in fibrotic tissues compared to healthy mice (Figure 38A). Treatment with ovo, on the other hand, induced a significant reduction in GGT activity. We also observed that the increase in GGT activity was very variable in the different mice affected by liver fibrosis, while the treatment with ovo reduced GGT activity at the physiological levels in all sick mice. Since GGT activity is closely related to GSH metabolism, we also evaluated total GSH levels in the hepatic tissues. As shown in figure 38B, total GSH levels increased in tissues from mice affected by liver fibrosis and treated with vehicle solution and decreased in liver tissues from mice treated with ovo.

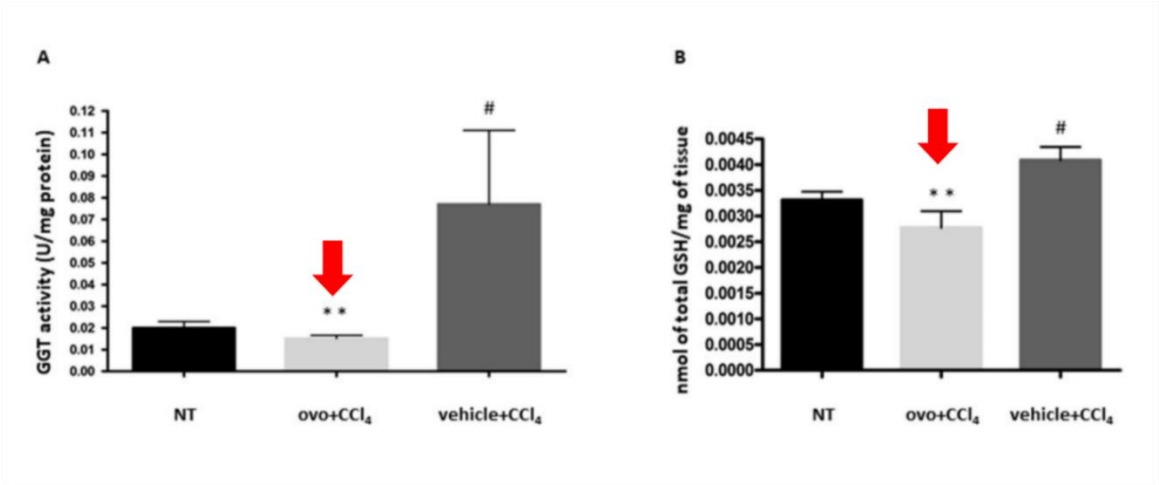

Figure 38. GGT activity and GSH content. (A) The enzymatic activity of GGT was evaluated on liver tissue microsomal extracts containing membrane-bound GGT. The activity of GGT was normalized compared to the mature protein band (50 kDa) detected by Western blot. **(B)** The levels of GSH were determined in hepatic tissue of mice treated with ovo or vehicle, after the induction of hepatic fibrosis, compared to samples of healthy tissue mice (NT). Data are expressed as mean ± SD, $n = 6$. The bars indicated the mean of 7 measures +/− SD (standard deviation). The significance was determined by the ANOVA and post hoc analysis: (#$p < 0$ 05) represents significance compared to healthy control; (∗∗$p < 0$ 01) represents significance compared to mice treated with vehicle + CCl4. (modified from Brancaccio et. al., 2018)

3.4. Discussion

In this study, to further investigate the effect of ovo in GGT-positive pathologies, we evaluated the effect of ovo in an *in vivo* model of liver fibrosis (Parsons et al., 2007; Puche et al., 2013). Since hepatic fibrosis is characterised by the accumulation of ECM and the activation of profibrogenic markers which result in the deposition of the collagene fibers (Novo et al., 2015), the reversion of the fibrotic phenotype is often associated with the eradication of the cause (abuse of alcohol, drugs and infectious microorganisms). If the cause of fibrosis is not removed in time, drug therapy is required to ameliorate the pathology (Schuppan and Kim 2013). Recent studies have shown that several sulfur-containing molecules can cause reversion of the fibrotic phenotype (D'argenio et al., 2010 and 2013; Schuppan and Kim 2013). In our study we decided to use a mouse model of liver fibrosis for two reasons, the first is that mouse is similar to human beings as regards development, physiology and genome, consequently the results obtained can then be translated to humans. Second, the studies conducted by Russo et al, had shown that treatment with ovo inhibited the proliferation of human hepatocellular carcinoma (HepG2) cells (Russo et al,2014). However, since hepatocarcinoma has an extremely severe prognosis, it was extremely interesting to investigate the action of ovo in an *in vivo* model of a pathological stage preceding liver cancer: like fibrosis. In addition, we decided to treat the mice with an introperitoneal injection of ovo at a single concentration because previous studies conducted by *Vamecq* and collaborators had shown that the introperitoneal injection of MFP-4MI (synthetic analogue of ovo) at a concentration of 50 mg/kg was not cytotoxic and produced no side effects in a mouse model of neurodegenerative disease (Vamecq et al., 2003). On the other hand, other types of administration of ovo were not documented in literature. Unfortunately, we had no possibility to treat mice affected by liver fibrosis with commercial inhibitors of GGT as positive controls, because these inhibitors were found to be cytotoxic (Ahluwalia et al., 1990; Lyons et al., 1990; Taylor et al., 1991). For the same reasons, the use of GGT knock-out mouse models could not be informative, because the elimination of GGT causes premature death of mice (Will et al.,2000).

In our study, ovo isolated from sea urchin eggs as disulphide and administered introperitoneally to mice at the dose of 50 mg/kgdemonstrated to be the form able to inhibit GGT activity. However, the

reduced form of ovo is unstable and it has ben reported that cells possess endogenous mechanisms to reduce ovo disulphide intracellulary (Vamecq et al., 2003).

Our results clearly indicate that ovo induced a significant reduction in the accumulation of collagen fibres in injured liver tissues associated with the reduction of serum levels of the liver enzymes AST and ALT (Figure 34).

In fact, in our experiments, ovo activated fibrinolytic processes on the extracellular matrix of ECM through the downregulation of various fibrotic markers (Figure 35). In particular, TGF-β, the most important profibrogenic cytokine, was significantly regulated by ovo at both gene and protein level (Figures 35 and 36B). Since TGF-β activation is essential for HSC activation and hepatic fibrogenesis, it is reasonable to deduce that a reduced expression of TGF-β, mediated by ovo, is consistent with a reduced amount of activated HSC, remodelling of the extracellular matrix and regeneration of liver function. The reduction of activated HSC after treatment with ovo was further confirmed by the reduction of the α-SMA protein isoform, which generally increases in acute liver disease while in normal liver is rarely detected. On the other hand, our results demonstrated that the administration of ovo had no effect on the gene regulation of Col1a1 (Figure 35). The deposition of this protein is responsible for the significant changes that occur in the ECM composition following liver damage and consequent alteration of the liver tissue anatomy. The reduction of the collagen fibres observed histologically was therefore probably caused by an indirect action exerted by ovo on the metalloproteinases and their inhibitors, which are involved in the degradation of the ECM and consequently in the inversion of the pathological phenotype. In fact, we found a higher protein expression of the TIMP1 metalloproteinase inhibitor in fibrotic tissues and a decrease after treatment with ovo (Figure 36C).

The analysis of the expression of GGT was more complex. At the transcriptional level, no change was evident. However, at protein level there was a clear difference between the precursor and its mature form (figure 37). Indeed, the mature and active form of GGT decreased in mice affected by fibrosis, whereas in mice treated with ovo it appeared to be comparable to healthy mice (Figure 37A and 37B). Finally, in the serum, only the mature form was detected (figure 37C). This finding suggests that the mature form is the only to be released in the extracellular milieu, while the precursor remains likely anchored to the membrane. This is particularly interesting because chronic

inflammation of the liver is known to cause damage to membranes resulting in the release of GGT into the blood (Yu et al., 2016), whose high serum levels are known markers of liver damage.

The main function of GGT is to regulate cellular homeostasis by catalysing the degradation of extracellular GSH and promoting the recycling of thiols within the cell (Castellano and Merlino 2012; 2013) (figure 39A). However, the regulation of enzymatic activity of GGT is crucial because, if on the one hand, GGT allows adequate use of the amino acids constituting new GSH, that has antioxidant properties, on the other hand, in the presence of transition metals such as iron [Fe (III)] and copper [Cu (II)], it can promote the formation of ROS in the extracellular environment. The balance between antioxidant and pro-oxidant function depends on the availability of metal ions, in particular of Fe (III), which promote the formation of ROS (figure 39B). It is known, that during hepatic fibrosis there is an increase in iron concentrations, thus causing an accumulation of ROS (Mehta et al., 2019).

The main targets of the ROS thus produced are both cell surface molecules (oxidation and thiolation of proteins, peroxidation of membrane lipids), and intracellular proteins sensitive to the redox state of the cell (e.g., nuclear factor-kappa B, activator protein 1) (Franzini et al., 2009; Whitfield J.B. 2001).

Here, we have shown that during the liver fibrosis process, the enzymatic activity of GGT as well as the GSH content increased in mice suffering from liver fibrosis; *viceversa*, in mice treated with ovo, we observed a decrease in both GGT activity and GSH content (figure 38A-B). These data confirm that *in vivo* ovo acts as an inhibitor of GGT activity, as demonstrated by our previous *in vitro* experiments with purified hGGT. By inhibiting the activity of GGT, ovo would prevent the accumulation of ROS thus avoiding cell damage. Consequently, this inhibition favours the reversion of the fibrotic phenotype.

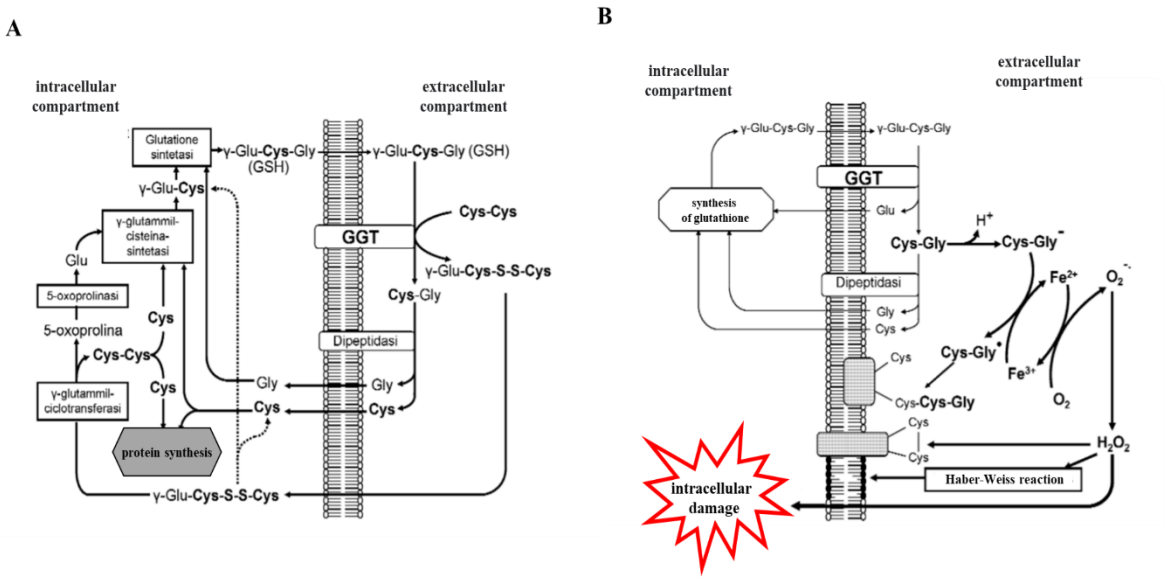

Figure 39. Enzymatic activity of GGT. (A) Extracellular degradation and intracellular resynthesis of glutathione (GSH) (γ-Glu-Cys-Gly, γ-glutamyl cycle). **(B)** Pro-oxidant activity of GGT in the presence of Fe^{3+} in the extracellular environment. (modified from Franzini et al.,2009)

3.5. Conclusions and perspectives

Currently, the pharmacological treatments to eradicate liver fibrosis are not considered to be highly efficient. Our study indicates that treatment with ovo significantly ameliorate liver fibrosis induced by repeated intraperitoneal injection of CCL_4, used to induce the deposition of the ECM and the activation of the profibrogenic cytokines. We demonstrated that, ovo inhibits the enzymatic activity of GGT and consequently affects the metabolism of GSH. This could be the specific mechanism by which ovo negatively regulates redox homeostasis and the activation of key fibrotic markers, TGF-β, α-SMA and TIMP1, which ultimately leads to a significant degradation of collagen fibres in the ECM (see diagram in figure 40).

Our study highlights that the inhibition of GGT by ovo could block the evolution of liver fibrosis. Overall, these results suggest that ovo can be considered a new class of sulfur-containing molecules with antifibrotic properties and possible applications as drugs or food supplement for the treatment of chronic liver inflammation and GGT positive pathologies.

Finally, recent studies have highlighted the discovery of dynamic epigenetic markers of fibrosis detectable in the plasma of patients with chronic liver disease that may be useful in the non-invasive diagnosis and staging of fibrosis (Yiğit et al., 2018). It would therefore be interested in future studies, to evaluate whether ovo treatment can affect these markers, causing epigenetic changes. At the same time, it would be interesting to evaluate the methylation of free circulating DNA (cfDNA). cfDNA are degraded DNA fragments released into the blood plasma. cfDNA can be used to describe various forms of DNA that freely circulate in the bloodstream, including circulating tumor DNA, cell-free mitochondrial DNA, and cell-free fetal DNA, which is now also extremely useful in pancreatic or breast cancer (Brancaccio et al.,2019; Jeschke et al., 2012).

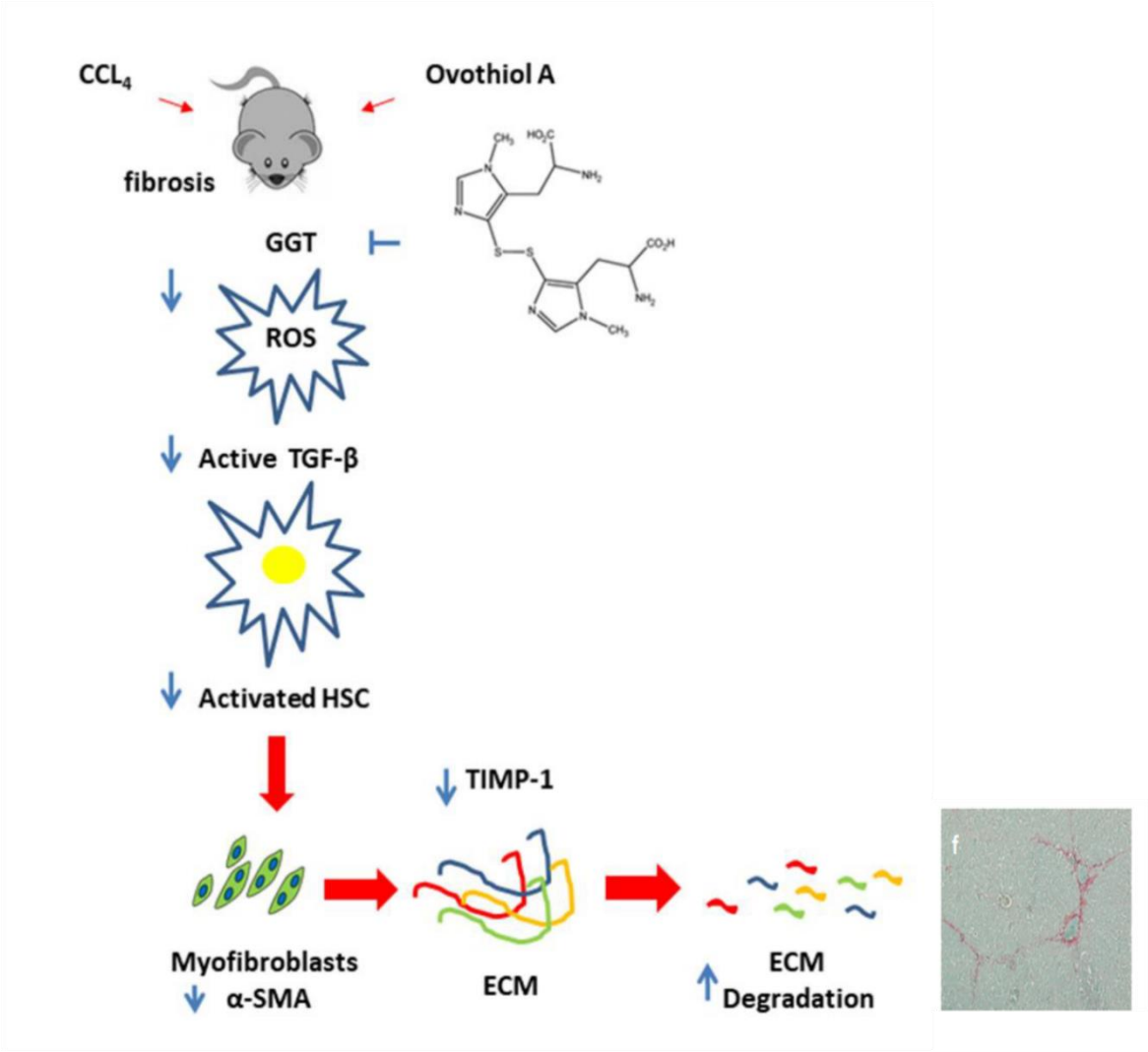

Figure 40. Proposed mechanism of action for ovothiol. During the development of liver fibrosis, membrane-bound GGT activity increases, leading to ROS overproduction. ROS can activate TGF-β, which in turn upregulates α-SMA and TIMP1, favouring ECM deposition. Ovothiol acts as a GGT inhibitor and in turn reduces TGF-β activation, thus inducing a cascade of events leading to downregulation of profibrogenic molecules and induction of fibrolytic enzymes. (modified from Brancaccio et. al., 2018)

CHAPTER 4

Dermo-protective properties of marine 5-thiohistidines

4.1. Aims of the study

Skin tissue is the largest organ in the human body. The skin is our outermost barrier and is therefore exposed to a high number of pathogenic microorganisms (Scudiero et al., 2020) and external insults such as UV rays (D'Orazio et al., 2013), consequently it represents the first line of defense of the human body. Numerous skin diseases arise in concomitance with a widespread inflammatory state, such as: psoriasis, dermatitis, infections caused by pathogenic microorganisms (*Candida albicans* or *Staphylococcus aureus*) and lesions caused by excessive exposure to UV rays. The common denominator of these pathologies is the cascade of pro-inflammatory cytokines that are activated post damage (Figure 40). The skin tissue has numerous sentinels of the immune system i.e. macrophages, lymphocytes T $CD4^+$ and dendritic cells (Figure 41) (Bangert and Brunner 2011) which, once activated, release the interleukins (IL-6, IL-8 and IL-β1) and induce an accumulation of TNF-α. TNF-α in turn mediates the activation of the nuclear factor NF-κB, thus causing an increase in the expression of pro-inflammatory genes. In this scenario, a fundamental role is played by protein kinases activated by MAPKs, which during inflammation can cause the accumulation of ROS and the dysregulation of skin homeostasis. ERK is a member of the MAPK family and it is involved in numerous cellular processes including proliferation, growth, differentiation, cell migration, cell survival, metabolism and transcription (Lu and Malemud 2019). ERK1/2 is activated (i.e. phosphorylated) in the cytosol and subsequently translocated to the nucleus, where it activates transcription factors (Lu and Malemud 2019). The perturbation of ERK 1/2 signalling is implicated in many pathological conditions, like cancer, arthritis, chronic inflammation and osteoporosis (Lu and Malemud 2019). Other members of MAPK family are the C-Jun N-terminal kinases, which consist of ten isoforms derived from three genes: JNK1 (four isoforms), JNK2 (four isoforms) and JNK3 (two isoforms) (Waetzig and Herdegen 2005). Each gene is expressed as a protein kinase of 46 kDa or 54 kDa, depending on how the 3 'coding regions of the corresponding mRNA is processed. No functional differences have been documented between the 46 kDa and 54 kDa isoform, however, a second form of alternative splicing occurs within the transcripts of JNK1 and JNK2, producing JNK1-α, JNK2-α and JNK1-β and JNK2 -β. Like ERK, JUN 1/2/3 are also involved in numerous biological processes such as differentiation, apoptosis and autophagy (Lu and Malemud 2019).

It is known that ROS production can downstream regulate Nrf-2, a transcription factor that in the absence of inflammatory stimuli is linked to Kelch -like ECH-associated protein 1 (Keap-1) and is found in the cytosol in an inactive form (Ahmed et al., 2016). In case of damage, Nrf-2 migrates into the nucleus, binds to small musculoaponeurotic fibrosarcoma protein (sMaf) and induces the transcription of detoxifying genes (Kaspar et al., 2009; Kim et al., 2010), thus inactivating the expression of pro-inflammatory genes (Figure 41) (Ahmed et al., 2016). The therapies currently in use in the case of skin disease include cortisone-based drugs (Uva et al., 2012) and in the case of a concomitant bacterial infection the administration of antibiotics (Scudiero et al., 2020).

Previous studies have shown that erg can inhibit the activation of pro-inflammatory cytokines and stimulate the migration of Nrf-2 into the nucleus, inhibiting the cascade of events of the inflammatory process caused by UV rays (Hsue et al., 2015). In addition, Markova et al. pointed out that skin cells and tissues are able to use erg as an antioxidant in their defence systems (Markova et al., 2008).

Previous experiments showing that ovo, purified from sea urchin *P. lividus* eggs, exhibits anti-inflammatory activity in an *in vitro* model of human endothelial cells (Castellano et al., 2018) and in an *in vivo* model of liver fibrosis (Brancaccio et al., 2018), prompted us to consider 5-thiohistidines as promising bioactive compounds to be used as dietary supplements or new drugs to prevent or cure human inflammatory diseases (Castellano and Seebeck 2018).

Therefore, another objective of my PhD thesis was to evaluate the effect of 5-thiohistidines and its methylated derivatives upon induction of inflammation of human skin tissues. To this aim, we used both an *in vitro* model of human keratinocytes (HaCat) and an *ex-vivo* model of human skin tissues in order to test the cytotoxicity of ovo, 5-thio and erg and their anti-inflammatory properties. In addition, in order to highlight the molecular mechanisms underlying such properties, we evaluated the gene expression of IL-6, IL-8, TNF-α and COX-2. Moreover, we measured the release of IL-6, IL-8 and TNF-α. Finally, we assessed the protein expression of ERK, JNK and Nrf2. Overall, our experiments provide novel information on the efficacy of 5-thiohistidines as new anti-inflammatory molecules against human skin disorders.

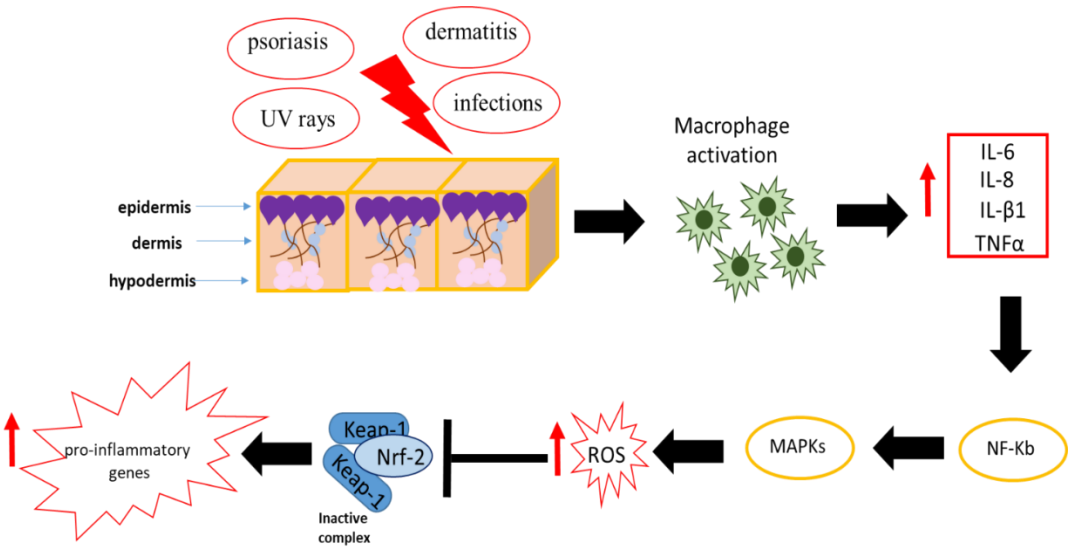

Figure 41. **Pathogenesis of skin disorders**. The skin receives external stimuli that cause the activation of macrophages, which activate the release of pro-inflammatory cytokines IL-6, IL-8, IL-β1 and TNF-α. The activation of TNF-α promotes the activation of NF-kb, which downstream activates the MAPKs. The activated MAPKs generate an increase in ROS, which inhibits the transfer of Nrf-2 to the nucleus, thus promoting the transcription of pro-inflammatory genes and consequently the skin damage.

4.2. Materials and methods

4.2.1. Cell cultures

The immortalised human skin keratinocyte cell line (HaCaT cells) was kindly provided by Prof.ssa Tiziana Angrisano (Department of Biology, University of Naples Federico II). HaCaT cells were maintained at 37 °C in a humidified atmosphere of 95% air and 5% CO_2 in Dulbecco's Modified Eagle Medium (DMEM; Gibco) supplemented with 10% of heat-inactivated Fetal Bovine Serum (FBS; Gibco), 1% glutamine and 1% antibiotics (100 U/ml Penicillin and 100 µg/ml Streptomycin; Gibco).

4.2.2. Human skin tissues sampling

The tissues were taken from patients undergoing cosmetic surgery at the Centro Hospitalar Universitário Lisboa Norte, Lisbon, Portugal. This study was approved by the Ethic Committee of the hospital. All principles of the Declaration of Helsinki were followed and written informed consent was obtained from all patients. Explanted tissues were set for 3h at 37 °C in a humidified atmosphere of 95% air and 5% CO_2 in Dulbecco's Modified Eagle Medium (DMEM; Gibco) supplemented with 10% of heat-inactivated Fetal Bovine Serum (FBS; Gibco), 1% glutamine and 1% antibiotics (100 U/ml Penicillin and 100 µg/ml Streptomycin; Gibco). The tissues were then cut with a biopsy punch to obtain 4mm fragments, which were incubated for 2h at 37 ° C in a humidified atmosphere as reported above. After that, we pre-treated the tissues with ovo, 5-thio, erg, and dexamethasone (DMX) at different concentrations for 24h. Subsequently, to induce inflammation, the tissues were treated with interleukin β1 (IL-β1) (Cat#200-01B, PeproTech) at a concentration of 10 ng/ml for other 24 h.

4.2.3. Cell viability assays

To test the cytotoxicity of the molecules, HaCat cells were plated in 384-multiwell plates (2×10^3 cell/well) by a pipetting robot (Freedom Evo-2 200 Liquids Handler, Tecan, Männedorf, Switzerland) and treated with ovo, 5-thio, and erg, at the indicated concentrations for 24, 48 and 72h. Cell viability was assessed by resazurin-based assays (CellTiter-Blue® Cell Viability Assay, Promega, Madison, WI, USA) according to the manufacturer's recommendations using a Spark® multimode microplate reader (TECAN). The fluorescence was measured at $560_{Ex}/590_{Em}$ nm. All experiments were performed in triplicate. The effect of molecules, on cell viability was assessed as the percentage of viable cells compared with not-treated control cells, which were arbitrarily assigned aviability of 100%. To test the anti-inflammatory activity of the molecules, HaCat cells were plated in 96-well plates (5×10^3 cell/well), pre-treated with ovo, 5-thio and erg at the indicated concentrations for 24h, and incubated with TNF-α at four different concentrations (1, 2, 5 and 10 ng/ml) for 24h to induce inflammation. Cell viability was assessed by CellTiter 96® Non-Radioactive Cell Proliferation Assay (MTT) (Promega, Madison, WI, USA). The absorbance was measured at 540 nm using the microplate reader. The effect of TNF-α on cell viability was assessed as the percentage of viable cells compared with the not-treated control cells, which were arbitrarily assigned aviability of 100%. All experiments were performed in triplicate. We decided to perform the resazurin test, after treatment with the compounds alone to evaluate cell viability and to test compounds cytotoxicity. Instead, to test the protective capacity of our molecules after the induction of the inflammatory process by TNF-α treatment, we performed as cell viability test the MTT assay that evaluates the metabolic capacity of living cells.

4.2.4. RNA Extraction and cDNA Synthesis

Total RNA was extracted from the skin fragments (three skin fragments/sample) by mechanical homogenisation with Ultra Turrax in Trizol Reagent according to the manufacturer's protocol (Life Technologies). The amount of total extracted RNA was estimated measuring the absorbance at 260nm and the purity by 260/280 and 260/230nm ratios by Nanodrop (ND-1000 UV-Vis Spectrophotometer; NanoDrop Technologies). The integrity of RNA was evaluated by agarose gel electrophoresis. For each sample, 1000 ng of total RNA were retro-transcribed with iScriptTM cDNA synthesis kit (Bio-Rad), following the manufacturer's instructions.

4.2.5. Gene Expression by Real-Time qPCR

For real-time qPCR experiments, the data from each cDNA sample were normalised using the human housekeeping gene RLP0 (ribosomal protein lateral stalk subunit P0). The specific primers used for amplification of RLP0, IL-6, IL-8, TNF-α and COX-2 were designed based on the nucleotide sequences downloaded by NCBI database (accession numbers) using Primer3WEB v.4.0.0. RLP0 primer forward 5'-TGGCAGCATCTACAACCCTG-3', primer reverse 5′-GACAAGGCCAGGACTCGTTT-3'; IL-6 primer forward 5'- CATCCTCGACGGCATCTCAG-3', primer reverse 5′- TCACCAGGCAAGTCTCCTCA-3'; IL-8 primer forward 5'-AAACCCAGGTGAGAGCTG-3', primer reverse 5′-TCTGAGATCCCGTCAGAGC-3'; COX-2 primer forward 5'-ATGATTGCCCGACTCCCTT-3', primer reverse 5′-ACTGATGCGTGAAGTGCTGG-3'; TNF-α primer forward 5'-CAAGGACAGCAGAGGACCA-3', primer reverse 5′-CGTCCCGGATCATGCTTTCA-3'. A final concentration of 1.4 pmol/μL for each primer, 1μL of 1:10 diluted cDNA having initial concentration of 1 μg and 1 FastStart SYBR Green Master Mix (total volume of 10 μL) were used for the reaction mixture. PCR amplifications were performed in a ViiATM 7 real-time PCR system (Applied Biosystems) thermal cycler using the following thermal profile: 95°C for 10 min, one cycle for cDNA denaturation; 95°C for 15 sec and 60°C for 1 min, 40 cycles for amplification; 72°C for 5 min, one cycle for final elongation; and one cycle for melting curve analysis (from 60°C to 95°C) to verify the presence of a single product.

Each assay included a no-template control for each primer pair. Specificity of amplification reactions was verified by melting curve analysis. The efficiency of each primers pair was calculated according to standard method curves using the equation $E = 10^{-1/slope}$. At least three serial dilutions 1:2, 1:10 and 1:100 were set up to determine Ct values and reaction efficiencies for all primer pairs. Standard curves were generated for each oligonucleotide pair using the Ct values versus the logarithm of each dilution factor, and PCR amplifications were performed in a ViiATM 7 real-time PCR system (Applied Biosystems) thermal cycler using the standard protocol described above. All real-time qPCR reactions were carried out in triplicate. The expression of the genes was analysed and normalised to RLP0 as housekeeping gene and not-treated samples as control condition using relative expression software tool (REST) software based on the Pfaffl method (2002). Relative expression ratios approaching two cycles were considered significant. Experiments were repeated at least three times.

4.2.6. Western blot analysis

HaCaT cells (5 x 10^5 cells/well) were seeded in 6-well plates and pre-treated with our compounds ovo, 5-thio and erg at a concentration of 2 μM for 24 h and subsequently exposed to TNF-α at a concentration of 10 ng/ml for another 24 h. Cells were then washed with cold PBS and resuspended in RIPA lysis buffer (1X) containing a 50 mM Tris-HCl (pH 7.6), 150 mM NaCl, 5 mM EDTA, 0.5% NP-40, 0.5% Sodium deoxycholate, 10% SDS, phosphatase, and protease inhibitor cocktail (Roche). Cell homogenates were centrifuged at 13,000 x g for 5 minutes at 4 ° C, and the obtained supernatant was used as the total extract. The protein content was determined with the Bio-Rad protein assay reagent using bovine serum albumin as standard. The samples were run on 12% SDS/polyacrylamide gel according to Laemnli. Following electrophoresis, proteins were transferred onto a PVDF (Millipore) membrane (Bio-Rad Trans-Blot Apparatus) and detected using a rabbit anti-ERK polyclonal antibody (Cell Signaling, #9102S) diluted 1:1000 in milk 5%, rabbit anti-phospho-ERK polyclonal antibody (Cell Signaling, #4370S) diluted 1:1000 in non-fat dried milk 5% (milk), rabbit anti-JNK polyclonal antibody (Cell Signaling, #9252) diluted 1:1000 in milk 5%, rabbit anti-phospo-JNK polyclonal antibody (Cell Signaling, #9251) diluted 1:500 in milk 5%, and as an internal control

the mouse anti-β-Actin monoclonal antibody (Santa Cruz Biotechnology, USA) diluted 1:1000 in milk 5%. All primary antibodies were incubated at 4°C overnight. The appropriate secondary antibody anti-mouse (NA931VS, Amersham ECL Mouse IgG, HRP-linked whole Ab from Citeab) diluted 1:10000 in milk 5% and anti-rabbit (GtxRb-003-DHRPX, Immunoreagents) diluted 1:10000 in Milk 5% were added at 37 °C for 1h and immunoreactive proteins were detected using the ECL (WesternBrightTM detection kit ECL, Advansta, USA) according to the manufacturer's instructions. Protein expression levels were analysed by means of densitometric analysis using the Image J software.

4.2.7. Preparation of cytosolic and nuclear extracts

HaCaT cells (5 x 10^5 cells/well) were seeded in 6-well plates, pre-treated with our compounds ovo, 5-thio and erg at a concentration of 2 μM for 24 h and then treated with TNF-α at a concentration of 10 ng/ml for other 24 h. Cells were then washed with cold PBS and resuspended in lysis buffer containing 10 mM Hepes (pH8.0), 0.1 mM EDTA, 10 mM KCl, 100 mM EGTA, 1mM DTT, 2.0 mg/mL leupeptin, 2.0 mg/mL aprotinin, NP-40 10%, phosphatase and protease inhibitor cocktail (Roche). The cells were allowed to swell on ice for 15 min. The samples were vortexed every 5 min for 20 min. The homogenates were centrifuged for 5 min at 12.000 g and the supernatant was used as the cytosolic extract. The nuclear pellet was resuspended in cold extraction buffer containing 20 mM Hepes (pH8.0), 1mM EDTA, 400 mM NaCl, 1mM EGTA, 1mM DTT, 2.0 mg/mL leupeptin, 20 mg/mL aprotinin, phosphatase and protease inhibitor cocktail (Roche). The samples were centrifuged at 15.000 g for 30 min and the obtained supernatant was used as the nuclear extract. The cytoplasmic and nuclear protein content was determined with the Bio-Rad protein assay reagent using bovine serum albumin as standard. Samples were run on 12% SDS/polyacrylamide gel according to Laemmli. Following electrophoresis, proteins were transferred onto a PVDF (Millipore) membrane (Bio-Rad Trans-Blot Apparatus) and detected using a mouse anti-Nrf2 monoclonal primary antibody (Santa Cruz Biotechnology, sc-365949) diluted 1:100 in MILK 5%, and as an internal controls mouse anti-Histone H3 monoclonal primary antibody (Cell Signaling, #3638) diluted 1:500 in milk 5% and mouse anti-β-Actin monoclonal antibody (Santa Cruz Biotechnology,

USA) diluted 1:1000 in milk 5%. The incubation with antibodies and the detection of immune-positive bands were performed as described above.

4.2.8. Nrf2 Immunofluorescence

HaCaT cells were plated in 96-well plates 5 x 10^4 cells/well). After treatments, cells were washed with 1X PBS (Phosphate Buffer Saline, Gibco) and then fixed with 4% paraformaldehyde for 10 min. After three washes in 1X PBS, cells were permeabilised with 0.5% Triton X-100 for 10 min and washed with 1X PBS. Cells were then blocked with 10% FBS (Gibco) in 1X PBS for 30 min and then incubated overnight at 4 °C with anti-Nrf2 mouse monoclonal primary antibody (Santa Cruz Biotechnology, sc-365949) diluted 1:250 in 1.5% FBS. Cells were then washed three times with 1X PBS and then incubated with goat anti-mouse (Abcam, Alexa Fluor 488, ab150113) secondary antibodies for an additional 1h, diluted 1:500 in 1.5% FBS. Then, cells were stained with 1 µg/mL DAPI (Life Technologies) for 10 min. Cells were examined with the DMI600 (Leica) fluorescence microscope and photographed using a DFC360-FX camera (Leica). Images were analyzed with ImageJ software to select Nrf2-positive cells. . The percentage of Nrf2 positive cells was obtained by normalizing the total number of nuclei to the Nrf2 positive nuclei. Each experiment was performed in triplicate.

4.2.9. ELISA Assay

Fragments of *ex-vivo* human skin tissues (4 mm diameter each) were plated in 24-multiwell plates (4 fragments/well), pre-treated with ovo, 5-thio and erg at the indicated concentrations for 24h, and incubated with IL-β1 (10 ng/ml) for 24h to induce inflammation. Conditioned media were collected and analysed for IL-6, IL-8 and TNF-α content through ELISA test (Human IL-6, IL-8 and TNF-α Standard ABTS ELISA Development Kit; PEPROTECH, USA) according to manufacturer's recommendations. Three fragments/condition were collected for RNA and protein extraction, stored at -80°C until use.

4.2.10 Statistical Analysis

All statistical analyses were performed using the GraphPad Prism 4 software (GraphPad Software Inc., La Jolla, USA). All data are the results of at least two independent experiments carried out in triplicate. Data were expressed as the mean ± standard deviation. Comparisons among groups were made by Student's t test. Values of $p < 0.05$ were considered as significant.

4.3. Results

4.3.1. Thiohistidine compounds are not cytotoxic on HaCat cells

To test the cytotoxicity of ovo, 5-thio and erg on human keratinocytes, the viability of HaCat cells was assessed following treatment for 24, 48 and 72h with these compounds at concentrations of 2, 5, 10, 50 and 100 µM. The results showed that ovo, 5-thio and erg were not cytotoxic at all the concentrations tested (Figure 42 A-C). Indeed, they induced a slight increase or decrease in cell viability at low or high concentrations, respectively (Figure 42 A-C).

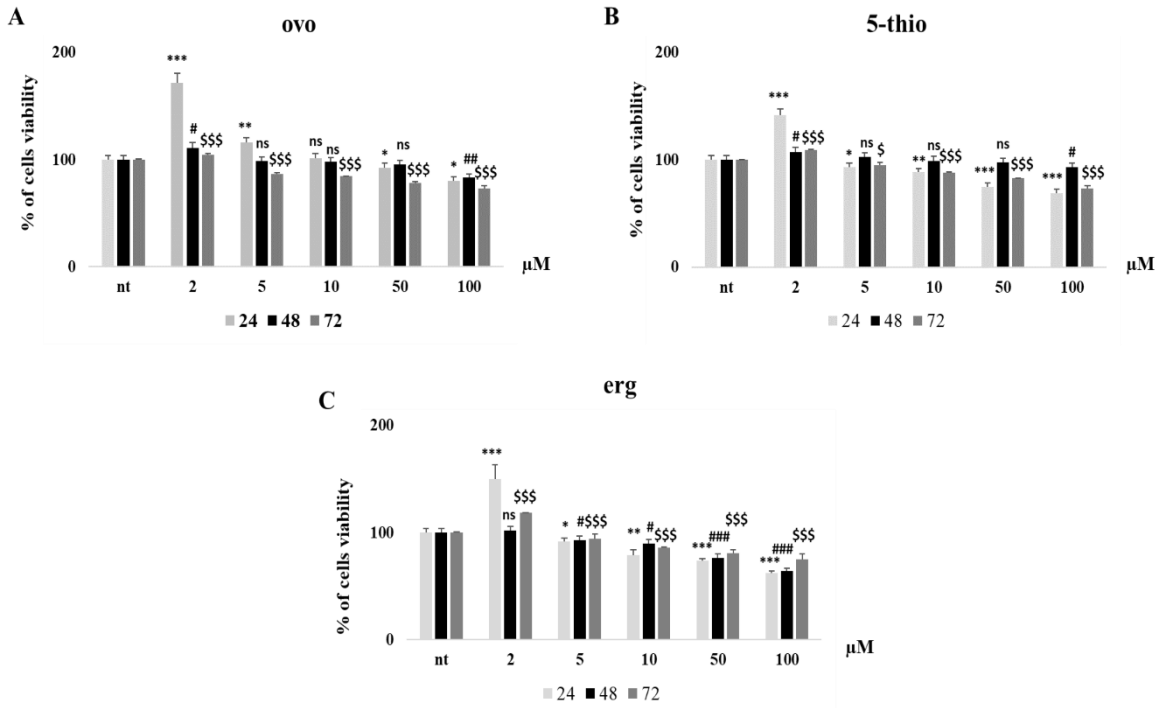

Figure 42. Cytotoxicity activity on HaCat cells. A) ovo, B) 5-thio and C) erg. Cells were treated for 24, 48 and 72h with **A)** ovo, **B)** 5-thio and **C)** erg. at five different concentrations (2, 5, 10, 50 and 100 µM) and cell viability was measured by a resazurin-based assay. Data are expressed as mean ± SD (standard deviation), *n* = 3. The significance was determined by the *t*-test student: * ($p < 0.05$), ** ($p < 0.01$) and *** ($p < 0.001$) represent significance compared to NT 24h (non-treated) control; $^{\#}$ ($p < 0.05$), $^{\#\#}$ ($p < 0.01$) and $^{\#\#\#}$ ($p < 0.001$) represent significance compared to NT 48h control; $^{\$}$ ($p < 0.05$), $^{\$\$}$ ($p < 0.01$) and $^{\$\$\$}$ ($p < 0.001$) represent significance compared to NT 72h.

4.3.2. Anti-inflammatory activity on HaCat cells

To understand if pretreatments with ovo, 5-thio and erg could protect human keratinocytes from inflammation, we pre-treated HaCat cells with these molecules at concentrations of 2, 5 and 10 µM for 24h. Then we induced inflammation by treating the cells with TNF-α at concentrations of 1, 2, 5 and 10 ng/ml for additional 24h and assessed cell viability by MTT assay (Figure 43 A-D). TNF-α-mediated inflammation caused a slight but significant reduction of viability at concentrations of 2, 5, and 10 ng/mL (Figure 43 B-D). On the other hand, pre-treatment with the molecules protected the cells from a decrease in viability caused by TNF-α (Figure 43 A-D). Finally, we highlighted an increase in viability following pretreatment with low concentration molecules compared to cells treated with TNF-α (Figure 43 B-D).

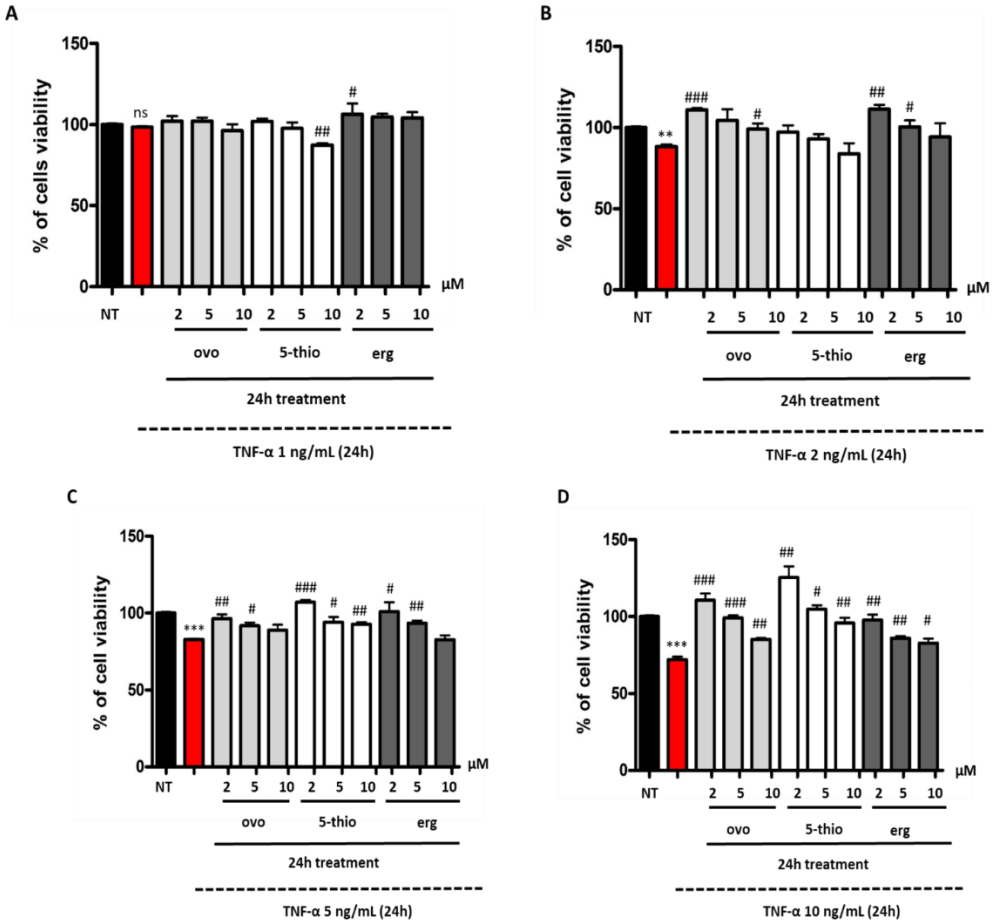

Figure 43. Anti-inflammatory activity on HaCat cells. Cells were pre- treated for 24h with ovo, 5-thio and erg at three different concentrations (2, 5 and 10 µM) and inflammation was stimulated for 24h with TNF-α at 1 **(A)**, 2 **(B)**, 5 **(C)** and 10 **(D)** ng/ml. Cell viability was measured by MTT assay. Data are expressed as mean ± SD, *n* = 3. The significance was determined by the t-test student: * ($p < 0.05$), ** ($p < 0.01$) *** ($p < 0.001$) represent significance compared to NT; $^{\#}$ ($p < 0.05$), $^{\#\#}$ ($p < 0.01$) $^{\#\#\#}$ ($p < 0.001$) represent significance compared to TNF-α treated cells. In all graphs, the red bar indicates the cells treated with TNF-α.

4.3.3 Effect of 5-thiohistidines on protein expression of key players in skin inflammation

To understand whether the pre-treatment with ovo, 5-thio and erg could affect the protein expression of MAPKs upon inflammation, we evaluated ERK and JNK phosphorylation by western blot analysis at the lowest effective concentration (2μM) of the compounds (Figures 44 A-C). The signals of p-ERK and p-JNK were normalised against the un-phosphorylated ERK and JNK (Figures 44 A-D).

The protein expression of ERK, normalized against β-actin, did not significantly vary in any sample after the treatments. From the densitometric analysis of p-ERK, we observed an increase of intensity of both bands (42 and 44 kDa) when the HaCats were treated with only TNF-α compared to not treated cells (NT) (Figures 43 B). In cells pre-treated with ovo, we observed a significant decrease in the protein expression of p-ERK for both bands (42 and 44 kDa) when compared with bands in cells treated only with TNF-α (Figure 43B). On the other hand, pre-treatment with 5-thio induced a significant increase of the 44 kDa band when compared to the cells treated only with TNF-α (Figure 43 B). An opposite trend was observed in the presence of erg pre-treatment with a significant decrease of intensity only of the 42 kDa band compared to cells treated only with TNF-α (Figure 44 B).

Furthermore, we also evaluated the protein expression of JKN, using β-actin as normaliser (Figure 43C). We chose β-actin as a normalizer because a recent study conducted by Riemer et al, showed that β-actin was found to be a good housekeeping in keratinocytes, being extremely stable even if they are stimulated with interferon-γ (Riemer et al., 2013). Also Hsue et al, when testing the use of erg in human keratinocytes exposed to UV, used β-actin (Hsue et al., 2015). Unfortunately, since the band recognized by β-actin overlaps at some extent with those of ERK and JNK, we were compelled to load different gels to monitor the different proteins.

In the case of JNK, we observed an increase in both bands (46 kDa and 54 kDa) in cells treated with TNF-α alone when compared to NT cells (Figure 44D). The increase in both bands (46 kDa and 54 kDa) also occurs in cells subjected to pre-treatment with 5-thio and erg (Figure 44D) when compared with NT; while in the cells subjected to pre-treatment with ovo we observed a slight decrease in band of 54 kDa when compared with NT (Figure 44D). Moreover, the increase of both bands (46 kDa and 54 kDa) in the cells subjected to pre-treatment with 5-thio and erg is not significant when compared

with TNF-α (Figure 44D). In addition, we observed also a significant decrease in both bands (46 kDa and 54 kDa) in cells pre-treated with ovo when compared with stimulation with TNF-α alone (Figure 44D).

Regarding the p-JNK protein expression, normalised against JNK content, both the band at 46 kDa and 54 kDa were not detected in cells treated with TNF-α as well as in NT cells (Figure 44D). Also after the pre-treatment with ovo, we did not observe the appearance of the p-JNK bands, whereas the pre-treatment with 5-thio and erg induced the phosphorylation of both bands of p-Jun. (Figure 44D).

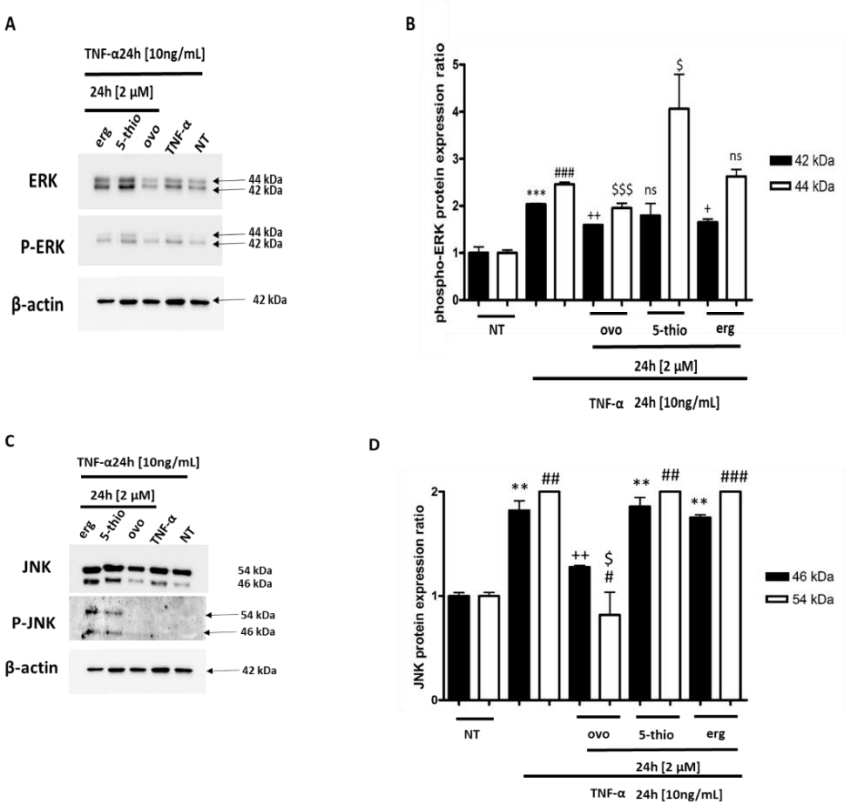

Figure 44. Protein expression of MAPKs signaling. (A) and **(C)** Representative experiments of Western blot analysis of cytosolic extracts obtained from HaCat cells pre-treated for 24h with ovo, 5-thio and erg at concentration of 2μM and stimulated for 24h with TNF-α at 10 ng/mL to induce inflammation. **(B-D)** Histograms of the densitometry analysis of protein bands obtained by Western blot using ImageJ software. **(B)** Data of P-ERK were normalized against ERK. **(D)** Data of JNK were normalized against β-actin. Data are expressed as mean ± SD, *n* = 3, the significance was determined by the t-test student. **(B)** *** ($p < 0.001$) represent significance compared to NT band at 42 kDa; ### ($p < 0.001$) represent significance compared to NT band at 44 kDa; + ($p < 0.05$), ++ ($p < 0.01$) represent significance compared to TNF-α treatment band at 42 kDa and $ ($p < 0.05$), $$$ ($p < 0.001$) represent significance compared to TNF-α treatment band at 44 kDa. **(D)** ** ($p < 0.01$) represent significance compared to NT band at 46 kDa; # ($p < 0.05$), ## ($p < 0.01$) and ### ($p < 0.001$) represent significance compared to NT band at 54 kDa; ++ ($p < 0.01$) represent significance compared to TNF-α treatment band at 46 kDa; $ ($p < 0.05$) represent significance compared to TNF-α treatment band at 54 kDa.

4.3.4 5-thiohistidines promotes Nrf2 nuclear translocation in human skin disease

To determine whether the pre-treatment with ovo, 5-thio and erg could mediate the nuclear translocation of Nrf-2, we evaluated both the cytoplasmic and nuclear fractions by western blot (Figures 45A-B). In this case, the cytoplasmic fraction was normalised against β-actin, while the nuclear fraction was normalised against Histone 3 (Figures 45A-B). The results showed a slight decrease of Nrf-2 at the cytoplasmic level and no significant nuclear variation in cells treated with TNF-α alone when compared with NT (Figure 45B). When HaCat cells were pre-treated with our molecules, a slight accumulation of Nrf-2 at the cytoplasmic level with a concomitant greater accumulation of Nrf-2 in the nucleus were observed when compared both to NT and to cells treated only with TNF-α (Figure 45B).

For further confirmation, nuclear import of Nrf-2 in control and treated cells was monitored by immunofluorescence. As illustrated in Figure 44C, Nrf-2 was tethered in the cytoplasm of control cells, reason why we did not observe any accumulation of Nrf-2 in the nucleus. Low nuclear Nrf-2 was indeed spontaneously detected after TNF-α treatment (Hsue et al, 2015). Additionally, pronounced Nrf-2 fluorescence intensity (also expressed as percentage of Nrf2 positive nuclei compared to total nuclei of cells) was observed in samples pre-treated with ovo, 5-thio and erg plus TNF-α compared to not treated cells (NT) and TNF-α alone (Figure 45C-D). These results indicate that our compounds promote Nrf-2 nuclear translocation after TNF-α (inflammation) treatment.

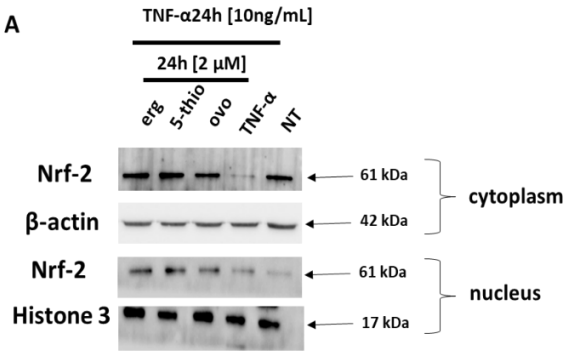

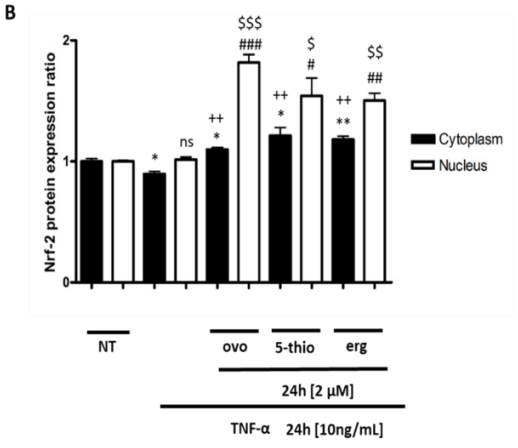

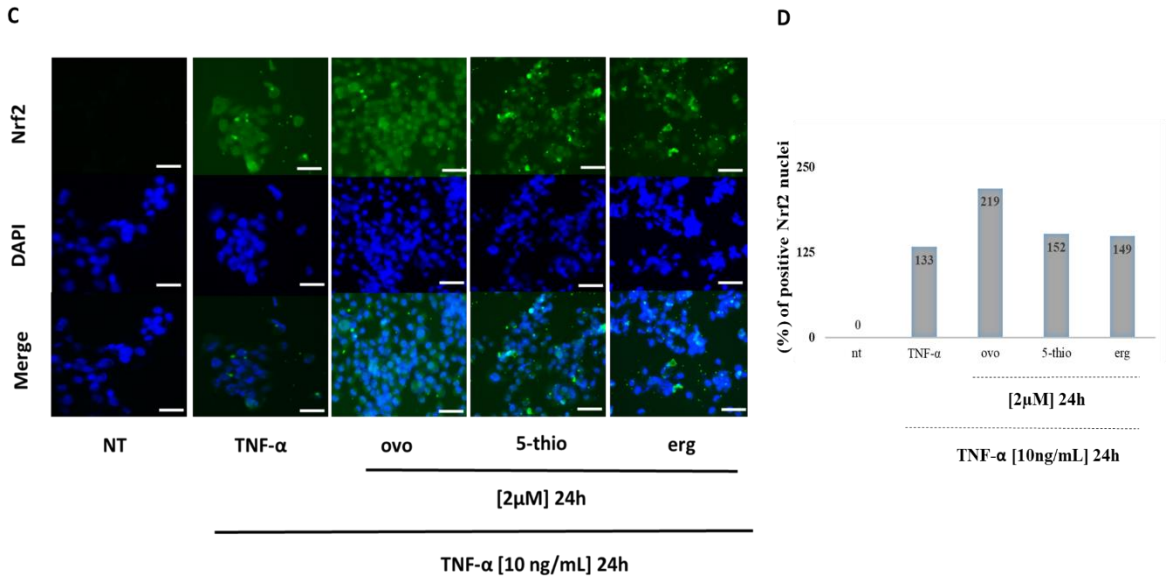

Figure 45. 5-thiohistidines promote nuclear translocation of NRF-2. (A) Representative experiment of Western blot analysis of cytosolic extracts obtained from HaCat cells pre-treated for 24h with molecules at concentration of 2µM and stimulated for 24h with TNF-α at 10 ng/mL to induce inflammation. **(B)** Histograms of the densitometry analysis of protein bands obtained by Western blot using ImageJ software. Data were normalized for β-actin and Histone 3. Data are expressed as mean ± SD, *n* = 3, the significance was determined by the t-test student, * ($p < 0.05$) represent significance compared to NT cytoplasmic fraction; $^{\#\#}$ ($p < 0.01$) and $^{\#\#\#}$ ($p < 0.001$) represent significance compared to NT nuclear fraction; $^{++}$ ($p < 0.01$) represent significance compared to TNF-α treated cytoplasmic fraction; $^{\$\$}$ ($p < 0.01$) and $^{\$\$\$}$ ($p < 0.001$) represent significance compared to TNF-α treated nuclear fraction. **(C)** Immunofluorescence staining showing the changes of Nrf-2 fluorescence. DAPI (1µg/mL) was stained for 10 min and examined by fluorescence microscopy. Scale bars, 10 µm. **(D)** Percentage of Nrf2 positive nuclei. The percentage of Nrf2 positive cells was obtained by normalizing the Nrf2 positive nuclei to the total number of nuclei. Nucleus counting was performed using Image J software

4.3.5. Anti-inflammatory activity of 5-thiohistidines on *ex vivo* human skin tissues

To further investigate on the anti-inflammatory properties of these molecules at the tissue level, we started a collaboration with University of Algarve, Portugal, in the framework of the EMBRIC Translation Access Program 2018. I personally visited the laboratory of Biochemistry led by Prof. Dina Simes in order to test these compounds in ex-vivo human skin tissues. ELISA test was performed in order to detect IL-6, IL-8 and TNF-α release from ex-vivo human skin tissues pre-treated with the molecules and then treated with IL-β1 10ng/mL, generally used in tissues to stimulate inflammation. IL-β1-induced inflammation caused an increase in IL-6, IL-8 and TNF-α release. (Figure 46 A-C). The 24 h pre-treatment with ovo and 5-thio, at the concentration of 2 and 5 µM, led to a drastic decrease of cytokines, especially for IL-6 and IL-8, thus exerting a strong anti-inflammatory effect (Figure 46 A-C) compared with 10µM concentration that was less effective. Pre-treatment with erg 10 µM resulted in a slight but significant decrease of IL-6, IL-8 and TNF-α, following inflammation stimulus. Interestingly, pre-treatment with ovo and 5-thio, was much more effective than pre-treatment with DMX, a type of corticosteroid medication, used in the treatment of many inflammatory conditions, including skin diseases (Uva et al., 2012) (Figure 46 A-C).

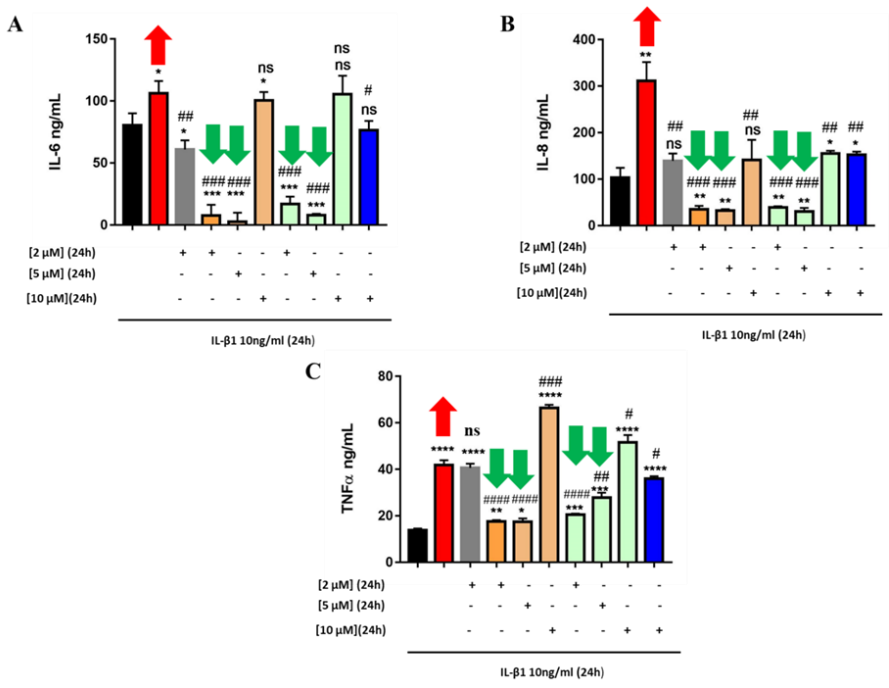

Figure 46. **ELISA assay on ex vivo human skin tissues**. Tissues were pre-treated for 24h with ovo, 5-thio and erg at three different concentrations (2, 5 and 10 µM) and inflammation was stimulated for 24h with IL-β1 10 ng/ml. Data are expressed as mean ± SD, n = 3. The significance was determined by the t-test student and post hoc analysis: * ($p < 0.05$), ** ($p < 0.01$) *** ($p < 0.001$) represent significance compared to NT (not treated only medium) control; # ($p < 0.05$), ## ($p < 0.01$) ### ($p < 0.001$) represent significance compared to IL-β1 10 ng/ml (24h). In the histogram, data referred to NT cells are in black, to cells after inflammation in red, to cells treat with DMX in grey, with ovo in orange, with 5-thio in green, with erg in blue.

4.3.6 5-thiohistidines affects gene expression of inflammatory markers

To evaluate the modulation of specific inflammatory markers involved in the progression of human skin damage, gene expression analysis of IL-6, IL-8, COX-2 and TNF-α was carried out by real-time qPCR after pre-treatment with 5 and 10 µM of ovo, 5-thio, and erg, using DMX as positive control. A significant increase in gene expression of IL-8, COX-2 and TNF-α was observed in ex-vivo human skin tissues treated with IL-β1 10 ng/ml compared to not treated tissues (Figure 47A), while we did not observe a significant increase in gene expression for IL-6 (Figure 47A). On the other hand, skin samples pre-treated for 24h with ovo, 5-thio at 2, 5 and 10 µM showed a significant downregulation of IL-8, COX-2 and TNF-α compared to skin tissues treated with IL-β1 10 ng/ml (Figure 47 B-D). The pre-treatment with erg at 2 and 5 µM induced a significant down-regulation of IL-8, COX-2 and TNF-α, while the pre-treatment with erg 10 µM of only COX-2 and TNF-α, whereas it did not affect in any way the gene expression of IL-6. Finally, the pre-treatment with DMX at 2 µM did not affect the gene expression of IL-6, IL-8, and TNF-α, but significantly induced the down-regulation of COX-2 (Figure 47 B-D).

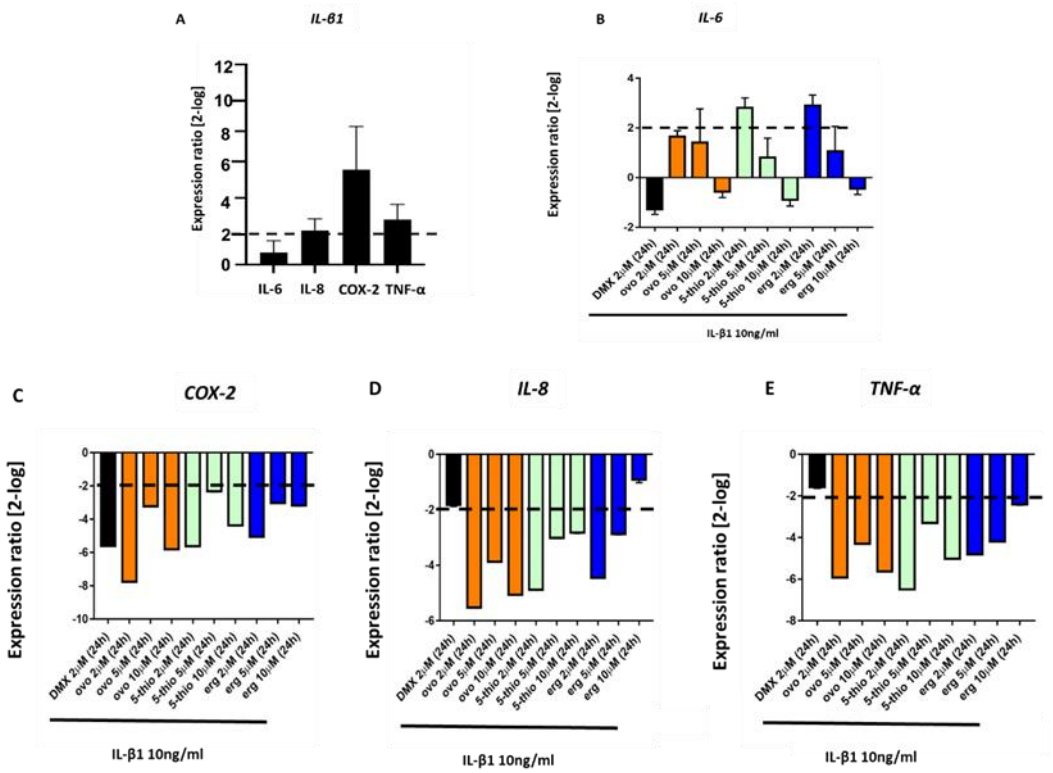

Figure 47. Gene expression analysis of inflammatory markers involved in human skin diseases by real-time qPCR. The levels of gene expression of inflammatory markers were assessed in skin tissues pre-treated with ovo, 5-thio and erg (see figures for concentrations) for 24h and then treated with IL-β1 10 ng/ml for other 24h to induce inflammation. **(A)** Tissues treated with only 10 ng/ml IL-1β for 24h were compared to tissues not treated (reference baseline). **(B-E)** Tissues pre-treated with ovo, 5-thio and erg 24h and then treated with IL-β1 10 ng/ml for other 24h were compared to tissues treated with only 10 ng/ml IL-1β for 24h (reference baseline). Data were analyzed through the REST software, relative expression ratios approaching two cycles were considered significant.

4.4. Discussion

Since in the first part of my PhD we demonstrated that ovo ameliorate liver fibrosis, which is a pathological condition caused by chronic inflammation of the liver tissue, in the second part we decided to further investigate the anti-inflammatory properties of thiohistidine compounds.

In particular, we treated both human keratinocytes and human skin tissues with ovo, 5-thio and erg, to evaluate their dermo-protective properties against pro-inflammatory stimuli: treatment with TNF-α 10 ng/ml or IL-β1 10 ng/ml, respectively.

For the first time, we have shown that the pre-treatment with ovo and 5-thio protects both human keratinocytes and skin tissue from inflammatory conditions.

We have shown that the treatment of human keratinocytes, also at high concentrations (up to 100µM) (Figure 42 A-C), does not appear to be cytotoxic, *viceversa* at low concentrations (2, 5 and 10µM) (Figure 42 A-C) we show a slight increase in proliferation. This phenomenon may account for an adaptive response of the cell known as hormesis, which deserves further investigations.

Furthermore, we underlined how the pre-treatment at low concentrations (2, 5 and 10µM for 24h) of ovo, 5-thio and erg protects human keratinocytes from inflammation induced by TNF-α (Figure 43), thus indicating that the tested compounds exert a protective activity against inflammation induced in human keratinocytes.

Considering that during an inflammatory process, the MAPK cascade is activated through increased ERK and JNK phosphorylation (Lu and Malemud 2019 we evaluated the protein expression of ERK and p-ERK (Figures 44 A-B), JNK and p-JNK in our samples (Figures 44 C-E). The pre-treatment with ovo is the most effective, in fact, it decreases the protein phosphorylation of the two ERK forms, ERK1 (p44) and ERK2 (p42) (Figures 44 A-B) compared to the inflammatory condition. By contrast, the pre-treatment with 5-thio does not have a significant effect on ERK2 (p42) while inducing an increase of phosphorylation of

ERK1 (p44) (Figures 44 A-B). On the other hand, the pre-treatment with erg acts only on ERK2 (p42) by decreasing phosphorylation. Most likely, the pre-treatment with ovo is more effective compared to the unmethylated form (5-thio) and erg due to the chemical and structural properties of ovo, which is probabily a more efficient scavenger of radicals and peroxides. Since during inflammation the production of ROS generally increases, together with the activation of MAPKs, leading to a dysregulation of the skin homeostasis, it is very likely that ovo reacts with ROS more actively, thus inducing the decrease of ERK phosphorylation and contributing to balance skin homeostasis again.

In addition, we analysed JNK and p-JNK (Figures 44 C-E). Regarding JNK, we noted an increase in protein for both forms (46 and 54 kDa) when subjected to treatment with TNF-α (induction of inflammation) and a decrease when the cells were pre-treated with ovo, indicating that ovo may act on the regulation of JNK biosynthesis/degradation (Figures 44 C-E). On the other hand, the pre-treatment with 5-thio and erg did not induce any effect on JNK protein content compared to the treatment only with TNF-α. Regarding p-JNK, we were not able to observe any phosphorylated band in NT, TNF- α treatment, and pre-treatment with ovo, whereas both isoform at 46 kDa and 54 kDa were activated after pre-treatment with 5-thio and erg.

These results indicate that ovo activates MAPKs by acting mainly on ERK phosphorylation which is sufficient to allow translocation of Nrf-2 into the nucleus (see figure 45), whereas 5-thio and erg act mainly on JNK signalling. However, these results need further investigations.

Nrf2 regulates the expression of antioxidant proteins that protect against oxidative damage triggered by injury and inflammation. Once in the nucleus Nrf-2 binds sMaf to form a complex that binds to the antioxidant response element (ARE), triggering the transcription of genes coding for phase II detoxification enzymes (Kaspar et al., 2009; Kim et al., 2010) and inhibiting the transcription of pro-inflammatory genes including COX-2 (Ahmed et al., 2016). Consequently, our finding that the compounds tested in this study increase the

accumulation of Nrf-2 in the nucleus and decrease the expression of downstream genes as COX-2 (Figure 45) further confirm that they exhibit anti-inflammatory activity. However, further investigations will be necessary to evaluate the activity of other detoxifying enzymes such as superoxide dismutase and catalase, both involved in the antioxidant cellular defenses.

Moreover, the anti-inflammatory activity of such compounds is validated by the decreased transcription of IL-6, IL-8, TNF-α and COX-2 (Figure 47 B-E) and the consequent inhibition of pro-inflammatory cytokines release in *ex-vivo* human skin tissue treated at low doses of ovo and 5-thio (Figure 46 A-C).

All these results suggest that 5-thiohistidine molecules can be considered dermoprotective agents. Moreover, future studies will be devoted to investigate their photoprotective properties considering that they have an absorption spectrum in UV-vis range (Figure 48).

Finally, it will be extremely interesting to integrate the results obtained in this study with others obtained on fibroblasts, because the skin is an organ in continuous development. In a young person, there is a balance between the synthesis of new collagen by fibroblasts and the degradation of collagen by MMPs activity that changes the recovery of collagen, causing a faster aging process of the skin. UV rays, both UVB and UVA are one of the key factors involved in premature skin aging. Therefore, the deepening and use of these cells will certainly be able to better clarify the mechanism of action of these molecules.

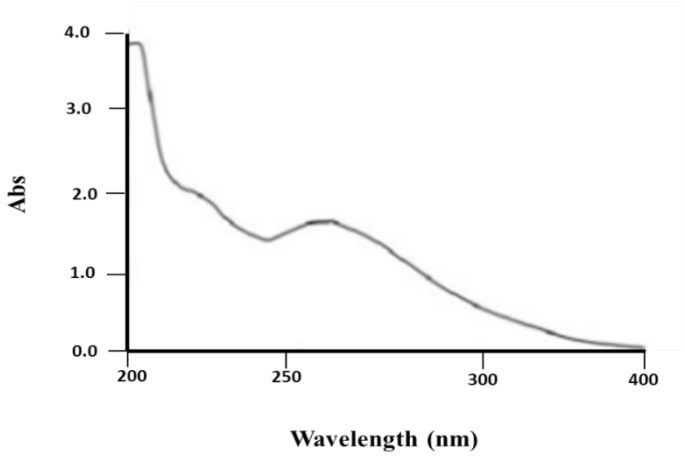

Figure 48. UV-Vis absorption spectrum of ovothiol A (modified from Russo et al., 2014).

4.5. Conclusions and perspectives

The results of our study demonstrated that micromolar concentrations of 5-thiohistidines are able to protect human keratinocytes from an inflammatory condition induced by TNF-α and at the same time to reduce the levels of pro-inflammatory interleukins in human skin tissues treated with IL-β1. The positive effects of 5-thiohistidines are certainly due to the differential ability to affect ERK or JNK signalling (Figure 49 A-B), thus favouring the nuclear translocation of Nrf-2 and down regulating the gene expression of IL-6, IL-8, COX-2 and TNF-α (Figure 49 A-B). In conclusion, our findings suggest that 5-thiohistidines could be used as effective substances to treat skin damage caused by inflammatory conditions. Consequently, it could be interesting to develop natural skin care products using the powerful properties of these molecules from the marine world.

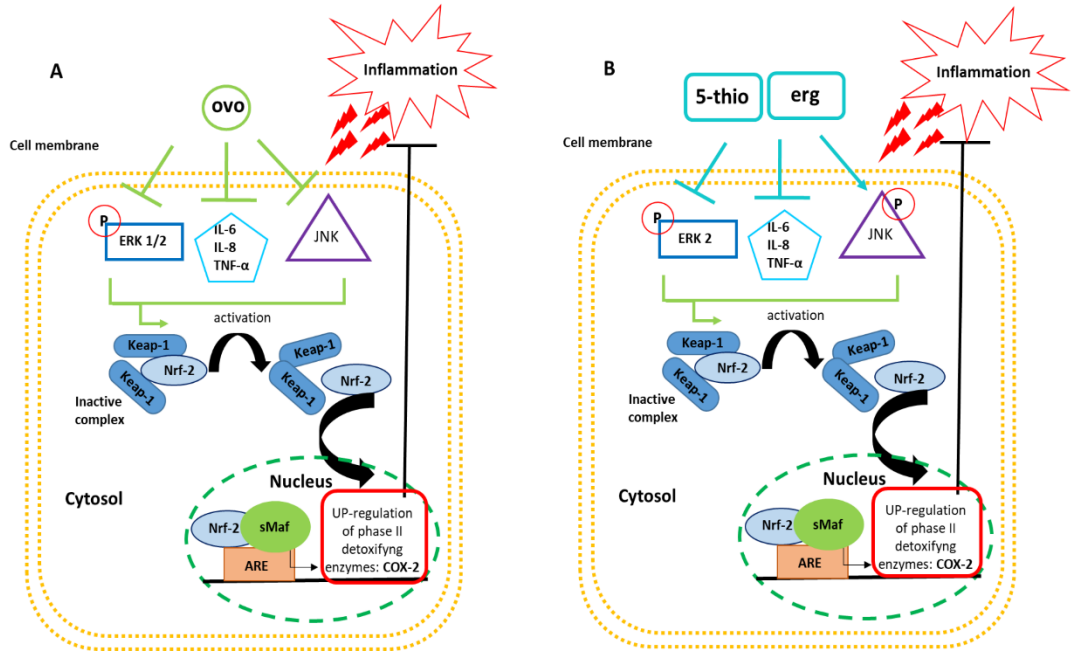

Figure 49. Proposed mechanism of action for thiohistidines. **(A)** Treatment with ovo, before inflammation of the skin tissue, inhibits the release of pro-inflammatory cytokines (IL-6, IL8 and TNF-α); blocks ERK 1/2 phosphorylation and inhibits JNK. **(B)** Treatment with 5-thio and erg, before inflammation of the skin tissue, inhibits the release of pro-inflammatory cytokines (IL-6, IL8 and TNF-α), blocks ERK 2 phosphorylation and promotes JNK phosphorylation. These mechanisms of action favours the activation of Nrf-2, which migrates into the nucleus and binds to sMaf causing the interaction with the ARE sequences and leading to the up-regulation of phase II detoxifying enzymes such as COX-2. These events block the inflammatory process.

CHAPTER 5

Unveiling the distribution and molecular diversity of ovothiol biosynthesis in bacteria

5.1. Aims of the study

The marine world offers numerous advantages for studying the evolution of metabolic pathways. Life originated in the seas, allowing the development of complex organisms from the simplest forms of life. The metabolic adaptation of these organisms is due to the presence of enzymes capable of developing beneficial functions that guarantee survival in changing environments (Sambamoorthy et al., 2019). Biological evolution and metabolic diversification are due to different factors, especially environmental constraints and ecological adaptation.

For these reasons, in this study, in order to shed new light on the biological roles of ovothiols, we decided to perform an in-depth analysis of the evolutionary history of the biosynthesis and environmental adaptations that led to the development of these compounds. Previous studies (Gerdol et al, 2019) have shown that the biosynthesis of ovo is conserved in several metazoans, while, it is lost in others like Nematoda, Arthropoda and bony vertebrates. In addition, the biosynthesis of ovo is conserved in most of diatoms, while it is lost in plants, for example (Milito et al., 2020). These results stimulated our curiosity in order to understand how organisms lacking this metabolic pathway could have developed alternative pathways to produce similar sulphur-containing molecules, or how they could have acquired these metabolites through diet (Yanshole et al., 2019) or symbiont organisms (Rizzo and Lo Giudice 2018).

In order to have an overall picture of the distribution and molecular diversification of ovo pathway, includind the sulfoxide synthase OvoA and the β-lyase OvoB, in nature, we decided to extend our analysis to the kingdom of bacteria, that, has a high variability in terms of pathogenic microorganisms, parasites and symbionts. At the same time, the study of this domain allows us to integrate, expand and intertwine the evolutionary history of ovo biosynthesis in prokaryotes with its evolution in single-cell eukaryotes and metazoans. Overall, the database of the biosynthetic enzyme sequences and taxonomic and metabolic information obtained in this study will provide a valuable source of concepts to highlight the evolutionary and biological role of this process and to identify the most performing enzyme in ovo production for future pharmacological uses.

Indeed, the chemical synstesis of ovo is difficult and time-consuming, on the other hand, the purification from sea urchin eggs is not eco-sustainable, therefore, the study of the biosynthetic

pathway in bacteria can prompt the development of protocols to produce ovo in a more eco-sustainable way as well as to obtain higher amounts of the molecule.

5.2. Materials and methods

5.2.1. Database creation

To establish the database of bacterial enzyme sequences, the fully annotated bacterial genomes available in the Ensembl and NCBI databases were used to perform a sequence screening similarity search for OvoA and OvoB; the criterion used is that of homology. The OvoA protein of *Erwinia tasmaniensis* (*Et*OvoA) (WP_012439783.1) was used as a query for BLASTp searches with respect to the expected protein collections. Positive hits were then used to highlight the presence of the three domains that make OvoA or domain similar to DinB (PF12867), domain FGE-sulfatase (PF03781) and domain C-terminal, belonging to the homologous methyltransferase homologous superfamily dependent on SAM (SSF53335). Amino acid sequence of OvoB from different sources was found by BLASTx and BLASTp homology search using as template OvoB from *E. tasmaniensis* (WP_012439783.1) *Et*OvoB.

5.2.2. OvoA and OvoB primary structural analysis

Both OvoA and OvoB protein sequence alignments were obtained by Clustal- Omega (Sievers et al., 2011). After the final curation step, the C-terminal regions of all OvoA sequences were trimmed, and aligned to create HMM profiles for the methyl transferase (MT) domains (PF13847, PF08242, PF13649 and PF08241) using the HMMer suite v3.2 (Eddy 2011); profile logos were created with Skylign program (Wheeler et al.,2014).

5.2.3. Description of habitat, metabolism and interspecific interactions

The habitat and interspecific interactions of the selected 233 bacterial species were inferred according to data available in the Pathosystems Resource Integration Center (PATRIC 3.6.2) free database and other public databases. PATRIC provides integrated data and analysis tools to support biomedical research on bacterial infectious diseases (Wattam et al, 2014).

5.2.4. 3D Models of Bacteroidetes OvoB-like sequences

Two selected proteins from *Bacteroidetes* species (NBV57240.1; NBC82978.1) were modelled using HHpred partition at MPI Bioinformatics Toolkit (Zimmermann et al., 2018), and selecting the best scoring hits. This analysis was performed with the help of Dr. Luca Ambrosino from the SZN Bioinformatic group. The atomic coordinates of the templates were obtained by scanning the PDB database (Berman et al., 2000). To predict 3D-models, two independent multiple sequence alignments, performed by Clustal-Omega (Sievers and Higgins 2018), between the two investigated protein sequences and the templates sequences, obtained in PIR format, were submitted to the homology modeling software Modeller 9v20 (Webb and Sali 2016). Modeller algorithm was set to generate 100 structural models for each protein structure. In order to evaluate the stereochemical quality of the generated structures and to select the best model, the models were uploaded, in the standard PDB file format, to the PDBsum server (de Beer et al.,2014), to carry out a full set of Procheck structural analyses (Laskowski et al., 1993), including an evaluation of the backbone conformations of all residues compared to the known allowed areas in the Ramachandran plot. The obtained models were displayed by using the molecular graphics software VMD (Humphrey et al., 1996). The comparisons between the modeled structures and the OvoB structure from *E. tasmaniensis* were carried out by VMD software and mTM-align (Dong et al., 2018).

5.2.5 Phylogenetic analysis

Phylogenetic analysis of the bacterial sequences was performed by Dr. Michael Tangherlini from the Integrative Marine Ecology Department of SZN. The 233 sequences within the database were first clustered to remove identical entries, leaving a total of 219 sequences, which were aligned using MAFFT (Katoh et al., 2019); the resulting alignment was used as an input for tree building using the IQ-TREE server (Minh et al.,2020) with the LG+R8 model. The tree was subsequently visualized using FigTree, manually rooted on the cyanobacterial OvoA-like proteins and clades manually identified. Distribution of the different metabolic strategies, oxygen requirements and methyl-transferase domains were assessed in each clade by means of the ggstatsplot (https://CRAN.R-project.org/package=ggstatsplot) R package, which considered the statistical significance of the results by means of Pearson's Chi-Squared tests.

5.3. Results

5.3.1. Ovothiol biosynthetic genes distribution in Bacteria

In order to understand the origin and distribution of ovo biosynthetic pathway in Bacteria, we searched for OvoA and OvoB-like sequences in reference genomes. We created a database, in particular, we found 233 sequences belonging to different bacteria featuring OvoA, 187 of which, besides OvoA, also exhibited OvoB-like sequences (selected using as cut off 30% identity with *E. tasmaniensis Et*OvoB). Most of the bacteria characterised by the presence of ovo gene pathway belonged to the phylum Proteobacteria (95%; Figure 50A), followed by Bacteroidetes (3%), Cyanobacteria (1%) and Verrucomicrobia (~1%). Among Proteobacteria, most belonged to Gamma-proteobacteria (74%), followed by Beta-proteobacteria (10%), Epsilon-proteobacteria (6%), Delta-proteobacteria (3%) and Acidithiobacillia (2%). Members of other classes included Bacteroidia (1%), Flavobacteria (1%), Oscillatoriophycideae (1 %), Alphaproteobacteria (~1%) and Verrucomicrobia (~1%; Figure 50B). Moreover, *Erwiniaceae* was the most represented family (28%), followed by *Piscirickettsiaceae* (8%), *Alteromonadaceae* (6%), *Aeromonadaceae* (6%), *Moraxellaceae* (4%) and *Campylobacteraceae* (3%). Interestingly, in some species like *Nitrosospira multiformis* (41370981), *Acidithiobacillus thiooxidans* (29720555), *Alteromonas macleodii* (29677280), *Alteromonas stellipolaris* (42913355) and *Pseudoalteromonas piscicida* (34018708) OvoA gene was found in cluster with an OvoB-like gene, annotated as C-S lyase or aminotransferase of class I/II, while in two cyanobacteria *Cylindrospermopsis raciborskii* (34474639) and *Microcystis aeruginosa* (5865063) OvoA was found in cluster with EgtD. Among the bacterial species analysed, 70% were chemoheterotrophic and 25% were chemoautotrophic; 56% of them exhibited an aerobic metabolism, including 7% aerobic sulfur-oxidisers, and 1% aerobic sulfur-reducers, 39% exhibited a facultative anaerobic metabolism, 5% were anaerobic (Figure 50C). Moreover, 46% of them were mainly found in aquatic environments, including 35% living in marine environments (5% of which in deep-sea hydrothermal vents), 6% living in lakes and 5% living in other freshwater environments, 38% living exclusively in terrestrial environments, and 16% in multiple environments (Figure 50D). Finally, we highlighted that, while most of them were free living, a consistent number established

intimate interactions with other organisms. In detail, 36% were parasites/pathogens of plants, animal and/or humans and 7% were symbionts of marine invertebrates, plants or insects; among symbionts we found 12 species with commensal behavior (Figure 50E).

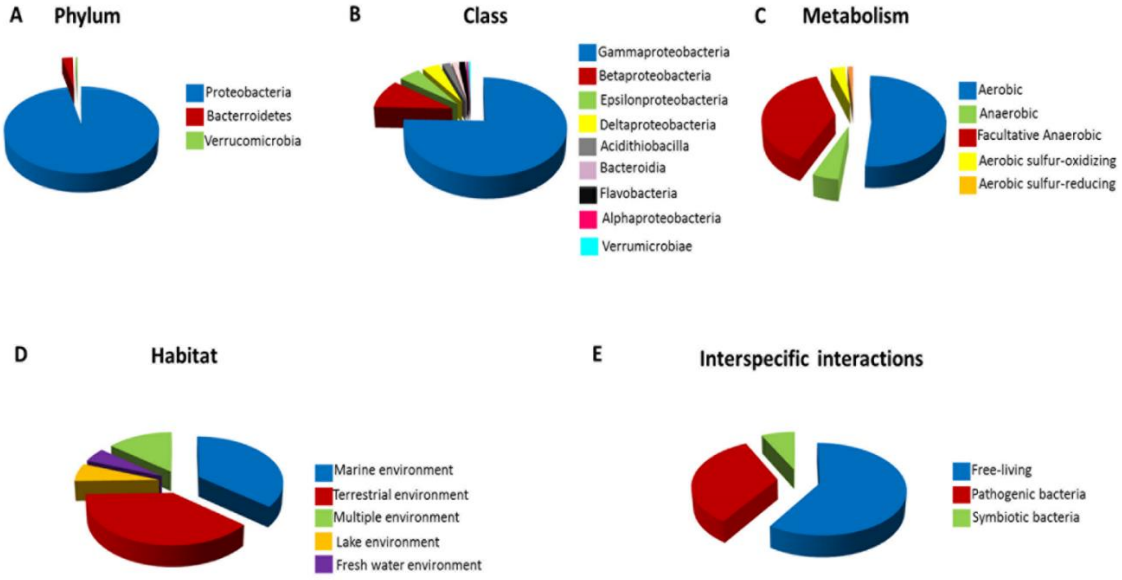

Figure 50. Taxonomy, habitat, metabolism, trophic interactions of bacteria with ovothiol-biosynthetic pathway. (A) *Phylum* classification **(B)** *Class* categorization **(C)** *Metabolism* diversification **(D)** *Habitat* **(E)** *Interspecific interactions***.** (Brancaccio et al., 2020 under review)

5.3.2. Characterization of bacterial OvoA-like proteins

To analyse the structural organisation of the bacterial OvoA proteins, we compared the 233 bacterial OvoA sequences selected for the presence of the three canonical domains (DinB, FGE-sulfatase, and methyl-transferase SAM domain) with the previously characterized *Et*OvoA structure (WP_012439783.1). Interestingly, bacterial OvoA orthologous differ in the C-terminal region for different annotated methyl-transferase SAM domains (MT11, MT12, MT25, and MT31); the most frequent being MT12, followed by MT31, MT25, and MT11 (Figure 50A). Regarding the residues necessary for enzymatic activities, all bacterial OvoA-like proteins preserved: the highly conserved iron binding motif HX3HXE in the DinB domain (Braunshausen and Seebeck 2011); all the residues proposed to be involved in substrates (cysteine and histidine) recognition/binding in the FGE-sulfatase domain (Castellano et al.,2016) and Tyr417, which plays a key role in sulfoxide synthase

activity (Chen et al., 2018); the residues G524, C525, G528, R529, D545, G599, D600, A601 considered to be involved in the formation of the SAM binding site (Figure 51B).

To reveal whether the four different methyl-transferase domain annotations had a specific sequence profile that could explain the diversification of their structure and function in bacterial OvoA orthologous, we compared the HMM profiles of all sequences restricted to the C-terminal region that included the SAM domain (Figure 51C). An HMM (Eddy 2011) profile is a probabilistic model that describes the position-dependent conservation of a given sequence family. Consequently, the use of an HMM profile turns out to be extremely useful for searching for sequence homology. The sequences of the MT domains showed a higher degree of similarity in the positions and motifs highlighted in figure 51C, while the remaining part of the sequences exhibited a high variability. Overall, MT12 and MT25 are more similar compared to MT11 and MT31 and are mostly found in *Erwiniaceae*, the most represented family of bacteria exhibiting OvoA orthologous.

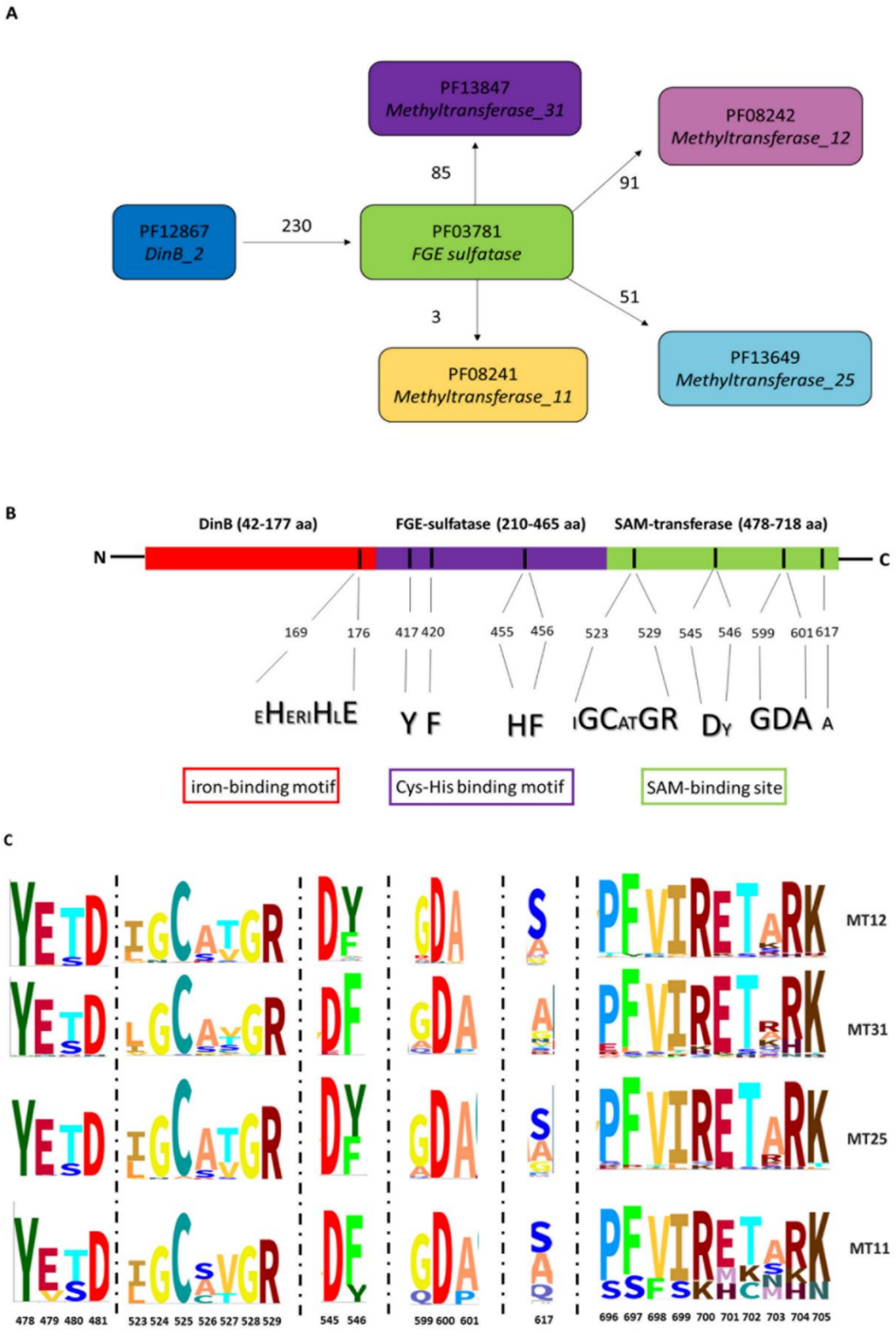

Figure 51. Characterization of OvoA proteins in Bacteria. (A) Structural domain organization of OvoA proteins in Bacteria. All OvoA share a common DinB domain boxed in blue, a FGE-sulfatase domain boxed in green, and differ in methyl-transferase SAM domain annotations: MT31 (violet), MT25 (light blue), MT12 (magenta) and MT11 (orange). **(B)** Schematic representation of OvoA primary structure. DinB domain is highlighted in red and the residues involved in the iron-binding site are indicated by arrows. FGE-sulfatase domain is highlighted in violet and the putative residues involved in the *Cys-His* binding motif are shown by arrows. SAM-transferase domain is highlighted in green and the residues involved in the SAM binding sites are reported by arrows. The indicated residues correspond to *Et*OvoA numeration. **(C)** Comparison of HMM profiles of the different annotated MT domains: MT12, MT31, MT25 and MT11 obtained from Skylign program [31]. (Brancaccio et al., 2020 under review)

5.3.3. Identification and characterization of OvoB-like proteins in Bacteria

To characterise the structural organization of bacterial OvoB orthologous proteins, we compared the previously characterised *Et*OvoB (Naowarojna et al., 2018) with the 187 OvoB-like sequences found among the bacteria analysed in the present study. These sequences shared the same structural organization of *Et*OvoB: the N-terminal (11-93 aa) domain, the catalytic domain (94-256 aa) and the C-terminal (257-389 aa) domain (Figure 52).

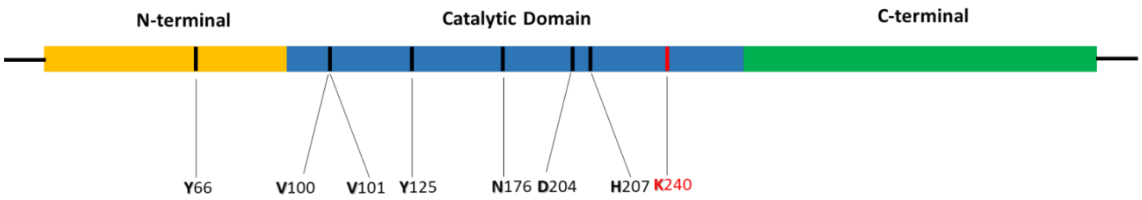

Figure 52. **Schematic representation of bacterial OvoB primary structure**. The N-terminal portion is highlighted in orange, the catalytic domain in blue, and the C-terminal portion in green. The residues involved in the enzymatic lyase activity are indicated by arrows. (Brancaccio et al., 2020 under review)

In *Et*OvoB the N-terminal and the C-terminal domains forms a lid that shelters the PLP-binding pocket and the active site (Naowarojna et al., 2018). Among the bacterial OvoB proteins, 91 shared from 50 to 93% aa identity with *Et*OvoB, while the others 96 shared from 30 to 49% aa identity. In all OvoB-like bacterial sequences sharing the higher identity with *Et*OvoB, all the residues responsible for the interaction with the PLP cofactor in the active site, K240, Y125, N176, D204, and H207, V100, and V101 in the catalytic domain, and Y66 in the N-terminal domain (Naowarojna et al., 2018) were highly conserved (see residues in Figure 52). In the sequences showing lower degree of similarity with *Et*OvoB, the residues N176, D204 and K240 were highly conserved; while Y66 was present in all sequences except in *Halomonas sp. TD01* (WP_009724024.1).

5.3.4. Comparison of bacterial OvoB-like proteins with OvoB-like domain in Hydrozoa

In bacteria, the C-S sulfoxide synthase and the PLP-dependent lyase activities are performed by two different enzymes (OvoA and OvoB), encoded by two different genes. In metazoans no OvoB-like sequence was found, except for species belonging to Hydrozoa, which display a unique polypeptide with both OvoA and OvoB-like activity (Gerdol et al., 2019) (Figure 53).

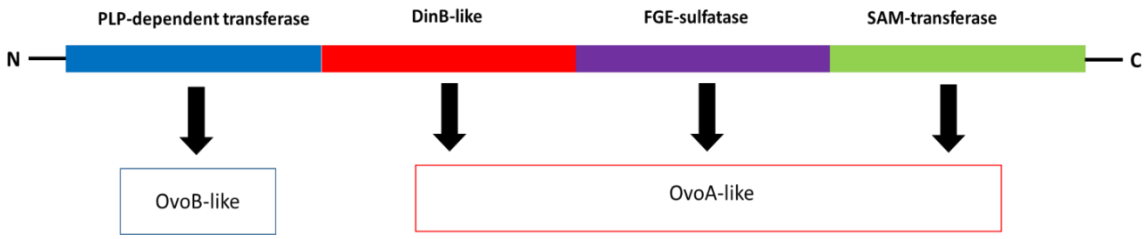

Figure 53. OvoB-OvoA fused protein in Hydrozoa. The PLP-dependent transferase domain, responsible for OvoB-like activity, is highlighted in blue, the DinB domain in red, the FGE-sulfatase domain in violet and the SAM-transferase domain in green. These three last domains are responsible for OvoA-like activities. (Brancaccio et al., 2020 under review)

Moreover, the OvoB-like domain in Hydrozoa was found to be encoded by a single exon, while the OvoA-like polypeptide was found to be encoded by four exons. For these reasons, to reveal whether the N-terminal OvoB-like domain fused with the OvoA in Hydrozoa could derive from an HGT event from bacteria, we carried out a similarity search comparison of the 262 aa of OvoB domain fused to OvoA protein in *Hydra vulgaris* against the NCBI database and we found that *H. vulgaris* N-terminal OvoB-like domain showed 30.7% identity with aminotransferase class V-fold PLP-dependent enzyme (NBV57240.1) of an uncharacterized bacterium from the Bacteroidetes phylum, identified in freshwater metagenome. This result was particularly interesting because Bacteroidetes live in close association with Hydrozoa (Di Camillo et al., 2012; Fraune amd Bosch 2017). Other metagenome-assembled genomes of bacteria belonging to this phylum, identified from Great Salt Lake, Utah, displayed both OvoA (KAA3624609.1) and a putative C-S lyase protein (NBC82978.1). Comparative analysis highlighted that OvoA-like proteins from these *Bacteroidetes* exhibit only the first two domains; DinB and FGE-sulfatase domain; while both OvoB-like proteins modelled trough HHpred gave as best templates C-S lyase or aminotransferase of class I/II (Figure 54A). In detail, the predicted models displayed superimposition with the 3D-structure of *Et*OvoB

(WP_042958836.1; [Naowarojna et al., 2018]) and high conservation of the residues involved in OvoB-like activity, especially for the putative C-S lyase (Figure 54B), thus suggesting bacterial origin.

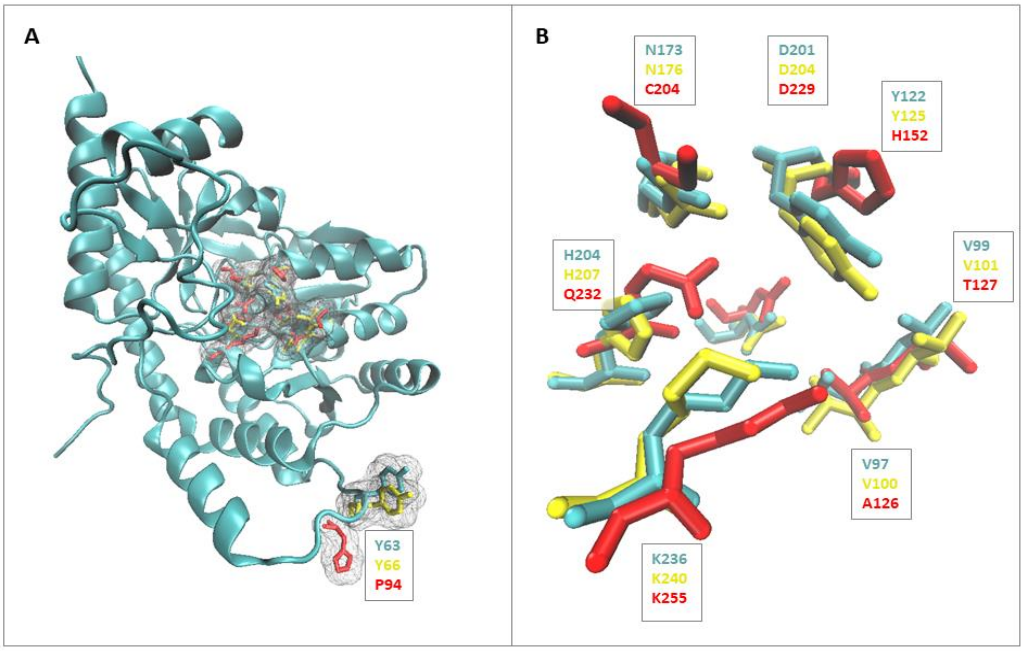

Figure 54. Protein structures superposition of the putative C-S lyase and Class5 aminotransferase from Bacteroidetes sp. and *Et*OvoB. A) Three-dimensional model of the putative C-S lyase (in cyan); amino acids involved in the catalytic activity are showed in a licorice view (in cyan for the putative C-S lyase, in red for the Class5 aminotransferase, in yellow for *Et*OvoB). **B)** Close-up view of amino acids in the active site and the corresponding position numbers (in cyan for the C-S lyase, in red for the Class5 aminotransferase, in yellow for *Et*OvoB). (Brancaccio et al., 2020 under review)

3.5.5. Phylogenetic analysis of the sulfoxide synthase OvoA in bacteria

The OvoA protein bacterial sequences retrieved from our database were used to reconstruct OvoA phylogeny in bacteria. Sequences from cyanobacteria were used as outgroups. The results showed that OvoA homologs clustered in 8 different clades (Figure 55).

Figure 55. Phylogenetic tree of OvoA-like sequences in bacteria. A phylogenetic tree was visualized using FigTree and colored according to each clade. (Brancaccio et al., 2020 under review).

We compared the distribution of metabolic traits, oxygen requirements and the diversification of the methyltransferase domains among the clades (Figure 56).

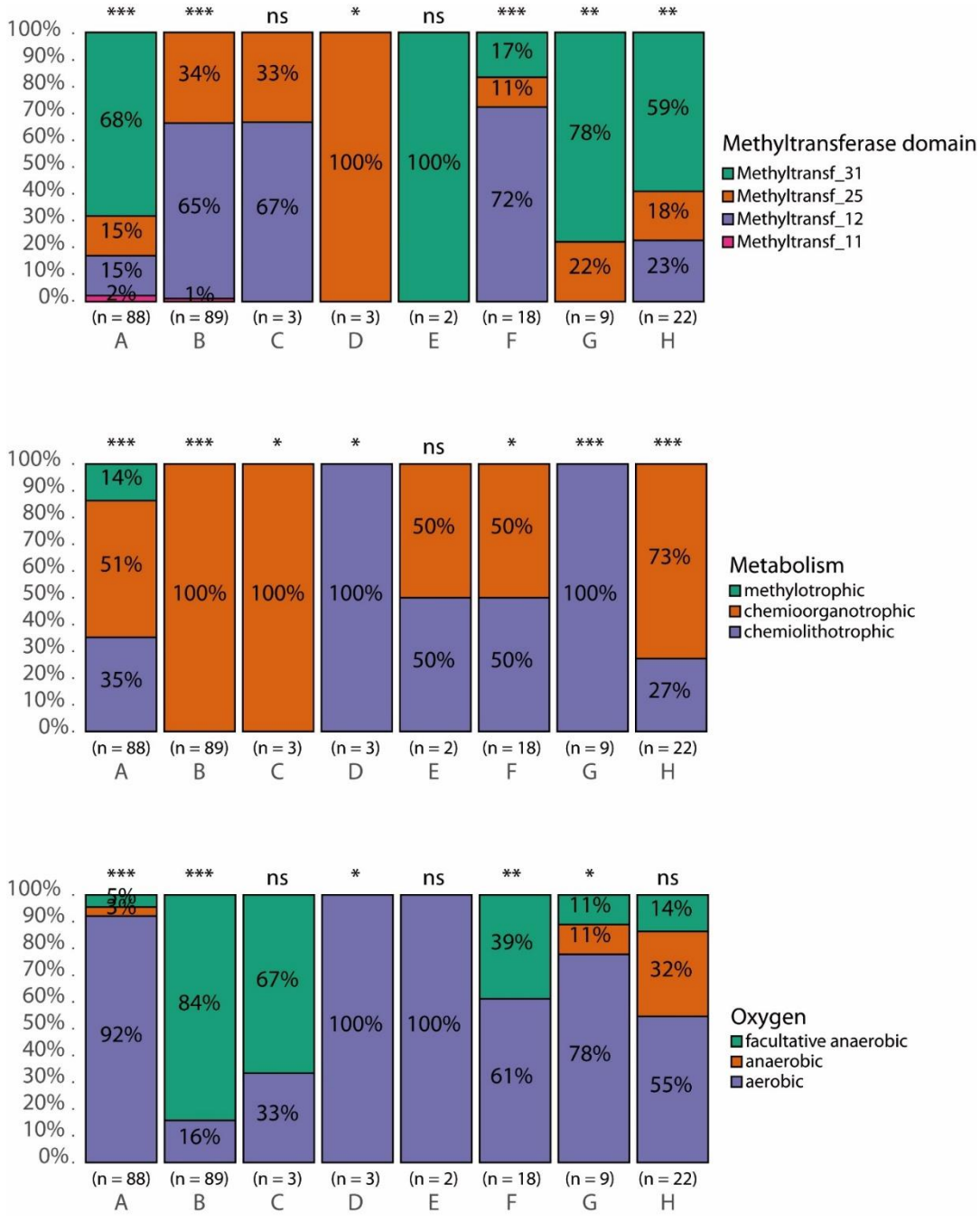

Figure 56. Significant differences in distribution of metabolic and sequence traits among clades. Relative abundances of each methyltransferase domains, metabolic pathways and oxygen requirements were calculated from metadata associated with each sequence. (Brancaccio et al., 2020 under review).

In detail, the two widest clades were A and B. Clade A was characterised by 92% of aerobic bacteria, 71% of the species belonging to Gammaproteobacteria, 25% to Betaproteobacteria and the remaining

4% to Acidithiobacillia, among these 51% were chemio-organotrophic. Clade B was characterised by 100% chemio-organotrophic Gammaproteobacteria, 73% belonging to the Erwiniaceae family, mostly facultative anaerobes (84%). Clades C and D were each represented by only 3 species, belonging to chemio-organotrophic Gammaproteobacteria, and aerobic autotropic Cyanobacteria, respectively. Clade E was composed of only two species, one belonging to Alphaproteobacteria, and one belonging to Gammaproteobacteria. Clade F was characterized by 18 species belonging to Gammaproteobacteria, while clade G was entirely characterized by lithotrophic organisms 89% belonging to Epsilonproteobacteria and the remaining 11% to Gammaproteobacteria. Finally, clade H was mainly characterized by heterotrophic organisms belonging to Deltaproteobacteria and Epsilonproteobacteria. Interestingly, clades A, G and H were significantly enriched in sequences with M31 domains (>50% in each clade), found mainly in aerobic organisms (>50% in each clade; fig. 54).

5.4. Discussion

The most accepted biological role for ovothiols is their involvement in cellular redox maintenance and molecular strategies to allow organisms to adapt to different environmental conditions (Castellano and Seebeck 2018). However, little is known about the ecological implications of the previous investigated functions, as the ability to protect eggs and embryos during sea urchin fertilization (Shapiro 1990), or their role in the defence from the immune response in trypanosome species (Krauth-Siegel and Leroux 2012; Ariyanayagam et al., 2001), as well as their protective role from environmental pollutants in starlet sea anemone and mussels (Tarrant et al., 2018; Diaz de Cerio et al., 2020).

Although, ovothiols have been found in different organisms, the biosynthetic pathway of these compounds has been characterised only in some microorganisms such as *E. tasmaniensis* and the trypanosome *Crithidia fasciculata* (Vogt et al., 2001; Braunshausen and Seebeck 2011), in the sea urchin *P. lividus* and in the diatom *S. marinoi* (Castellano et al., 2016; Milito et al., 2020).

In this section, we describe, for the first time, the distribution and diversification of the enzymes involved in ovo biosynthesis in bacteria, in order to shed light on the evolutionary link between bacteria, eukaryotes and metazoans and to understand how organisms that have lost this metabolic pathway have differently adapted their metabolic capabilities.

Our results show that ovo biosynthetic pathway is mainly conserved in proteobacteria. Proteobacteria represent the most abundant bacteria in the marine world and, consequently, they are the perfect candidates for studying links between metabolic adaptation and environmental niches (Zhou et al., 2020).

The beginning of life originated in the marine environment; thus, the presence of this biosynthetic pathway mostly in marine bacteria and in particular in anaerobic ones (5%) and in bacteria that live in deep hydrodermal vents (5%) could highlight that ovo biosynthesis is a very ancient pathway during evolution. The presence of ovo biosynthetic genes in the genomes of anaerobic bacteria is surprising, because, we known that the enzymes belonging to the family of sulphoxide synthase are dependent on oxygen. This may suggest some ancient oxygen-independent enzymatic activities, as already reported for erg biosynthesis (Leisinger et al., 2019). Probably, oxygen appearance in the

atmosphere caused a selective pressure against the ancient sulfoxide synthase enzymes, bringing them to become oxygen dependent. In addition, we have found biosynthetic genes of ovo in chemosynthetic bacteria that oxidise or reduce sulfur. This one is another interesting aspect considering that these compounds could have played a key role in evolution as electron and sulfur donors in chemical reactions.

Bacterial OvoA proteins have a canonical organization with three domains, with a higher degree of conservation for the DinB and FGE-sulphatase domains, in particular for the residues involved in iron bonding and the sulfoxide synthase activity, while the methyltransferase domain is more variable. This finding suggests that there has been a selective pressure for the conservation of the domains involved in the sulfoxide synthase activity that generates the production of the 5-thiohistine compound. Instead, the final methylation on the imidazole ring of histidine may not be so necessary, as also suggested by the finding that some OvoA-like proteins from Bacteroidetes lack the MT domain. In support of this hypothesis, both ovo and the unmethylated form of 5-thiohistidine have been found in nature in complex with other secondary marine metabolites, like adenochromines in cephalopods, discorhabdins in sponges and imbricatine in sea stars (Castellano and Seebeck 2018). The biological implications of the formation of these building blocks are still unclear. Furthermore, 5-thiohistidine chemical and biological properties are similar to ovo, as demonstrated also by the efficacy of the non-methylated form in inhibiting the activity of GGT in human cancer cells to the same extent as ovo (Brancaccio et al., 2018; Milito et al., 2019).

Previous studies on biosynthesis of ovo in metazoans did not reveal any presence of OvoB, except for hydrozoans, which have an additional N-terminal domain similar to OvoB appearing to be fused with OvoA in a single polypeptide (Gerdol et al., 2019). Concerning bacteria, we have observed a strong association between the presence of both OvoA and OvoB-like proteins encoded by two different genes. This finding supports a bacterial origin of the domain similar to OvoB in Hydra probably originated by bacterial symbionts. In fact, our analysis showed that 7% of bacteria showing ovo gene groups are symbionts and the OvoB-like hydrozoan domain shares a high similarity to proteins of uncultured Bacteroidetes OvoB-like, a phylum to which the symbiotic bacteria in Hydra belong (Di Camillo et al., 2012; Fraune and Bosch 2017).

The OvoB-like domain fused with OvoA in Hydra represents the unique case reported so far of a single polypeptide chain that combines all three enzymatic activities (sulfatase, lyase and methyltransferase) responsible for ovo biosynthesis (Gerdol et al., 2019). This is particularly relevant when one considers that the transcripts of at least one third of the genes in Hydra undergo trans-spliced (Chapman et al., 2010). Trans-splicing occurs in several hydrozoans, but not in the anthozoan *Nematostella*, and it may be an ancestral feature of this class, which is why perhaps OvoB has merged with OvoA. Furthermore, the fused OvoB-OvoA gene in Hydra shows a significantly lower number of exons (5 instead of 17) than the other metazoans including other cnidarians (Gerdol et al., 2019). This may be due to the intron loss high rate in the Hydra lineage compared to other anthozoans (Chapman et al., 2010). Interestingly, the additional domain similar to the N-terminal OvoB in Hydra is entirely encoded by the first exon (Gerdol et al., 2019), suggesting that its acquisition could be the result of the horizontal transfer of a bacterial intron-less gene, later merged with OvoA.

The presence of ovo biosynthetic genes in parasites and pathogens of host organisms without the same metabolic pathway is another feature that could have important evolutionary and biological implications. Almost 36% of the bacteria presenting OvoA and OvoB genes are parasites and/ or pathogens of plants or animals, which do not produce ovo. This suggests that ovo-producing organisms may be protected from the infection by these pathogenic microbes. On the other hand, these pathogens can use ovo to protect themselves from the immune response of those hosts that do not produce this antioxidant (Krauth-Siegel and Leroux 2012). This is also consistent with the lack of OvoA in obligate parasites having lost primary host-supplied metabolic pathways: Platyhelminthes (Jackson 2015; Zarowiecki and Berriman 2015) and Myxozoa (Chang et al., 2015). Furthermore, these data strongly support our discoveries on the anti-inflammatory activities of ovo in mammalian models that do not contain ovo biosynthetic pathway (Castellano et al., 2018; Brancaccio et al., 2018; Brancaccio et al., 2019; Milito et al., 2019), opening some promising scenarios in the field of the exploitation of these molecules as new marine drugs. At the same time, ovothiol biosynthesis by pathogens may emerge as a target for new anti-infectious therapies.

From a phylogenetic point of view, our studies have shown that the occurrence of the ovo pathway in bacteria reflects significant differences in the distribution of metabolic traits and oxygen requirements. In particular, regarding the two most representative clades, A and B, bacteria are

characterized by marked differences in terms of oxygen requirement (mainly aerobic bacteria 92% in clade A compared to 84% of the facultatives anaerobes in clade B). In clade A we find also an abundance of MT31, while in clade B there is a majority of MT12. These characteristics suggest that the methyltransferase domains can be shared between organisms with different metabolisms, with MT31 favored between aerobes and MT12 or MT25 preferred in optional anaerobes. More importantly, chemoorganotrophic bacteria (clade B) and chemo-lithotrophic bacteria (clade G) cluster separately, suggesting a clear divergence of OvoA enzymes in heterotrophic and autotrophic bacteria. This data may suggest that OvoA evolved in basal metazoans through the ancient endosymbiosis of heterotrophic Proteobacteria and in protists, like microalgae, from the endosymbiosis of autotrophic Proteobacteria. The endosymbiotic events involving cyanobacteria instead likely favoured OvoA spread first in red and green algae, and then in diatoms (Milito et al., 2020).

Conservation of the metabolic pathway of ovo is likely due to its ability to provide efficient regulation of redox sensitive signalling pathways, the modulation of which is critical for key life cycle transitions in marine invertebrates (Castellano et al., 2015) and/or light-modulated physiological processes in bacteria and microalgae (Milito et al., 2020). On the other hand, the loss of the ability to produce ovo can be related to the independent evolution of alternative and more sophisticated mechanisms for the control of redox homeostasis. These could involve erg in mycobacteria and fungi (Seebeck 2013), as well as the more widespread glutathione, whose metabolism in mammals, we have here demonstrated to be influenced by exogenous ovos produced by invertebrates (Brancaccio et al., 2019). In addition, it is possible that certain organisms can accumulate this molecule in specific organs through the diet: for example, an accumulation of ovo have been found in the lens and gills of the bony fish (Yanshole et al., 2019). Further, *in silico* analyses aimed to investigate coevolution of ovo and other thiol biosynthetic pathways, as well as their receptors/transporters could shed light on these aspects in the near future.

5.5. Conclusions and perspectives

Our study indicates that most bacteria retain ovo biosynthetic pathways, in particular, OvoA and OvoB which are the enzymes involved in the biosynthesis of this metabolite, are encoded by two different genes. We then discovered how most of the bacteria that preserve this metabolic pathway are aerobic and live in aquatic environment, however, a small part of them are anaerobic and live in deep waters. It is likely that originally the sulfoxide synthase activity was oxygen independent. In addition, we have revealed that some of these bacteria live in symbiosis with, or are parasites/pathogens of plants and/or animals, which do not possess the biosynthetic pathway of ovo. These findings indicate a role for the molecule in mutualistic associations and/or in the protection of plants and animals from any infections. Finally, we found evidences in support of the hypothesis that the OvoB-like domain in *Hydra* likely originated from a horizontal gene transfer event from bacterial symbionts. In conclusion, our results point out to a complex evolutionary history of ovothiol biosynthesis from bacteria to unicellular and multicellular eukaryotes. Moreover, the conservation of this secondary metabolic pathway in many marine organisms suggests that molecules similar to ovo are necessary for survival in specific environmental niches. In the future, further studies, that will involve both the biochemical and evolutionary aspects of sulphoxide synthase, will help us to improve our knowledge on marine world, and, at the same time, they could provide some important information allowing us to use biotechnology and metabolic engineering to exploit the chemical, physical and biological properties of these enzymes and their behaviour.

CHAPTER 6

6.1. General discussion and conclusions

The aim of my thesis was to investigate the biological roles and pharmacological potential of marine 5-thiohistidines. During evolution the biosynthesis of these compounds has developed in bacteria, microalgae, and invertebrates, but has been lost in vertebrates and consequently in humans. Therefore, we considered extremely interesting to investigate whether the administration of such compounds could have therapeutic effects on mammals.

To shed new light on the biological role of this metabolite and to fulfil a general picture on the distribution and molecular diversification of the ovothiol pathway in nature, we conducted an *in silico* study on bacterial genomes. We highlighted that most bacteria evolved the biosynthetic pathways of ovo, in particular OvoA and OvoB which are the enzymes involved in the biosynthesis of this metabolite. Most of the bacteria that preserve this metabolic pathway are aerobic and live in an aquatic environment. Curiously, we have revealed that some of these bacteria live in symbiosis with or are parasites of plants/animals, which have not developed the biosynthetic pathway of ovo. These results indicate a role in mutual associations and/or in the protection of parasites from the immune response of the host lacking the same defence system. Finally, we underlined the hypothesis that the OvoB-like domain in *Hydra* originated from a horizontal gene transfer event from bacterial symbionts. The conservation of this secondary metabolic pathway in many marine organisms suggests that ovo-like molecules are required for survival in specific environmental niches. The involvement of ovo in the response to environmental cues well fits with the anti-inflammatory properties we found to be exerted by 5-thiohistidines on mammals. Indeed, our finding that ovo from marine invertebrates inhibits human GGT and therefore affects GSH metabolism, opens new questions about the differential evolution of alternative thiols metabolic pathways in invertebrates and vertebrate for example.

In the first part of my PhD study, I investigated the interaction between 5-thiohistidines and GGT, a membrane-bound enzyme most expressed in the liver and considered a target of action in pathologies associated with high level of GGT activity. We discovered that 5-thiohistidines are reversible and non-competitive inhibitors of GGT activity (Brancaccio et al, 2019; Milito et al., 2019). Furthermore,

these molecules appear to be non-cytotoxic towards normal cells and more efficient compared to GGT inhibitors abandoned in clinical trials for the treatment of GGT-positive pathologies (Brancaccio et al, 2019; Milito et al., 2019). Future studies devoted to the modulation of GGT activity through RNA interference techniques may provide new insight into the role of this enzyme in mediating the biological activities of these compounds.

However, to verify the efficacy of such compounds in ameliorating GGT-positive pathologies, we chose an *in vivo* model of hepatic fibrosis, characterized by high levels of GGT activity. We first confirmed that the treatment with ovo inhibited the enzymatic activity of GGT *in vivo*, causing a down regulation of the main actors of hepatic fibrosis: TGF-β, α-SMA, TIMP-1 thus generating a block in the activation of HSCs and an increase ECM degradation (Brancaccio et al., 2018). These results suggest that ovos can be considered as a new class of sulfur-containing molecules with anti-fibrotic properties.

Since liver fibrosis is the consequence of a chronic state of inflammation, we then decided to test the anti-inflammatory properties of 5-thiohistidines in other models of human inflammation, like *in vitro* model of human keratinocytes and in an *ex vivo* model of human skin tissue. We first pre-treated the cells with 5-thiohistidines (ovo and 5-thio) and then induced inflammation either with TNF-α or with IL-β1. The results obtained shed light on how pretreatment with low concentrations of 5-thiohistidines inhibits the release of pro-inflammatory cytokines (IL-6, IL-8 and TNF-α), induces ERK phosphorylation and then the nuclear translocation of Nrf-2 which activates the transcription of phase II detoxifying enzymes to inhibit the oxidative stress caused by the inflammatory process. These results allow us to hypothesize a possible use of 5-thiohistidines as new pharmacological agents for skin disorders or as formulation in a protective cream against inflammatory processes associated with sunburn, dermatitis, and psoriasis, for example.

In conclusion, our results indicate that ovos are promising natural products to be used as drugs or dietary supplements for the treatment of chronic liver disease (Brancaccio et al., 2018; Milito et al., 2019), and in general, 5-thiohistidines can be considered powerful anti-inflammatory agents in the treatment of skin disorders.

Previous *in vitro* studies of bioavailability indicated that when ovo is administered to GGT-positive cells as HepG2, most of the molecule remain outside the cells likely bound to the membrane enzymes

(Russo et al. 2014), viceversa when ovo is administered to endothelial cells (not overexpressing GGT), most of the molecule enter cells and there exerts its antioxidant and anti-inflammatory action (Castellano et al. 2018). These differences also account for the the different mechanisms of action in the two systems: in the first case, we observe inhibition of GGT activity and induction of autophagy (Brancaccio et al. 2019); in the second, we observe the decrease of intracellular ROS and RNS and of the adhesion molecules to the endothelium (Castellano et al, 2018). However, *in vivo* bioavailability studies are necessary for a future therapeutic application of 5-thiohistidines in human disorders. In fact, these studies would allow to identify the best route of administration (in addition to the peritoneal one), understand which is the fraction of the molecule / drug administered that reaches the systemic circulation without undergoing any chemical modification compared to the total administered, underline the speed with which the drug is made available in the systemic circulation

These studies are fundamental because the choice of molecules with high bioavailability allows to obtain the desired pharmacological effects using a lower dose of active ingredients, also limiting the possible adverse effects at local level.

From a biological and evolutionary point of view, further studies, which will involve both the biochemical and evolutionary aspects of the enzymes involved in the biosynthesis of ovo, could provide some important advances in the use of biotechnology and metabolic engineering to exploit the chemical, physical and biological properties of these enzymes and their behaviour.

In addition, having demonstrated that the non-methylated form of ovo, 5-thio, obtained from chemical synthesis by Prof. Florian Seebeck exhibits ovo-like biological activities, opens new scenarios for the future exploitation of these compounds.

Therefore, we are sure that the results obtained in this thesis can represent the springboard for obtaining an industrial and sustainable production of these compounds with numerous and advantageous properties from a parmacological point of view.

References:

Ahluwalia, G. S., Grem, J. L., Hao, Z., and Cooney, D. A. (1990) Metabolism and action of amino acid analog anti-cancer agents. *Pharmacol. Ther*., **46**, 243–271.

Ahmed, S.M.U., Luo, L., Namani, A., Wang, X.J., Tanga, X. (2016) Nrf2 signaling pathway: Pivotal roles in inflammation. *Biochimica et Biophysica Acta*., **1863** (2), 585-597

Aitken, A.E., Richardson, T.A., Morgan, E.T. (2006) Regulation of drug-metabolizing enzymes and transporters in inflammation. *Ann. Rev. Pharmacol. Toxicol*., **46**, 123–149.

Arauz, J., Ramos-Tovar, E., Muriel, P. (2016) Redox state and methods to evaluate oxidative stress in liver damage: From bench to bedside. *Ann. Hepatol*., **15**, 160–173.

Ariyanayagam, M. R. & Fairlamb, A. H. (2001) Ovothiol and trypanothione as antioxidants in trypanosomatids. *Molecular and Biochemical Parasitology*, **115** (2), 189-198.

Bailly, F., Zoete, V., Vamecq, J., Catteau, J.-P. & Bernier, J.-L. (2000) Antioxidant actions of ovothiol-derived 4-mercaptoimidazoles: glutathione peroxidase activity and protection against peroxynitrite-induced damage. *FEBS Letters*, **486** (1), 19-22.

Bailly, F., Azaroual, N. & Bernier, J.-L. (2003) Design, synthesis and glutathione peroxidase-Like properties of ovothiol-Derived diselenides. *Bioorganic & Medicinal Chemistry*, **11** (21), 4623-4630.

Bangert, C. & Brunner, P.M., Stingl, G. (2011) Immune functions of the skin. *Clin Dermatol*., **29**, 360-76.

Bataller, R. & Brenner, D.A. Liver fibrosis.(2015) *J. Clin. Investig*., **115**, 209–218.

Bailly, F., Zoete, V., Vamecq, J., Catteau, J.-P. & Bernier, J.-L. (2000) Antioxidant actions of ovothiol-derived 4-mercaptoimidazoles: glutathione peroxidase activity and protection against peroxynitrite-induced damage. *FEBS Letters*, **486** (1), 19-22.

Bedossa, P.& Paradis, V. (2003) Liver extracellular matrix in health and disease. *J. Pathol.*, **200**, 504–515.

Benlloch, M., Ortega, A., Ferrer, P., Segarra, R., Obrador, E., Asensi, M., Carretero, J., and Estrela, J. M. (2005) Acceleration of glutathione efflux and inhibition of γ-glutamyltranspeptidase sensitize metastatic B16 melanoma cells to endothelium-induced cytotoxicity. *J. Biol. Chem.*, **280**, 6950–6959

Benlloch, M., Mena, S., Ferrer, P., Obrador, E., Asensi, M., Pellicer, J. A., Carretero, J., Ortega, A., and Estrela, J. M. (2006) Bcl-2 and Mn-SOD antisense oligodeoxynucleotides and a glutamine-enriched diet facilitate elimination of highly resistant B16 melanoma cells by tumor necrosis factor-α and chemotherapy. *J. Biol. Chem.*, **281**, 69–79.

Berman, H.M., Westbrook, J., Feng, Z., Gilliland, G., Bhat, T.N., Weissig, H., Shindyalov, I.N., Bourne, P.E. (2000) The Protein Data Bank. *Nucleic Acids Res*., **28**, 235-242.

Breithaupt, T. & Hardege, J. D. (2012) Pheromones mediating sex and dominance in aquatic animals. *Chemical ecology in aquatic systems*. 1 ed., Oxford University Press.

Bradford, M. M. (1976) A rapid and sensitive method for the quantitation of microgram quantities of protein utilizing the principle of protein-dye binding. *Anal. Biochem.*, **72**, 248–254

Brancaccio, M., D'Argenio, G., Lembo, V., Palumbo, A., Castellano, I. (2018) Antifibrotic Effect of Marine Ovothiol in an In Vivo Model of Liver Fibrosis. *Oxid. Med. Cell. Longev*., **2018**, 5045734.

Brancaccio, M., Russo, M., Masullo, M., Palumbo, A., Russo, G.L., Castellano, I. (2019) Sulfur-containing histidine compounds inhibit γ-glutamyl transpeptidase activity in human cancer cells. *J. Biol. Chem*. **294**, 14603–14614.

Brancaccio, M., Natale, F., Falco, G., Angrisano, T. (2019) Cell-Free DNA Methylation: The New Frontiers of Pancreatic Cancer Biomarkers' Discovery. *Genes (Basel)*, **11**(1):14

Braunshausen, A. & Seebeck, F. P. (2011) Identification and Characterization of the First Ovothiol Biosynthetic Enzyme. *Journal of the American Chemical Society*, **133** (6), 1757-1759.

Burgoyne, D. L., Miao, S., Pathirana, C., Andersen, R. J., Ayer, W. A., Singer, P. P., Kokke, W. C. M. C. & Ross, D. M. (1991) The structure and partial synthesis of imbricatine, a benzyltetrahydroisoquinoline alkaloid from the starfish Dermasterias imbricata. *Canadian Journal of Chemistry*, **69** (1), 20-27.

Carlsen, H., Alexander G, Austenaa LM, Ebihara K and Blomhoff R: (2004) Molecular imaging of the transcription factor NF-kappaB, a primary regulator of stress response. *Mutat Res.*, **551**, 199-211,

Castellano, I. & Merlino, A. (2012). γ-Glutamyltranspeptidases: Sequence, structure, biochemical properties, and biotechnological applications. *Cell Mol. Life Sci*., **69**, 3381–3394.

Castellano, I.; Merlino, A. (2013) Gamma-Glutamyl Transpeptidases: Structure and Function. In Springer Briefs in Biochemistry and Molecular Biology; *Springer: Basel, Switzerland.*

Castellano, I., Ercolesi, E., Romano, G., Ianora, A., Palumbo, A. (2015) The diatom-derived aldehyde decadienal affects life cycle transition in the ascidian Ciona intestinalis through nitric oxide/ERK signalling. *Open Biol*., **5**, 140182.

Castellano, I., Migliaccio, O., D'Aniello, S., Merlino, A., Napolitano, A., Palumbo, A. (2016) Shedding light on ovothiol biosynthesis in marine metazoans. *Scientific reports*, **6**, 21506.

Castellano, I. & Seebeck, F. P. (2018) On ovothiol biosynthesis and biological roles: from life in the ocean to therapeutic potential. *Nat Prod Rep*., **35** (12),1241-1250.

Castellano, I., di Tomo, P., di Pietro N., Mandatori, D., Pipino, C., Formoso,G.,Napolitano, A., Palumbo, A., Pandolfi, A. (2018) Anti-inflammatory activity of marine ovothiol A in an in vitro model of endothelial dysfunction induced by hyperglycemia. *Oxidative Medicine and Cellular Longevity*, **2018** (2087373).

Chapman, J.A., Kirkness, E.F., Simakov, O., Hampson, S.E., Mitros, T., Weinmaier, T., Rattei, T., Balasubramanian, P.G., Borman, J., Busam, D., et al. (2010) The dynamic genome of Hydra. *Nature*, **464**, 592–596.

Chang, E.S., Neuhof, M., Rubinstein, N.D., Diamant, A., Philippe, H., Huchon, D., Cartwright, P. (2015) Genomic insights into the evolutionary origin of Myxozoa within Cnidaria. *Proc. Natl. Acad. Sci*., **112**, 14912–14917.

Chen, L., Naowarojna, N., Song, H., Wang, S., Wang, J., Deng, Z., Zhao, C., Liu, P. (2018) Use of a Tyrosine Analogue To Modulate the Two Activities of a Nonheme Iron Enzyme OvoA in Ovothiol Biosynthesis, Cysteine Oxidation versus Oxidative C-S Bond Formation. *J Am Chem Soc*., **140**, 4604-4612.

Corti, A., Franzini, M., Paolicchi, A., Pompella, A. (2010) γ-Glutamyltransferase of cancer cells at the crossroads of tumor progression, drug resistance and drug targeting. *Anticancer Res*. **30**, 1169–1181.

Costanzo, P., Cariati, L., Desiderio, D., Sgammato, R., Lamberti, A., Arcone, R., Salerno, R., Nardi, M., Masullo, M., Oliverio, M. (2016) Design, synthesis, and evaluation of donepezil-like compounds as ache and bace-1inhibitors. *ACS Med. Chem. Lett*., **7**, 470–475.

D'Argenio, G., Amoruso, D.C., Mazzone, G., Vitaglione, P., Romano, A., Ribecco, M.T.; D'Armiento, M.R., Mezza, E., Morisco, F., Fogliano, V., Caporaso, N. (2010) Garlic extract prevents CCl4-induced liver fibrosis in rats: The role of tissue transglutaminase. *Dig. Liver Dis*., **42**, 571–577.

D'Argenio, G., Mazzone, G., Ribecco M. T., Lembo, V., Vitaglione, P., Guarino, M., Morisco, F., Napolitano, M., Fogliano, V., Caporaso, N (2013) Garlic extract attenuating rat liver fibrosis by inhibiting TGF-β1. *Clinical Nutrition*, **32** (2), 252-8.

Damjanov, N., & Vojinovic, J. (2009) Biologic therapy of rheumatoid arthritis. *Srp Arh Celok Lek.*, **137**, 205-210.

Daunay, S., Lebel, R., Farescour, L., Yadan, J.-C. & Erdelmeier, I. (2016) Short protectinggroup-free synthesis of 5-acetylsulfanyl-histidines in water: novel precursors of 5- sulfanyl-histidine and its analogues. *Organic & Biomolecular Chemistry*, **14** (44), 10473-10480.

de Beer, T.A., Berka, K., Thornton, J.M., Laskowski, R.A.(2014) PDBsum additions. *Nucleic Acids Res*., **42**, D292-D296.

Diaz de Cerio, O., Reina, L., Squatrito, V., Etxebarria, N., Gonzalez-Gaya, B., Cancio, I. (2020) Gametogenesis-Related Fluctuations in Ovothiol Levels in the Mantle of Mussels from different Estuaries: Fighting Oxidative Stress for Spawning in Polluted Waters. *Biomolecules*, **10** (3), 373.

Di Camillo, C.G., Luna, G.M., Bo, M., Giordano, G., Corinaldesi, C., Bavestrello, G. (2012) Biodiversity of Prokaryotic Communities Associated with the Ectoderm of Ectopleura crocea (Cnidaria, Hydrozoa). *PLoS ONE*., **7**, e39926.

Ding C, Cicuttini F, Li, J., Jones, G. (2009) Targeting IL-6 in the treatment of inflammatory and autoimmune diseases. *Expert Opin Investig Drugs*, **18**, 1457-1466.

D'Orazio, J., Jarrett, S., Amaro-Ortiz, A., Scott, T. (2013) UV Radiation and the Skin. *Int J Mol Sci*., **14** (6), 12222–12248.

Dong, R., Peng, Z., Zhang, Y., Yang, J. (2018) mTM-align: an algorithm for fast and accurate multiple protein structure alignment. *Bioinformatics*., **34**, 1719-1725.

Eddy, S.R. (2011) Accelerated profile HMM searches. *PLoS Comput Biol*., **7**, e1002195

Elliott, J.K., Ros,s D.M., Pathirana, C., Miao, S., Andersen, R. J., Singer, P.P., Kokke, W.C.M.C., Ayer, W.A. (1989) Induction of swimming in Stomphia (Anthozoa: Actiniaria) by imbricatine, a metabolite of the asteroid Dermasterias imbricate. *Biol. Bull*., **176**, 73-78.

Esfahani, K., Gold, P., Wakil, S., Michel, R.P., Solymoss ,S. (2011) Acute liver failure because of chronic lymphocytic leukemia: case report and review of the literature. *Curr Oncol*., **18**(1):39-42.

Fairlamb, A. H., Blackburn, P., Ulrich, P., Chait, B. T., Cerami, A. (1985) Trypanothione: a novel bis (glutathionyl) spermidine cofactor for glutathione reductase in trypanosomatids. *Science*, **227** (4693), 1485-1487.

Fairlamb, A. H. & Cerami, A. (1992) Metabolism and Functions of Trypanothione in the Kinetoplastida. *Annual review of microbiology*, **46** (1), 695-729.

Fliedl, L., Wieser, M., Manhart, G., Gerstl, M.P., Khan, A, Grillari, J., Grillari-Voglauer, R. (2014) Controversial role of gamma-glutamyl transferase activity in cisplatin nephrotoxicity. *ALTEX*. **31**(3), 269-78

Franzini, M., Corti, A., Mammini C. (2009) γ-Glutammiltransferasi: biochimica clinica e fisiopatologia umana. *Biochimica clinica*, vol. 33, n. 1.

Fraune, S. & Bosch, T.C. (2007) Long-term maintenance of species-specific bacterial microbiota in the basal metazoan Hydra. *Proc Natl Acad Sci U S A*., **104**, 13146-13151.

Gerdol, M., Sollitto, M., Pallavicini, A., Castellano, I. (2019) The complex evolutionary history of sulfoxide synthase in ovothiol biosynthesis. *Proc Biol Sci*, **286** (1916), 20191812.

Goncharenko, K. V., Vit, A., Blankenfeldt, W. & Seebeck, F. P. (2015) Structure of the Sulfoxide Synthase EgtB from the Ergothioneine Biosynthetic Pathway. *Angewandte Chemie International Edition*, **54** (9), 2821-2824.

Hampel, P.J., King, R.L., Hanson, C.A., Simonetto, D., Chaffee, K.G., Call, T.G., Ding, W., Kenderian, S.S., Slager, S.L., Kay, N.E., Shanafelt, T.D., Parikh, S.A. (2016) Liver Biopsy in Patients with Chronic Lymphocytic Leukemia: Indications and Pathological Findings. *Blood Journal, American Society of Hematology*, **128** (22), 5592.

Hampel, P. J, Chaffee, K.G., King, R.L., Simonetto, D., Larson, M.C., Achenbach, S., Call, T.G., Ding, W., Kenderian, S.S., Leis, J.F., Chanan-Khan, A.A., Bowen, D.A., Conte, M.G., Schwager, S.M., Hanson, C.A., Slager, S.L., Kay, N.E., Shanafelt, T.D., Parikh, S.A. (2017) Liver dysfunction in chronic lymphocytic leukemia: Prevalence, outcomes, and pathological findings. *Am J Hematol*., **92** (12), 1362-1369.

Hand, C. E. & Honek, J. F. (2005) Biological chemistry of naturally occurring thiols of microbial and marine origin. *Journal of natural products*, **68** (2), 293-308.

Hanigan, M. H., Gallagher, B. C., Townsend, D. M., and Gabarra, V. (1999) γ-Glutamyl transpeptidase accelerates tumor growth and increases the resistance of tumors to cisplatin in vivo. *Carcinogenesis*, **20**, 553–559.

Hanigan, M. H., Frierson, H. F. Jr, Swanson, P. E., and De Young, B. R. (1999) Altered expression of γ-glutamyl transpeptidase in human tumors. *Hum. Pathol*., **30**, 300–305.

Hanigan, M. H. (2014) γ-Glutamyl transpeptidase: redox regulation and drug resistance. *Adv. Cancer Res*. **122**, 103–141.

Han, L., Hiratake, J., Tachi, N., Suzuki, H., Kumagai, H., and Sakata, K. (2006) γ-(Monophenyl) phosphono glutamate analogues as mechanismbased inhibitors of γ-glutamyl transpeptidase. *Bioorg. Med. Chem*., **14**, 6043–6054,

Han, L., Hiratake, J., Kamiyama, A., and Sakata, K. (2007) Design, synthesis, and evaluation of γ-phosphono diester analogues of glutamate as highly potent inhibitors and active site probes of γ-glutamyl transpeptidase. *Biochemistry*, **46**, 1432–1447.

Haubrich, WS. (2004) Kupffer of Kupffer cells. *Gastroenterology* 127:16.

Haywood, R., Wardman, P., Sanders, R., Linge, C. (2003) Sunscreens inadequately protect against ultraviolet-A-induced free radicals in skin:implications for skin aging and melanoma? *J. Invest. Dermatol.*, **21**, 862–868.

Hemmann, S., Graf, J., Roderfeld, M., Roeb, E. (2007) Expression of MMPs and TIMPs in liver fibrosis a systematic review with special emphasis on anti-fibrotic strategies. *J Hepatol*., **46** (5), 955-975.

Higdon, A., Diers, A. R., Oh, J. Y., Landar, A. & Darley-Usmar, V. M. (2012) Cell signalling by reactive lipid species: new concepts and molecular mechanisms. *Biochemical Journal*, **442** (Pt 3), 453-464.

Holler, T. P. & Hopkins, P. B. (1988) Ovothiols as biological antioxidants. The thiol groups of ovothiol and glutathione are chemically distinct. *Journal of the American Chemical Society*, **110** (14), 4837-4838.

Holler, T. P., Ruan, F., Spaltenstein, A. & Hopkins, P. B. (1989) Total synthesis of marine mercaptohistidines: ovothiols A, B, and C. *The Journal of Organic Chemistry*, **54** (19), 4570-4575.

Holler, T. P. & Hopkins, P. B. (1990) Ovothiols as free-radical scavengers and the mechanism of ovothiol-promoted NAD(P)H-O2 oxidoreductase activity. *Biochemistry*, **29** (7), 1953-1961.

Hseu, Y.C., Chou, C.W., Senthil Kumar, K., Fu, K.T., Wang, H.M., Hsu, L.S., Kuo, Y.H., Wu, C.R., Chen, S.C., Yang, H.L. (2012) Ellagic acid protects human keratinocyte (HaCaT) cells against UVA-induced oxidative stress and apoptosis through the up regulation of the HO-1and Nrf-2 antioxidant genes. *Food Chem.Toxicol*., **50**, 12451255.

Hseu, Y.C., Lo, H.W., Korivi, M., Tsai, Y.C., Tang, M.J., Yang, H.L.(2015) Dermato-protective properties of ergothioneine through induction of Nrf2/ARE-mediated antioxidant genes in UVA-irradiated Human keratinocytes. *Free Radic Biol Med*., 86:102-17

Humphrey, W., Dalke, A., Schulten, K. (1996) VMD: Visual molecular dynamics. *J Mol Graph*., **14**, 33-38.

Iluz-Freundlich, D., Zhang, M., Uhanova, J, Minuka, G.Y. (2019) The relative expression of hepatocellular and cholestatic liver enzymes in adult patients with liver disease. *Annals of Hepatology*., **19** (2), 204-208.

Irie, M., Suzuki, N., Sohda, T., Anan, A., Iwata, K., Takeyama, Y., Watanabe, H., Fischer, P., Scherberich, J.E., Sakisaka, S. (2007) Hepatic Expression of Gamma-Glutamyltranspeptidase in the Human Liver of Patients With Alcoholic Liver Disease. *Hepatol Res*., **37** (11), 966-73.

Issa, R., Zhou, X., Trim N., Millward-Sadler, H., Krane, S., Benyon, C., Iredale, J. (2003) Mutation in collagen-1that confers resistance to the action of collagenase resultsin failure of recovery from CCl4-induced liver fibrosis, persistence of activated hepatic stellate cells, and diminished hepatocyte regeneration. *FASEB J*., **17** (1), 47-9.

Ito, S., Nardi, G., Palumbo, A. & Prota, G. (1979a) Isolation and characterization of adenochrome, a unique iron (III)-binding peptide from Octopus vulgaris. *Journal of the Chemical Society*, Perkin Transactions **1**, 0, 2617-2623.

Ito, S., Nardi, G., Palumbo, A. & Prota, G. (1979b) A possible pathway for the biosynthesis of adenochromines. *Experientia,* **35** (1), 14-15.

Ivanova, I.A., Nakrieko, K.A. & Dagnino L. (2009) Phosphorylation by p38 MAP kinase is required for E2F1 degradation and keratinocyte differentiation. *Oncogene*, **28**, 52-62.

Jacob, C. (2006) A scent of therapy: pharmacological implications of natural products containing redox-active sulfur atoms. *Natural Product Reports*, **23** (6)**,** 851-863.

Jackson, A.P. (2015) The evolution of parasite genomes and the origins of parasitism. *Parasitology*, **142** Suppl 1:S1-5.

Jeschke J., Van Neste L., Glöckner S.C., Dhir M., Calmon M.F., Deregowski V., Van Criekinge W., Vlassenbroeck I., Koch A., Chan T.A., et al. (2012) Biomarkers for detection and prognosis of breast cancer identified by a functional hypermethylome screen. *Epigenetics*, 7:701–709

Jiang, C.; Zhou, Q.; Jin, M.; Niu, J.; Gao, Y. (2019) Congenital hepatic fibrosis with polycystic kidney disease:Two case reports. *Medicine*, **98**, e15600.

Kamiyama, A., Nakajima, M., Han, L., Wada, K., Mizutani, M., Tabuchi, Y., Kojima-Yuasa, A., Matsui-Yuasa, I., Suzuki, H., Fukuyama, K., Watanabe, B., and Hiratake, J. (2016) Phosphonate-based irreversible inhibitors of human γ-glutamyl transpeptidase (GGT). GGsTop is a non-toxic and highly selective inhibitor with critical electrostatic interaction with an active-site residue Lys562 for enhanced inhibitory activity. *Bioorg. Med.Chem*., **24**, 5340–5352.

Katoh, K., Rozewicki, J., Yamada, K.D. (2019) MAFFT online service: multiple sequence alignment, interactive sequence choice and visualization. *Briefings in bioinformatics*., **20**,1160-1166.

Kaspar, J.W., Niture, S.K., Jaiswal, A.K. (2009) Nrf2:INrf2(Keap1) signalling in oxidative stress. *Free Radic.Biol.Med*., **47** (9),1304-9.

Kassambara, A. (2017) ggpubr:"ggplot2" based publication ready plots. R package version 0.1, 6. https://cran.r-project.org/web/packages/ggpubr/index.html.

Kim, J.; Cha, Y.N., Surh, Y.J.A. (2010) protective role of nuclear factor-erythroid 2-related factor-2(Nrf2) in inflammatory disorders. *Mutat. Res*., **690** (1-2),12-23.

King, J. B., West, M. B., Cook, P. F., and Hanigan, M. H. (2009) A novel, species-specific class of uncompetitive inhibitors of γ-glutamyl transpeptidase. *J. Biol. Chem*. **284**, 9059–9065.

Koenig, G. & Seneff, S. (2015) Gamma-Glutamyltransferase: A Predictive Biomarker of Cellular Antioxidant Inadequacy and Disease Risk. *Dis Markers*., **2015**, 818570.

Kovarikova, M., Hofmanova, J., Soucek, K., & Kozubik, A. (2004) The effects of TNF-alpha and inhibitors of arachidonic acid metabo¬lism on human colon HT-29 cells depend on differentiation status. *Differentiation*, **72**, 23-31.

Krauth-Siegel, R.L. & Leroux, A.E. (2012) Low-molecular-mass antioxidants in parasites. *Antioxid. Redox Signal.*, **7** (4), 583-607.

Kreiniz, N., Katz, O.B., Polliack, A., Tadmor, T. (2017) The Clinical Spectrum of Hepatic Manifestations in Chronic Lymphocytic Leukemia. *Clin Lymphoma Myeloma Leuk*., **17** (12), 863-869.

Laemmli, U. K. (1970) Cleavage of structural proteins during the assembly of the head of bacteriophage T4. *Nature*, **227**, 680–685.

Lyons, S. D., Sant, M. E., and Christopherson, R. I. (1990) Cytotoxic mechanisms of glutamine antagonists in mouse L1210 leukemia. *J. Biol. Chem*., **265**, 11377–11381.

Lancaster, J.E., Shaw, M.L. (1994) Characterization of purified gamma-glutamyl transpeptidase in onions: evidence for in vivo role as peptidase. *Phytochemistry*, **36**, 1351–1358.

Laskowski, R.A., MacArthur, M.W., Moss, D.S., Thornton, J.M. (1993) PROCHECK: a program to check the stereochemical quality of protein structures. *J. Appl. Cryst*., **26**, 283-291.

Leng H, Luo X, Ma L, Kang., K. & Zheng, Z. (2009) Reversal of ultraviolet B-induced immunosuppression by inhibition of the extracellular signal-regulated mitogen-activated protein kinase. *Photodermatol Photoimmunol Photomed*., **25**, 264-269.

Leisinger, F., Burn, R., Meury, M., Lukat, P., Seebeck, F.P. (2019) Structural and Mechanistic Basis for Anaerobic Ergothioneine Biosynthesis. *J Am Chem Soc*., **141**, 6906-6914.

Lherbet, C., & Keillor, J. W. (2004) Probing the stereochemistry of the active site of γ-glutamyl transpeptidase using sulfur derivatives of L-glutamic acid. *Org. Biomol. Chem*., 2, 238–245.

Liao, C. & Seebeck, F. P. (2017) Convergent Evolution of Ergothioneine Biosynthesis in Cyanobacteria. *Chembiochem: a European journal of chemical biology*, **18** (21), 2115-2118.

Lieberman, M. W., Wiseman, A. L., Shi, Z. Z., Carter, B. Z., Barrios, R., Ou, C. N., Che´vez-Barrios, P., Wang, Y., Habib, G. M., Goodman, J. C., Huang, S. L., Lebovitz, R. M., and Matzuk, M. M. (1996) Growth retardation and cysteine deficiency in γ-glutamyl transpeptidase-deficient mice. *Proc. Natl. Acad. Sci. U.S.A.*, **93**, 7923–7926.

Li, H.-Y., Ju, D., Zhang D.-W., Li, H., Kong, L.M., Guo, Y., Li, C., Wang, X.L., Chen, Z.N., Bian,H. (2015) Activation of TGF-β1- CD147 positive feedback loop in hepatic stellate cells promotes liver fibrosis. *Scientific Reports*, **12**, 5, 16552.

LoPachin, R. M., Gavin, T., Geohagen, B. C. & Das, S. (2007) Neurotoxic Mechanisms of Electrophilic Type-2 Alkenes: Soft–Soft Interactions Described by Quantum Mechanical Parameters. *Toxicological Sciences*, **98** (2), 561-570.

Lottenberg, R. & Jackson, C. M. (1983) Solution composition dependent variation in extinction coefficients for p-nitroaniline. *Biochim. Biophys. Acta*, **742**, 558–564.

Lozy, F. & Karantza, V. (2012) Autophagy and cancer cell metabolism. *Seminars in cell & developmental biology*, **23** (4), 395-401.

Lu, N., Malemud, C.J. (2019) Extracellular Signal-Regulated Kinase: A Regulator of Cell Growth, Inflammation, Chondrocyte and Bone Cell Receptor-Mediated Gene Expression. *Int J Mol Sci*., 20 (15), 3792.

Lyons, S. D., Sant, M. E., Christopherson, R. I. (1990) Cytotoxic mechanisms of glutamine antagonists in mouse L1210 leukemia. *J. Biol. Chem*., **265**, 11377–11381.

Marchesini, G., Avagnina, S., Barantani, E.G., Ciccarone, A.M., Corica, F., Dall'Aglio, E., Dalle Grave, R., Morpurgo, P.S., Tomasi, F., Vitacolonna, E. (2005) Aminotransferase and gamma-glutamyltranspeptidase levels in obesity are associated with insulin resistance and the metabolic syndrome. *J Endocrinol Invest*., **28** (4), 333–339.

Markova, N.G., Karaman-Jurukovska, N., Dong, K., Damaghi, N., Smiles, K.A., Yarosh, D.B. (2009) Skin cells and tissue are capable of using L-ergothioneine as an integral component of their antioxidant defense system. *Free Radic Biol Med*., **46** (8), 1168-1176.

Marjanovic, B., Simic, M. G. & Jovanovic, S. V. (1995) Heterocyclic thiols as antioxidants: Why Ovothiol C is a better antioxidant than ergothioneine. *Free Radical Biology and Medicine*, **18** (4), 679-685.

Martin, M.N., Slovin, J.P. (2000) Purified gamma-glutamyl transpeptidases from tomato exhibit high affinity for glutathione and glutathione S-conjugates. *Plant Physiol*., **122** (4), 1417–1426.

Mashabela, G. T. M. & Seebeck, F. P. (2013) Substrate specificity of an oxygen dependent sulfoxide synthase in ovothiol biosynthesis. *Chemical Communications*, **49** (70), 7714-7716.

Medlin L.K. (2016) Evolution of the diatoms: major steps in their evolution and a review of the supporting molecular and morphological evidence. *Phycologia*, **55** (1), 79–103.

Mehta, K.J., Farnaud, S.J., Sharp P.A. (2019) Iron and liver fibrosis: Mechanistic and clinical aspects. *World J Gastroenterol*, **25**(5), 521–538

Mena, S., Benlloch, M., Ortega, A., Carretero, J., Obrador, E., Asensi, M., Petschen, I., Brown, B. D., and Estrela, J. M. (2007) Bcl-2 and glutathione depletion sensitizes B16 melanoma to combination therapy and eliminates metastatic disease. *Clin. Cancer Res*. **13**, 2658–2666.

Milito A, Brancaccio M, D'Argenio G, and Castellano I. (2019) Natural Sulfur-Containing Compounds: An Alternative Therapeutic Strategy against Liver Fibrosis. *Cells*, **8** (11), 0.

Milito, A., Brancaccio, M., Lisurek, M., Masullo, M., Palumbo, A., Castellano, I. (2919) Probing the Interactions of Sulfur-Containing Histidine Compounds with Human Gamma-Glutamyl Transpeptidase. *Marine Drugs*, **17** (12), 650.

Milito A, Castellano I, Burn R, Seebeck FP, Brunet C, Palumbo A (2020). First evidence of ovothiol biosynthesis in marine diatoms. *Free Radic Biol Med*., **152**, 680-688.

Minh, B.Q., Schmidt, H.A., Chernomor, O., Schrempf, D., Woodhams, M.D., Von Haeseler, A., Lanfear, R. (2020) IQ-TREE 2: New models and efficient methods for phylogenetic inference in the genomic era. *Molecular Biology and Evolution*, **37**, 1530-1534.

Murray, H. W. & Nathan, C. F. (1999) Macrophage Microbicidal Mechanisms In Vivo: Reactive Nitrogen versus Oxygen Intermediates in the Killing of Intracellular Visceral Leishmania donovani. *The Journal of Experimental Medicine*, **189** (4), 741-746.

Muthusamy, V., & Piva, T. J. (2009) The UV response of the skin: a review of the MAPK, NFkappaB and TNFalpha signal transduction pathways. *Arch Dermatol Res Sep*., **302** (1), 5-17.

Nagy, P. (2013) Kinetics and Mechanisms of Thiol–Disulfide Exchange Covering Direct Substitution and Thiol Oxidation-Mediated Pathways. *Antioxidants & Redox Signaling*, **18** (13), 1623-1641.

Nakayama, R., Kumagai, H., Tochikura, T. (1984) Purification and properties of gamma-glutamyltranspeptidase from Proteus mirabilis. *J Bacteriol*., **160** (1), 341–346.

Naowarojna, N., Huang, P., Cai, Y., Song, H., Wu, L., Cheng, R., Li, Y., Wang, S., Lyu, H., Zhang, L., Zhou, J. & Liu, P. (2018) In Vitro Reconstitution of the Remaining Steps in Ovothiol A Biosynthesis: C–S Lyase and Methyltransferase Reactions. *Organic letters*, **20** (17), 5427-5430.

Neves, B.M., Cruz, M.T., Francisco, V., Garcia-Rodriguez, C., Silvestre, R., Cordeiro-da-Silva, A., Dinis, A.M., Batista, M.T., Duarte, C.B. & Lopes, M.C. (2009) Differential roles of PI3-kinase, MAPKs and NF-kappaB on the manipulation of dendritic cell T(h)1/T(h)2 cytokine/chemokine polarizing profile. *Mol Immunol*, **46**, 2481-2492.

Newton, G. L., Arnold, K., Price, M. S., Sherrill, C., Delcardayre, S. B., Aharonowitz, Y., Cohen, G., Davies, J., Fahey, R. C. & Davis, C. (1996) Distribution of thiols in microorganisms: mycothiol is a major thiol in most actinomycetes. *Journal of bacteriology*, **178** (7), 1990-1995.

Novo, E., Cannito, S., Morello, E., Paternostro, C., Bocca, C., Miglietta, A., Parola, M. (2015) Hepatic myofibroblasts and fibrogenic progression of chronic liver diseases. *Histology and Histopathology*, **30** (9), 1011-113.

Ogawa Y, Hosoyama H, Hamano M, Motai H (1991) Purification and properties of gamma-glutamyltranspeptidase from Bacillus subtilis (natto). *Agric Biol Chem*, **55** (12), 2971–2977.

O'Neill, E. C., Trick, M., Hill, L., Rejzek, M., Dusi, R. G., Hamilton, C. J., Zimba, P. V., Henrissat, B. & Field, R. A. (2015) The transcriptome of Euglena gracilis reveals unexpected metabolic capabilities for carbohydrate and natural product biochemistry. *Molecular BioSystems*, **11** (10), 2808-2820.

Palumbo, A., D'Ischia, M., Misuraca, G. & Prota, G. (1982) Isolation and structure of a new sulphur-containing aminoacid from sea urchin eggs. *Tetrahedron Letters*, **23** (31), 3207-3208.

Palumbo, A., Misuraca, G., D'Ischia, M., Donaudy, F. & Prota, G. (1984) Isolation and distribution of 1-methyl-5-thiol-l-histidine disulphide and a related metabolite in eggs from echinoderms. Comparative Biochemistry and Physiology Part B. *Comparative Biochemistry*, **78** (1), 81-83.

Palumbo A, Castellano I, Napolitano A. (2018) Ovothiol: a potent natural antioxidant from marine organisms. In Blue Biotechnology: Production and Use of Marine Molecules, pp. 583–610. Hboken, NJ, USA: Stephane La Barre, Stephen S. Bates.

Parsons, C. J., Takashima, M., Rippe, R. A. (2007) Molecular mechanisms of hepatic fibrogenesis. *Journal of Gastroenterology and Hepatology*, **22**, S79–S84.

Pathirana, C. & Andersen, R. J. (1986) Imbricatine, an unusual benzyltetrahydroisoquinoline alkaloid isolated from the starfish Dermasterias imbricata. *Journal of the American Chemical Society*, **108** (26), 8288-8289.

Pompella, A., De Tata, V., Paolicchi, A., and Zunino, F. (2006) Expression of γ-glutamyltransferase in cancer cells and its significance in drug resistance.*Biochem. Pharmacol*., **71**, 231–238.

Povero, D.; Busletta, C.; Novo, E.; Di Bonzo, L.V. (2010) Cannito, S.; Paternostro, C.; Parola, M. Liver fibrosis:A dynamic and potentially reversible process. *Histol. Histopathol*., **25**, 1075–1091.

Puche, J. E., Saiman, Y., Friedman, S. L. (2013) Hepatic stellate cells and liver fibrosis. *Comprehensive Physiology*, **3,** 4.

R Core Team. R (2019) A language and environment for statistical computing. R Foundation for Statistical Computing, Vienna, Austria. https://www.R-project.org/.

Ramsay, R.R. & Tipton, K.F. (2017) Assessment of enzyme inhibition: a review with examples from the development of monoamine oxidase and cholinesterase inhibitory drugs. *Molecules*., **22**, 1192.

Riemer, A. B., Keskin, D. B., & Reinherz, E. L. (2012). Identification and validation of reference genes for expression studies in human keratinocyte cell lines treated with and without interferon-γ - a method for qRT-PCR reference gene determination. *Experimental dermatology*, **21**(8), 625–629.

Rizzo, C. & Lo Giudice, A. (2018) Marine Invertebrates: Underexplored Sources of Bacteria Producing Biologically Active Molecules. *Diversity*., **10** (3), 52.

Rhee, S. G., Yang, K.-S., Kang, S. W., Woo, H. A., Chang, T.-S. (2005) Controlled Elimination of Intracellular H2O2: Regulation of Peroxiredoxin, Catalase, and Glutathione Peroxidase via Post-translational Modification. *Antioxidants & Redox Signaling*, **7** (5-6), 619-626.

Rohl, I., Schneider, B., Schmidt, B., Zeeck, E. (1999) L-ovothiol A: the egg release pheromone of the marine polychaete Platynereis Dumerilii: Anellida: Polychaeta. *Zeitschrift für Naturforschung C*, **54c**, 1145–1147.

Rossi, F., Nardi, G., Palumbo, A. & Prota, G. (1985) 5-thiolhistidine, a new amino acid from eggs of Octopus vulgaris. *Comparative Biochemistry and Physiology Part B: Comparative Biochemistry*, **80** (4), 843-845.

Ruoso, P. & Hedley, D. W. (2004) Inhibition of γ-glutamyl transpeptidase activity decreases intracellular cysteine levels in cervical carcinoma. *Cancer Chemother. Pharmacol*., **54**, 49–56.

Russo, G., Russo, M., Castellano, I., Napolitano, A., Palumbo, A. (2014) Ovothiol isolated from sea urchin oocytes induces autophagy in the Hep-G2 cell line. *Marine Drugs*, **12** (7), 4069-4085.

Sambamoorthy, G., Sinha, H., Raman, K. (2019) Evolutionary design principles in metabolism. *Proc Biol Sci.*, **286** (1898), 20190098.

Schuppan, D. & Kim, O.Y. (2013) Evolving therapies for liver fibrosis. *J Clin Invest*., **123**(5):1887-901.

Scudiero O, Brancaccio M, Mennitti C, Laneri S, Lombardo B, De Biasi MG, De Gregorio E, Pagliuca C, Colicchio R, Salvatore P, Pero R. (2020) Human Defensins: A Novel Approach in the Fight against Skin Colonizing Staphylococcus aureus. *Antibiotics (Basel)*, **9**(4):198.

Seebeck, F. P. (2010) In Vitro Reconstitution of Mycobacterial Ergothioneine Biosynthesis. *Journal of the American Chemical Society*, **132** (19), 6632-6633.

Seebeck, F. P. (2013) Thiohistidine Biosynthesis. CHIMIA *International Journal for Chemistry*, **67** (5), 333-336.

Selman-Reimer, S., Duhe, R. J., Stockman, B. J. & Selman, B. R. (1991) L-1-N-methyl-4-mercaptohistidine disulfide, a potential endogenous regulator in the redox control of chloroplast coupling factor 1 in Dunaliella. *Journal of Biological Chemistry*, **266** (1), 182-188.

Shapiro, B. M., Turner, E. E., Hopkins, P. B., Klevit, R. E., Holler, T. P. & Spaltenstein, A. (1990) *Antioxidant thiohistidine compounds.*

Shimamura, Y., Takeuchi, I., Terada, H., and Makino, K. (2019) Therapeutic effect of GGsTop, selective γ-glutamyl transpeptidase inhibitor, on a mouse model of 5-fluorouracil-induced oral mucositis. *Anticancer Res*., **39**, 201–206.

Sievers, F., Wilm, A., Dineen, D., Gibson, T. J., Karplus, K., Li, W., Lopez, R., McWilliam, H., Remmert, M., Söding, J., Thompson, J.D., Higgins, D.G. (2011) Fast, scalable generation of high-quality protein multiple sequence alignments using Clustal Omega. *Mol Syst Biol*., **7**, 529.

Sievers, F. & Higgins, D,G. (2018). Clustal Omega for making accurate alignments of many protein sequences. *Protein Sci*., **27**, 135-145.

Song, H., Leninger, M., Lee, N. & Liu, P. (2013) Regio-selectivity of the Oxidative C-S Bond Formation in Ergothioneine and Ovothiol Biosyntheses. *Organic letters*, **15** (18), 4854-4857.

Song, H., Her, A. S., Raso, F., Zhen, Z., Huo, Y. & Liu, P. (2014) Cysteine Oxidation Reactions Catalyzed by a Mononuclear Non-heme Iron Enzyme (OvoA) in Ovothiol Biosynthesis. *Organic letters*, **16** (8), 2122-2125.

Spies, H. S. & Steenkamp, D. J. (1994) Thiols of intracellular pathogens. Identification of ovothiolA in Leishmania donovani and structural analysis of a novel thiol from Mycobacterium bovis. *European Journal of Biochemistry*, **224**, 203-213.

Steenkamp, D. J., Weldrick, D. & Spies, H. S. C. (1996) Studies on the Biosynthesis of Ovothiol A. *European Journal of Biochemistry*, **242** (3), 557-566.

Suzuki, H., Kumagai, H., Tochikura, T. (1986) gamma-Glutamyltranspeptidase from Escherichia coli K-12: purification and properties. *J Bacteriol*, **168** (3), 1325–1331.

Tarrant, A.M., Payton, S.L., Reitzel, A.M., Porter, D.T., Jenny, M.J. (2918) Ultraviolet radiation significantly enhances the molecular response to dispersant and sweet crude oil exposure in Nematostella vectensis. *Mar Environ Res*., **134**, 96-108.

Tate, S. S., and Meister, A. (1978) Serine-borate complex as a transitionstate inhibitor of γ-glutamyl transpeptidase. *Proc. Natl. Acad. Sci. U.S.A.*, 75, 4806–4809.

Taylor, S. A., Crowley, J., Pollock, T. W., Eyre, H. J., Jaeckle, C., Hynes, H. E., and Stephens, R. L. (1991) Objective antitumor activity of acivicin in patients with recurrent CNS malignancies: a Southwest Oncology Group trial. J. *Clin. Oncol*., **9**, 1476–1479.

Terzyan, S. S., Cook, P. F., Heroux, A., and Hanigan, M. H. (2017) Structure of 6-diazo-5-oxo-norleucine-bound human γ-glutamyl transpeptidase 1, a novel mechanism of inactivation. *Protein Sci*. **26**, 1196–1205.

Turner, E., Klevitj, R., Hopkinsj, P. B. & Shapiro, B. M. (1986) Ovothiol: A Novel Thiohistidine Compound from Sea Urchin Eggs That Confers NAD(P)H-02 Oxidoreductase Activity on Ovoperoxidase. *The Journal of biological chemistry*, **261**, 13056-13063.

Turner, E., Klevit, R., Hager, L. J. & Shapiro, B. M. (1987) Ovothiols, a family of redoxactive mercaptohistidine compounds from marine invertebrate eggs. *Biochemistry*, **26** (13), 4028-4036.

Turner, E., Hager, L. J. & Shapiro, B. M. (1988) Ovothiol replaces glutathione peroxidase as a hydrogen peroxide scavenger in sea urchin eggs. *Science*, **242** (4880), 939-941.

Tuzova, M., Jean, J. C., Hughey, R. P., Brown, L. A., Cruikshank, W. W., Hiratake, J., and Joyce-Brady, M. (2014) Inhibiting lung lining fluid glutathione metabolism with GGsTop as a novel treatment for asthma. *Front. Pharmacol*., **5**, 179.

Uva, L., Diana, M., Catarina, P., Joana, A., Ferreira, C.D.J., Paulo, F. (2012) Mechanisms of Action of Topical Corticosteroids in Psoriasis. *Int J Endocrinol*., **2012**, 561018.

Vamecq, J., Maurois, P., Bac, P., Bailly, F., Bernier, J. L., Stables, J. P., Husson, I. & Gressens, P. (2003) Potent mammalian cerebroprotection and neuronal cell death inhibition are afforded by a synthetic antioxidant analogue of marine invertebrate cell protectant ovothiols. *The European journal of neuroscience*, **18** (5), 1110-1120.

Vogt, R.N., Spies, H.S., Steenkamp, D.J. (2001) The biosynthesis of ovothiol A (N-methyl-4-mercaptohistidine). Identification of S-(4'-L-histidyl)-L-cysteine sulfoxide as an intermediate and the products of the sulfoxide lyase reaction. *Eur. J. Biochem*., **268**, 5229–5241.

Vogt, R. N., Spies, H. S. C. & Steenkamp, D., J. (2001) The biosynthesis of ovothiol A (N1-methyl-4-mercaptohistidine). *European Journal of Biochemistry*, **268** (20), 5229-5241.

Vogt, R. N. & Steenkamp, D. J. (2003) The metabolism of S-nitrosothiols in the trypanosomatids: the role of ovothiol A and trypanothione. *Biochemical Journal*, **371** (Pt 1), 49-59.

Wall, S., B., Oh, J.-Y., Diers, A. R. & Landar, A. (2012) Oxidative Modification of Proteins: An Emerging Mechanism of Cell Signaling. *Frontiers in Physiology*, **3**, 369.

Wang, L., Qu, X., Xie, Y. & Lv, S. (2017) Study of 8 Types of Glutathione Peroxidase Mimics Based on β-Cyclodextrin. *Catalysts*, **7** (10), 289.

Wattam, A.R., Abraham, D., Dalay, O., Disz, T.L., Driscoll, T., Gabbard, J.L., Gillespie, J.J., Gough, R., Hix, D., Kenyon, R., Machi, D., Mao, C., Nordberg, E.K., Olson, R., Overbeek, R., Pusch, G.D, Shukla, M., Schulman, J., Stevens, R.L., Sullivan, D.E., Vonstein, V., Warren, A., Will, R., Wilson, M.J.C., Yoo, H.S., Zhang, C., Zhang, Y., Sobral, B.W. (2014) PATRIC, the bacterial bioinformatics database and analysis resource. *Nucleic Acids Res*., **42**, D581-D591.

Weaver, K. H. & Rabenstein, D. L. (1995) Thiol/Disulfide Exchange Reactions of Ovothiol A with Glutathione. *The Journal of Organic Chemistry*, **60** (6), 1904-1907.

Webb, B. & Sali, A. (2016) Comparative Protein Structure Modeling Using MODELLER. *Curr Protoc Bioinformatics.*, **54**, 5.6.1-5.6.37.

Weng, H. L., Liu, Y., Chen J. L., Huang, T., Xu,L.J., Godoy, P., Hu, J.H., Zhou, C., Stickel, F., Marx, A., Bohle, R.M., Zimmer, V., Lammert, F., Mueller, S., Gigou, M., Samuel, D., Mertens, P.R., Singer, V.M., Seitz, H.K., Dooley S. (2009) The etiology of liver damage imparts cytokines transforming growth factor beta1 or interleukin-13 as driving forces in fibrogenesis. *Hepatology*, **50** (1), 230-243.

Westley, A. M., and Westley, J. (1996) Enzyme inhibition in open systems. Superiority of uncompetitive agents. *J. Biol. Chem*., **271**, 5347–5352.

West, M.B., Wickham, S., Quinalty, L.M., Pavlovicz, R.E., Li, C., Hanigan, M.H. (2011) Autocatalytic cleavage of human gammaglutamyl transpeptidase is highly dependent on N-glycosylation at asparagine 95. *J Biol Chem*, **286** (33), 28876–28888.

Wheeler, T.J., Clements, J., Finn, R.D. (2014) Skylign: a tool for creating informative, interactive logos representing sequence alignments and profile hidden Markov models. *BMC Bioinformatics*, **15**, 7.

Whitfield J.B. (2001) Gamma glutamyl transferase. *Crit Rev Clin Lab Sci*, **38**(4), 263-355

Will, Y., Fischer, K.A., Horton, R.A., Kaetzel, R.S., Brown, M.K., Hedstrom, O., Lieberman, M.W., Reed, D.J. (2000) gamma-glutamyltranspeptidase-deficient knockout mice as a model to study the relationship between glutathione status, mitochondrial function, and cellular function. *Hepatology*, **32**(4 Pt 1), 740-9.

Winterbourn, C. C. & Hampton, M. B. (2008) Thiol chemistry and specificity in redox signaling. *Free Radical Biology and Medicine*, **45** (5), 549-561.

Yanshole, V.V., Yanshole, L.V., Zelentsova, E.A., Tsentalovich Y.P. (2019) Ovothiol A is the Main Antioxidant in Fish Lens. *Metabolites*, **9** (5): 95.

Yamamoto, S., Watanabe, B., Hiratake, J., Tanaka, R., Ohkita, M., and Matsumura, Y. (2011) Preventive effect of GGsTop, a novel and selective γ-glutamyl transpeptidase inhibitor, on ischemia/reperfusion-induced renal injury in rats. *J. Pharmacol. Exp. Ther*., **339**, 945–951.

Yu, Y., Fan, Y., Yang, Z., Lu, Y., Xu, Q., Chen, X. (2016) Elevated serum gamma-glutamyltransferase predicts advanced histological liver damage in chronic hepatitis B. *Discov Med*., **21**, (113), 7-14.

Yiğit, B., Boyle, M., Özler, O., Erden, N., Tutucu, F., Hardy, T., Bergmann, C., Distler, J., Adalı, G., Dayangaç, M., Mann, D. A., Zeybel, M., & Mann, J. (2018). Plasma cell-free DNA methylation: a liquid biomarker of hepatic fibrosis. Gut, **67**(10), 1907–1908.

Zimmermann, L., Stephens, A., Nam, S.Z., Rau, D., Kübler, J., Lozajic, M., Gabler, F., Söding, J., Lupas, A.N., Alva, V. (2018) A Completely Reimplemented MPI Bioinformatics Toolkit with a New HHpred Server at its Core. *J Mol Biol*., **430**, 2237-2243.

Zoete, V., Bailly, F., Catteau, J.-P. & Bernier, J.-L. (1997) Design, synthesis and antioxidant properties of ovothiol-derived 4-mercaptoimidazoles. *Journal of the Chemical Society*, Perkin Transactions **1**, 0 (20), 2983-2988.

Zoete, V., Bailly, F., Vezin, H., Teissier, E., Duriez, P., Fruchart, J.-C., Catteau, J.-P. & Bernier, J.-L. (2000) 4-Mercaptoimidazoles derived from the naturally occurring antioxidant ovothiols 1. Antioxidant properties. *Free Radical Research*, **32** (6), 515-524.

Zhou, Z., Tran, P.Q., Kieft, K., Anantharaman, K. (2020) Genome diversification in globally distributed novel marine Proteobacteria is linked to environmental adaptation. *ISME J*., **14** (8):2060-2077.

Zarowiecki, M. & Berriman, M. (2015) What helminth genomes have taught us about parasite evolution. *Parasitology*, **142** Suppl 1,S85-S97.